UNIVERSITEIT VAN PRETORIA
UNIVERSITY OF PRETORIA
YUNIBESITHI YA PRETORIA

# Chemical and genetic interrogation of *Plasmodium falciparum* mitochondrial pyruvate carriers

By Shanté da Rocha
16224494

Submitted in fulfilment of the requirements for the degree
*Magister Scientiae* in Biochemistry

in the Faculty of Natural and Agricultural Sciences
Department of Biochemistry, Genetics and Microbiology Division of Biochemistry
University of Pretoria

December 2022

UNIVERSITEIT VAN PRETORIA
UNIVERSITY OF PRETORIA
YUNIBESITHI YA PRETORIA

# SUBMISSION DECLARATION

I, Shanté da Rocha, declare that the dissertation, which I hereby submit for the degree *Magister Scientiae* in the Department of Biochemistry, Genetics, and Microbiology at the University of Pretoria, is my own work and has not previously been submitted by me for a degree at this or any other tertiary institution.

Signature: 

Date: 20/10/2022

# DECLARATION OF ORIGINALITY

University of Pretoria

Faculty of Natural and Agricultural Sciences

Department of Biochemistry, Genetics, and Microbiology

| | |
|---|---|
| Full names of student: | Shanté da Rocha |
| Student number: | 16224494 |

**Declaration**

1. I understand what plagiarism is and am aware of the University's policy in this regard.

2. I declare that this project proposal is my original work. Where other people's work has been used (either from a printed source, Internet, or any other source), this has been properly acknowledged and referenced in accordance with requirements.

3. I have not used work previously produced by another student or any other person to hand in as my own.

4. I have not allowed and will not allow anyone to copy my work with the intention of passing it off as his or her own.

Signature**:** 

Date**:** 20/10/2022

# Table of Contents

Table of Contents……iv
List of Figures……vi
List of Tables……viii
List of Abbreviations……ix
Acknowledgements……xi
Summary……xii
1. Literature review……1
1.1 Malaria: the disease burden……1
1.2 *P. falciparum* life cycle……2
1.3 Malaria control strategies ……4
1.4 Membrane transport proteins……6
1.5 Central carbon metabolism of the intraerythrocytic *P. falciparum* parasite……8
1.6 Mitochondrial pyruvate carriers……11
1.7 *P. falciparum* genetic editing techniques……12
Aim ……16
Hypothesis……16
Objectives……16
2. Materials and Methods……17
2.1 *In silico* analyses of putative MPCs ……17
2.2 *In vitro P. falciparum* parasite cultivation ……18
2.2.1 Ethical clearance statement ……18
2.2.2 *In vitro* asexual parasite cultivation ……18
2.2.3 Sorbitol synchronisation of asexual *P. falciparum* parasites ……19
2.2.4 *In vitro P. falciparum* early gametocyte cultivation ……19
2.3 Evaluating asexual proliferation using a SYBR Green I fluorescence assay ……19
2.4 Evaluating gametocyte viability using the lactate dehydrogenase assay……20
2.5 Generation of SLI-TGD and SLI-*glmS* transgenic parasite lines……21
2.5.1 Preparation of SLI constructs for transfection ……23
2.5.2 Transfection of SLI constructs into NF54 parasites……24
2.5.3 Drug selection and screening of transgenic parasites……24

2.6 Generation of a transgenic ectopic expression line ..... 28
2.6.1 *In silico* design of *mpc1-myc-mpc2-HA* fragment ..... 29
2.6.2 Cloning of the *mpc1-myc-mpc2-HA* fused fragment into pCR2.1-*cam* ..... 30
2.6.3 Putative recombinant colony screening ..... 31
2.6.3.1 Bacterial colony-screening PCR ..... 31
2.6.3.2 Restriction enzyme digestion of putative recombinant plasmid ..... 32
2.6.3.3 Sanger sequencing of putative recombinant plasmid ..... 32
2.6.4 Recombinant ectopic expression system plasmid preparation ..... 32
2.6.5 Transfection of ectopic expression system plasmids ..... 33
2.6.6 Drug selection and transgenic parasite screening ..... 33
3. Results ..... 35
3.1. *In silico* analyses of putative MPC proteins ..... 35
3.2. *In vitro* cultivation of *P. falciparum* parasites ..... 39
3.3. MPC inhibitor effect on *P. falciparum* parasites ..... 40
3.4. Genetic manipulation of putative MPCs to evaluate biological function ..... 42
3.4.1. Investigation of MPC essentiality in asexual stage parasites using SLI-TGD ..... 42
3.4.2. Generation of conditional knockdown lines with the SLI-*glmS* system ..... 46
3.4.3. Generation of an MPC ectopic expression line ..... 50
3.4.3.1. Cloning the *mpc1-myc-mpc2-HA* fragment into Bxb1 ectopic expression system ..... 50
3.4.3.2. Generation of ectopic expression lines in *P. falciparum* ..... 54
4. Discussion ..... 57
5. Conclusio ..... 61
6. References ..... 62
7. Supplementary informatio ..... 71

# List of Figures

Figure 1.1: Global distribution of malaria infection in 2020. ..... 1
Figure 1.2: *P. falciparum* life cycle. ..... 3
Figure 1.3: Schematic representation of membrane transport protein classes. ..... 7
Figure 1.4: Schematic diagram of *P. falciparum* central carbon metabolism. ..... 9
Figure 2.1: Plasmid representation of the SLI-based systems. ..... 22
Figure 2.2: Schematic representation of transgenic parasite line generation using the SLI-systems ..... 25
Figure 2.3: Schematic representation of the primer combinations used in screening the SLI-transgenic parasite lines. ..... 27
Figure 2.4: Schematic representation of the BXB1 ectopic expression system. ..... 28
Figure 2.5: Schematic representation of the *mpc1-myc-mpc2-HA* fragment ..... 29
Figure 2.6: Schematic representation of screening the ectopic transgenic parasite lines generated with the ectopic expression system. ..... 34
Figure 3.1: Evolutionary analysis of putative MPC1 and MPC2 proteins. ..... 35
Figure 3.2: Protein sequence alignment of *P. falciparum* MPC1 and MPC2 to MPC orthologues with experimentally confirmed function. ..... 37
Figure 3.3: Schematic representation of the predicted MPC1 and MPC2 protein topology. ..... 38
Figure 3.4: *P. falciparum* NF54 parasite morphology. ..... 39
Figure 3.5: The chemical structure of the MPC inhibitor, UK-5099. ..... 40
Figure 3.6: The inhibitory effect of UK-5099 and DMSO on asexual parasites and early stage gametocytes. ..... 41
Figure 3.7: Summary of pSLI-*mpc1*-GFP and pSLI-*mpc2*-GFP cloning and validation process. ..... 43
Figure 3.8: Parasitaemia of *P. falciparum* NF54 parasites transfected with pSLI-*mpc1*-GFP and pSLI-*mpc2*-GFP during episomal selection and recovery. ..... 44
Figure 3.9: PCR screening for episomal plasmid presence in NF54 parasites transfected with pSLI-*mpc1*-GFP and pSLI-*mpc2*-GFP plasmids. ..... 45
Figure 3.10: Parasitaemia of *P. falciparum* NF54-epi(pSLI-*mpc1*-GFP) and NF54-epi(pSLI-*mpc2*-GFP) parasite lines during G418 selection and recovery. ..... 46
Figure 3.11: Summary of pSLI-*mpc1-glmS/glmS-mut* and pSLI-*mpc2-glmS/glmS-mut* cloning and validation process. ..... 47
Figure 3.12: Parasitaemia of *P. falciparum* NF54 parasites transfected with pSLI-*mpc1-glmS/glmS-mut* and pSLI-*mpc2-glmS/glmS-mut* during episomal selection and recovery ..... 48

Figure 3.13: PCR confirmation of the episomal uptake into NF54 parasites transfected with pSLI-*glmS/glmS-mut*. ..... 48
Figure 3.14: Parasitaemia of *P*. *falciparum* NF54-epi(pSLI-*mpc1-glmS/glmS-mut*) and NF54-epi(pSLI-*mpc2-glmS/glmS-mut*) parasite lines during G418 selection and recovery. ..... 49
Figure 3.15: Restriction enzyme digest of pUC57-*mpc1-myc-mpc2-HA.* ..... 50
Figure 3.16: Restriction enzyme digest of pCR2.1-*cam-glmS* and pCR2.1-*cam-glmS-mut*. .. 51
Figure 3.17: Bacterial colony screening for a recombinant pCR2.1-*cam-glmS* and *pCR*2.1-*cam-glmS* plasmid. ..... 52
Figure 3.18: Validation of recombinant pCR2.1-*cam-mpc1-myc-mpc2-HA-glmS* and pCR2.1-*cam-mpc1-myc-mpc2-HA-glmS-mut* plasmids. ..... 53
Figure 3.19 Parasitaemia of *P*. *falciparum* transfected *P. falciparum* NF54$^{attB}$ parasites during G418 and WR99210 selection and recovery. ..... 54
Figure 3.20: Genomic integration confirmation of the NF54-*cam-mpc1-myc-mpc2-HA-glmS* parasite line. ..... 55

# List of Tables

Table 1.1: The advantages and disadvantages of genetic editing strategies used in *P. falciparum.* ..... 13
Table 2.1: UniProt accession codes for MPC1 and MPC2 amino acid sequences for various organisms. ..... 17
Table 2.2: SLI-TGD and SLI-*glmS* construct information. ..... 22
Table 2.3: Primers used for screening the episomal presence of SLI constructs and the allelic exchange at the *mpc* loci in *P. falciparum* NF54 parasites. ..... 26
Table 2.4: Primers used to identify bacterial clones containing the ectopic expression plasmids. ..... 31
Table 2.5: Primers used for identifying transgenic *P. falciparum* parasites with genomic integration into NF54$^{attB}$ parasites. ..... 34
Table 3.1: Likelihood prediction of MPC1 and MPC2 export to the mitochondria in eukaryotic organisms. ..... 39

# List of Abbreviations

| | |
|---|---|
| Aco | Aconitase |
| ACT | Artemisinin-based combination therapy |
| $Amp^R$ | Ampicillin resistance gene |
| APAD | 3-acetylpyridine adenine dinucleotide |
| ATP2 | Aminophospholipid-transporting P-ATPase |
| BCKDH | Branched-chain keto-acid dehydrogenase |
| BSL2 | Biosafety level 2 |
| CHC | α-Cyano-4-hydroxycinnamate |
| CRT | Chloroquine resistance transporter |
| CS | Citrate synthase |
| DD | Destabilisation domain |
| DMSO | Dimethyl sulfoxide |
| DV | Digestive vacuole |
| EDTA | Ethylenediaminetetraacetic acid |
| EPM | Erythrocyte plasma membrane |
| EtBr | Ethidium bromide |
| FAD | Flavin adenine dinucleotide |
| FDA | Food and Drug Administration |
| FH | Fumarate hydratase |
| FKBP | FK506-binding protein |
| FRB | FKBP rapamycin binding |
| GABAT | GABA transaminase |
| GDP | Guanosine diphosphate |
| GFP | Green fluorescent protein |
| Glcn | Glucosamine |
| GOI | Gene of interest |
| GTP | Guanosine triphosphate |
| HA | Hemagglutinin |
| hDHFR | Human dihydrofolate reductase |
| hpi | Hours post-invasion |
| $IC_{50}$ | Half-maximal inhibitory concentration |
| IDC | Intraerythrocytic development cycle |
| IDH | Isocitrate dehydrogenase |
| IMM | Inner mitochondrial membrane |
| IRS | Indoor residual spraying |
| KGDH | α-ketogluterate dehydrogenase |
| LB | Luria Bertani broth |
| LB-Ampicillin | LB supplemented with 50 mg/mL ampicillin |
| LDH | Lactate dehydrogenase |
| LLIN | Long-lasting insecticidal nets |
| MEGA | Molecular Evolutionary Genetics Analysis |
| MPC | Mitochondrial pyruvate carrier |
| MQO | Malate-quinone oxidoreductase |
| MSA | Multiple sequence alignment |

| | |
|---|---|
| MTP | Membrane transport protein |
| NAD | Nicotinamide adenine dinucleotide |
| NAG | N-acetyl glucosamine |
| NBT | Nitroblue tetrozoleum |
| Neo-R | Neomycin resistance |
| OAA | Oxaloacetate |
| $OD_{600}$ | Optical density at 600 nm |
| OMM | Outer mitochondrial membrane |
| PCR | Polymerase chain reaction |
| PDH | Pyruvate dehydrogenase |
| PEP | Phosphoenolpyruvate |
| PEPC | Phosphoenolpyruvate carboxylase |
| PEPCK | Phosphoenolpyruvate carboxykinase |
| PES | Phenoethosulphate |
| PfNCR1 | Niemann-Pick type C1-related protein |
| PfNT1 | Nucleoside transporter |
| PK | Pyruvate kinase |
| PlasmoDB | *Plasmodium* database |
| pLDH | Parasite lactate dehydrogenase |
| PPM | Parasite plasma membrane |
| PV | Parasitophorous vacuole |
| PVM | Parasite vacuolar membrane |
| SCS | Succinyl-CoA synthetase |
| SDH | Succinate dehydrogenase |
| SLI | Selection-linked integration |
| TAE | Tris-acetate-EDTA buffer |
| TCA | Tricarboxycyclic acid |
| TGD | Targeted gene disruption |
| WHO | World Health Organization |

# Acknowledgements

I would like to express my heartfelt gratitude to my supervisor, Dr. Jandeli Niemand, for her mentorship, encouragement, and willingness to brainstorm for the betterment of the project and my personal growth as a scientist. I also thank, Professor Lyn-Marie Birkholtz, my co-supervisor, for her contributions and insights to this project. Furthermore, I would like to extend my gratitude to all members of the Malaria Parasite Molecular Laboratory (M2PL) team and to Dr. Elisha Mugo for their guidance, no matter the nature of each inquiry.

Thank you to my parents, Edna and Rocky da Rocha, for their unwavering support and guidance throughout my academic journey. I also thank my sister and brother-in-law, Tania and Leo Morais, for their advice after lending a listening ear to level my thought processes. I am grateful to my fellow lab partners and colleagues who have become invaluable friends, including Henrico Langeveld, Daniel Opperman, Martha Muruya, Jean Thomas, Sizwe Tshabalala, and Marché Maré. I thank them for their support, friendship, and much-needed distractions during times when science seemed uncertain.

Lastly, I acknowledge the National Research Foundation for funding this degree through the NRF Grantholder-linked bursary.

# Summary

Despite efforts to reduce the global spread and severity of malaria infection, resistance towards current frontline antimalarials has halted malaria elimination progress. Thus, malaria parasite biology should be continually investigated in hopes of finding resistance mechanisms and targetable biology to develop new compounds. *Plasmodium falciparum*, the most clinically important malaria-causing parasite, employs energy metabolism pathways differently from one intraerythrocytic form to the next. The proliferative asexual stage, the disease-causing form, fulfils its high energy demand through anaerobic glycolysis. However, the slow-maturing gametocyte, the transmissible form, relies on a canonical TCA cycle and oxidative phosphorylation for energy production. Membrane transport proteins crucially maintain the metabolite link between these pathways in both stages of parasite development. For instance, pyruvate production, from extracellularly sourced glucose, is important for glycolysis and the TCA cycle, yet its translocation mechanism across the inner mitochondrial membrane is unknown. In the last decade, the mitochondrial pyruvate carrier (MPC) heterocomplex which consists of MPC1 and MPC2 was identified as the transport complex responsible for pyruvate translocation in humans, yeast, and other eukaryotic organisms. In *P. falciparum,* two *mpc* genes, *mpc1* (PF3D7_1340800) and *mpc2* (PF3D7_1470400) are putatively annotated but have not yet been characterised.

Here, we aimed to develop both chemical and genetic mechanisms to characterise the function of the putative MPCs within *P. falciparum* parasites. A known MPC inhibitor, UK-5099, was used to chemically investigate the asexual parasite and gametocytes' physiological response to the inhibition of these putative MPCs. Additionally, this study developed three approaches to genetically interrogate MPC function in transgenic *P. falciparum* lines. In the first instance, genetic disruption and conditional knockdown of these *mpc* genes were investigated. Low native promoter activity complicated the production of pure integrant lines for these systems. Therefore, an alternative system was investigated in which the two *mpc* genes would be ectopically expressed under a constitutive promoter to produce a functional MPC heterocomplex for later investigations of the importance of this transporter to parasite development. In the future, a greater catalogue of MPC inhibitors should be screened alongside the characterisation of the ectopic *mpc* expression line to characterise the MPC heterocomplex to expand our understanding of how the overexpressed MPC heterocomplex phenotype affects parasite biology and the response to MPC inhibitors.

# 1. Literature review

## 1.1 Malaria: the disease burden

Globally, malaria is a major public health concern, impacting the socioeconomic development of malaria-endemic countries. In 2020, 241 million malaria cases were reported, of which 627 000 resulted in death, with cases in the African region of the World Health Organization (WHO) accounting disproportionately for 95 % of this burden (Figure 1.1) [1]. Most malaria-endemic countries are impoverished with limited access to healthcare and malaria intervention aids, hindering their progress toward a malaria-free status [2]. Additionally, the COVID-19 pandemic has hampered progress from 2019 to 2020, with increases of 6 and 12 % in reported malaria cases and deaths, respectively [1].

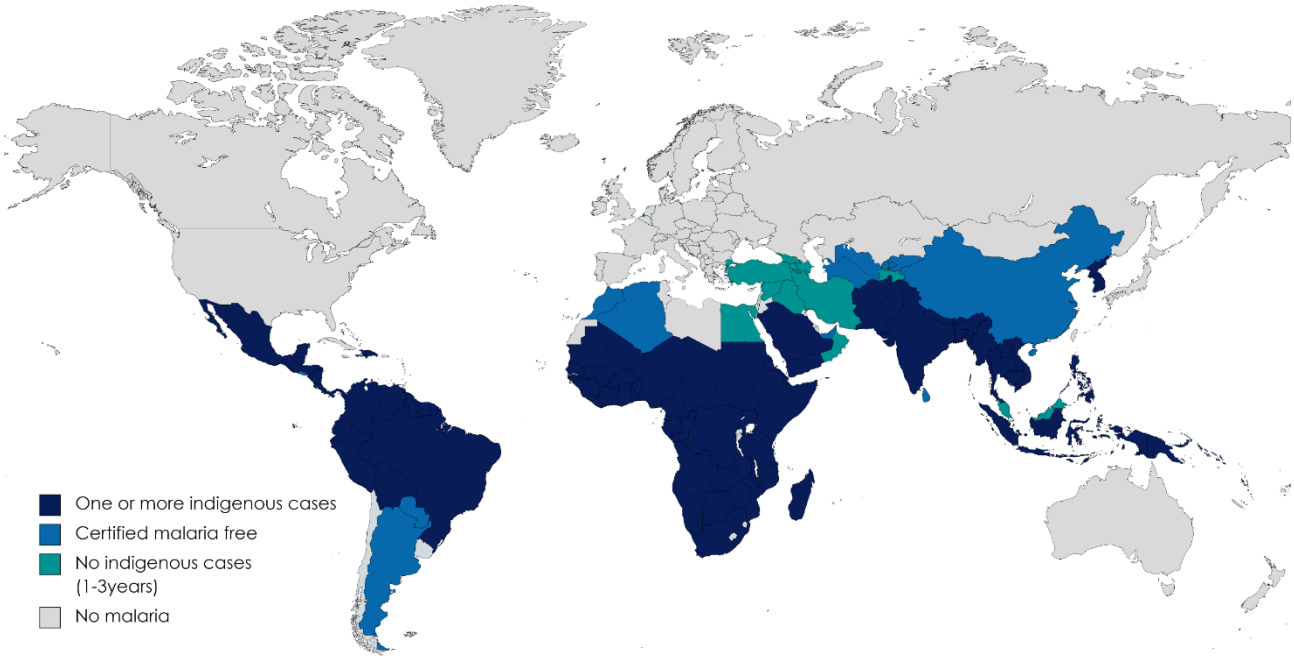


**Figure 1.1: Global distribution of malaria infection in 2020.** Malaria infection predominantly occurs in Africa, Asia, and South America (indicated in dark blue), with the African region reporting the most indigenous cases annually. Image adapted from the WHO Malaria Report 2021 and produced in MapChart (URL: https//:mapchart.net/).

Malaria is caused by a unicellular protist in the genus *Plasmodium* [3]. Currently, there are six species of *Plasmodium* that infect humans with varying severity, namely: *Plasmodium falciparum, Plasmodium malariae, Plasmodium ovale curtisi, Plasmodium ovale wallikeri, Plasmodium vivax* and *Plasmodium knowlesi* [4, 5]. Infection in Africa is predominantly caused by *P. falciparum*, the most virulent and lethal of these pathogens, while in Asia infection is predominantly caused by *P. vivax* [1]. Malaria infected patients commonly present with periodic fevers as well as myalgia and fatigue. In more severe cases, infection

can lead to anaemia, respiratory distress, cerebral malaria, and eventually death if untreated [6]. Young children, especially those under the age of five, and pregnant women are at the greatest risk of mortality from this disease [1]. Although malaria is considered a preventable and treatable disease, this consistent burden on malaria-endemic populations highlights the need to understand the causative agent to effectively adapt control strategies.

## 1.2 *P. falciparum* life cycle

*P. falciparum* parasites ensure survival and transmission by using the vector, a female *Anopheles* mosquito, and the human host. During a blood meal by a parasite-infected mosquito, sporozoites from mosquito saliva are deposited into host tissue to initiate infection (Figure 1.2) [3]. The injected sporozoites travel along the lymphatic system to the liver, where it invades hepatocytes, forming hepatic schizonts [3]. The hepatic schizonts, upon rupture, release merozoites into the bloodstream where the merozoite is exposed for a short time to the host immune system [7]. However, a merozoite can escape immune pressure by expressing variable forms of surface proteins [8]. Upon contact with the surface of a host erythrocyte, the apical surface of a merozoite forms weak interactions with the surface proteins and receptors on the erythrocyte to orient itself for the formation of tight junctions to initiate erythrocyte invasion [9, 10]. This causes the erythrocyte membrane to move inwards to generate a parasitophorous vacuolar membrane (PVM) enveloping the parasite. This results in a favourable environment for the parasite within the infected erythrocyte [9, 10] where the parasite is ultimately surrounded by three membranes: the erythrocyte plasma membrane (EPM), the PVM, and the parasite plasma membrane (PPM) [3].

Merozoite infection and conversion to the ring stage marks the beginning of the disease-causing intraerythrocytic development cycle (IDC), during which asexual reproduction of the parasite occurs [11]. The ring stage develops into a trophozoite, metabolising haemoglobin from the erythrocyte to obtain amino acids and convert toxic haem into haemozoin [12]. Additionally, this creates space in the erythrocyte for parasite growth and development into a schizont [7]. During schizogony, multiple asynchronous nuclear divisions occur to produce 16-32 daughter merozoites [13]. Eventually, the schizont ruptures, releasing merozoites into the bloodstream for the subsequent invasion of other erythrocytes, which physiologically manifests as a fever spike within the host [11]. This process is cyclical in nature, repeated every 48 h for *P. falciparum* and leads to the periodic fever associated with tertian malaria [6].

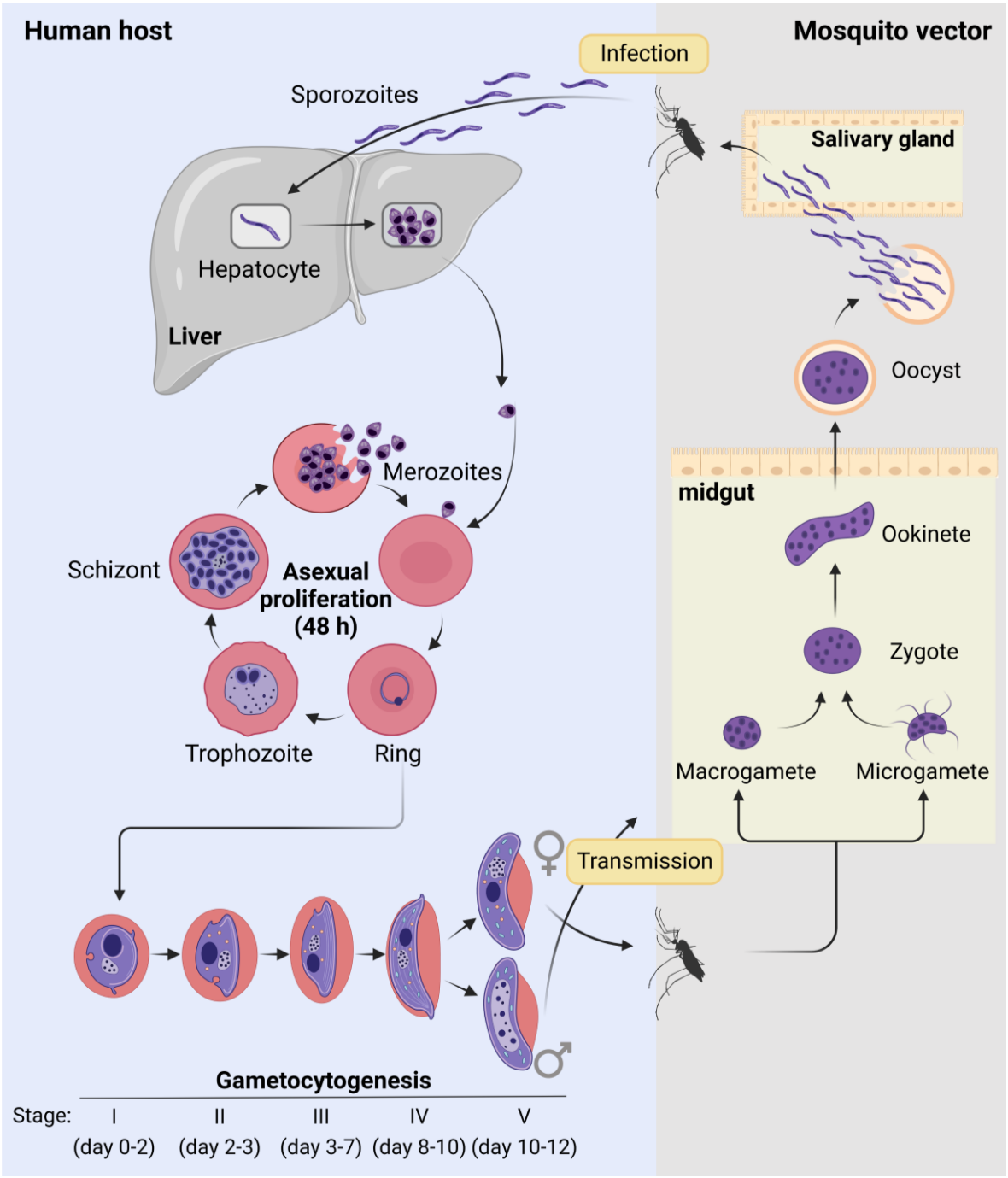


**Figure 1.2: *P. falciparum* life cycle.** *P. falciparum* infection begins during the blood meal from a parasite-infected female mosquito, during which sporozoites are deposited into the host's tissue. Sporozoites invade hepatocytes to form hepatic schizonts that rupture to release merozoites. These invade erythrocytes initiating the 48 h asexual proliferation cycle. A portion of asexual parasites will commit to sexual differentiation and undergo gametocytogenesis. Mature gametocytes are transmissible to a mosquito vector during subsequent blood meals. Once taken up by the mosquito, the male microgamete and female macrogamete fuse to form a zygote. This matures to form an ookinete that embeds in the intestinal wall, differentiating into an oocyst, where asexual sporogony occurs. These sporozoites are released and migrate to the salivary duct, to be deposited into other hosts during subsequent blood meals, reinitiating the infection cycle. Created with BioRender.com**.**

Less than 10 % of asexual parasites diverge from the proliferative cycle to differentiate into male and female gametocytes, the transmissible forms of malaria parasites [14]. In *P. falciparum*, a mature gametocyte forms over a 10-14 day period by the process known as gametocytogenesis consisting of five distinct stages (stages I-V) (Figure 1.2) [15, 16]. Stage I

gametocytes are morphologically similar to asexual trophozoites [17], whereas stage II-V gametocytes are morphologically distinct. Stage II gametocytes are short and hemispherical/lemon-like in shape [18]. As the gametocyte progresses into stage III its nucleus and mitochondria elongate due to ultrastructural alterations associated with subpellicular tubulin deposits that cause flattening of one edge of the parasite and rounding of the other to form a D shape with distortion of the erythrocyte [18, 19]. Stage IV gametocytes maximally distort the surrounding erythrocyte as the stage IV crescent and rigid form with tapered ends takes shape. Stage V gametocytes are a falciform shape with rounded ends, a distinct characteristic of *P. falciparum* [20]. Immature gametocytes, stage I-IV, sequester within the bone marrow and spleen until maturation to prevent splenic clearance [14, 21]. Mature stage V gametocytes re-enter the blood circulation through their flexible shape and migrate toward the dermal capillaries to ensure accessibility to the next feeding mosquito [22].

Sexual reproduction occurs exclusively within the mosquito [11] and is marked by the fusion of macrogametes (female) and microgametes (male) to form a zygote within the midgut of the mosquito [23]. The zygote forms an ookinete capable of transcellular migration between the endothelial cells that line the mosquito gut. The ookinete differentiates into an oocyst, which undergoes asexual nuclear division to form sporozoites. The sporozoites migrate toward the salivary glands, where these will remain until the mosquito feeds next, furthering parasite transmission [9].

## 1.3 Malaria control strategies

A multifaceted approach is used to simultaneously control the spread and decrease the severity of malaria infection, with strategies targeted at both the mosquito vector and the causative *Plasmodium* parasite. Current vector control methods involve the seasonal use of indoor residual spraying (IRS) and insecticide-treated materials such as long-lasting insecticidal nets (LLIN) in malaria-endemic areas. The use of LLIN and IRS is estimated to have averted 78 % of global cases since 2000 [24, 25]. Pyrethroids are the main insecticide class used in both strategies due to its minimal toxic effect on humans and efficacy against mosquitoes [26]. Despite the success of insecticides, resistance has emerged against all insecticidal classes, challenging the efficacy of implemented strategies [24].

Although vector control constitutes an important part of malaria control, antimalaria drugs remain important in reducing the pathogenesis caused by the asexual stage of the parasite in the human host with chemotherapeutics, preventing parasite infection with chemoprophylaxis and limiting the spread of the disease by preventing host-to-vector transmission with

transmission-blocking drugs [24]. Chemoprophylactics aim to reduce the overall incidence of malaria through the administration of protective drugs to travelling individuals and people who live in endemic areas during the seasons of greatest infection [27]. The current gold standard chemotherapeutics used in malaria-endemic regions are artemisinin-based combination therapies (ACT). ACTs combine a short half-life artemisinin or one of its derivatives with a longer lasting drug such as piperaquine or lumefantrine to significantly reduce parasite number and prevent recurrence while minimising the risk of resistance development [28]. However, ACT resistance has been reported in Southeast Asia [29] and more recently been detected in Africa [30, 31]. This resistance towards ACTs in parasite populations has major implications for malaria control efforts and highlights the urgency of developing new drugs by exploring alternative aspects of parasite biology that may be targeted with chemotherapeutics. Although chemotherapeutic drugs contribute to the treatment and survival of malaria-infected patients, these patients remain able to transmit malaria further through gametocyte reservoirs. Therefore, the development and administration of transmission-blocking drugs or dual active drugs (compounds with the ability to target the asexual and sexual parasite stages) such as primaquine are an important part of the objectives of malaria elimination strategies to prevent further transmission in endemic populations, as well as to reduce the spread of parasite resistance mechanisms [32-34].

Vaccines are being developed as an alternative protection strategy to prevent the establishment of parasite infections by inducing an immune response against pre-erythrocytic stages. Malaria vaccine development presents a major challenge due to the complexity of the parasite and its life cycle. The recombinant vaccine RTS,S/AS01$_B$ targets the circumsporozoite protein of *P. falciparum,* a sporozoite surface protein, and induces a protective immune response after three intermittent doses in young children (<18 months of age) [35]. In 2019, this vaccine was implemented in Kenya, Malawi, and Ghana to establish a real-world model surrounding efficacy, safety, and feasibility [36]. Recently, the WHO has approved the use of this vaccine despite its low efficacy (<40 % 12 months after vaccination) to mitigate malaria infection in areas of high transmission for the vulnerable child population [37, 38]. Other vaccines are also in development, including the PfSPZ live attenuated vaccine and the R21 recombinant vaccine, currently progressing through phase II and III clinical trials, respectively [39-42]. The R21/Matrix-M vaccine has recently shown promising efficacy of 70-80 % in children in a high malaria transmission setting after a 12 month booster was administered [42] and has now entered phase III clinical evaluation in a larger pool of children located in different transmission settings [42].

Although these control approaches have been responsible for the downward trend in malaria infection observed since 2000, progress began to plateau in 2015, presenting an obstacle to malaria elimination and highlighting inadequacies in current eradication strategies [1]. Inefficient policy implementation, lack of community support, and drug resistance are contributing factors to this stagnation in malaria elimination. To move closer to global malaria eradication, research is needed on new strategies. One particular avenue of research is the targetable biological processes that are essential to the *P. falciparum* parasite.

## 1.4 Membrane transport proteins

To maintain the functional complexity of a cell and inherently the cell's health and survival, the translocation of ions, nutrients, metabolites, or waste across the phospholipid membranes is required, which is mediated by integral membrane transport proteins (MTPs) [43, 44]. MTPs are commonly classified as channels, carriers, or pumps based on the mechanism of transport (Figure 1.4) [44]. Channels facilitate the rapid and selective translocation of solutes of specific charges or sizes through an aqueous passage in the channel down the solute's transmembrane concentration gradient [44, 45]. A channel can be 'non-gated', indicating that the channel is constitutively open, or 'gated', requiring a physiological signal to induce the opening of the 'gate' to expose the aqueous passageway to the solute [44]. Carriers undergo a conformational change upon substrate binding to allow substrate translocation through the membrane [46]. Carriers are designated as uniporters, symporters, or antiporters. Uniporters translocate a single substrate down its concentration gradient. Symporters and antiporters translocate a substrate and co-substrate in the same or opposite directions, respectively. These carriers use the energy stored in the concentration gradient of the co-substrate to facilitate the movement of the substrate of interest against its concentration gradient [44, 45]. ATP-powered pumps facilitate the transport of a molecule against its concentration gradient by using a primary source of energy, such as ATP hydrolysis [45]. The USA Food and Drug Administration (FDA) has approved multiple drugs for human use which target various MTPs [47-49].

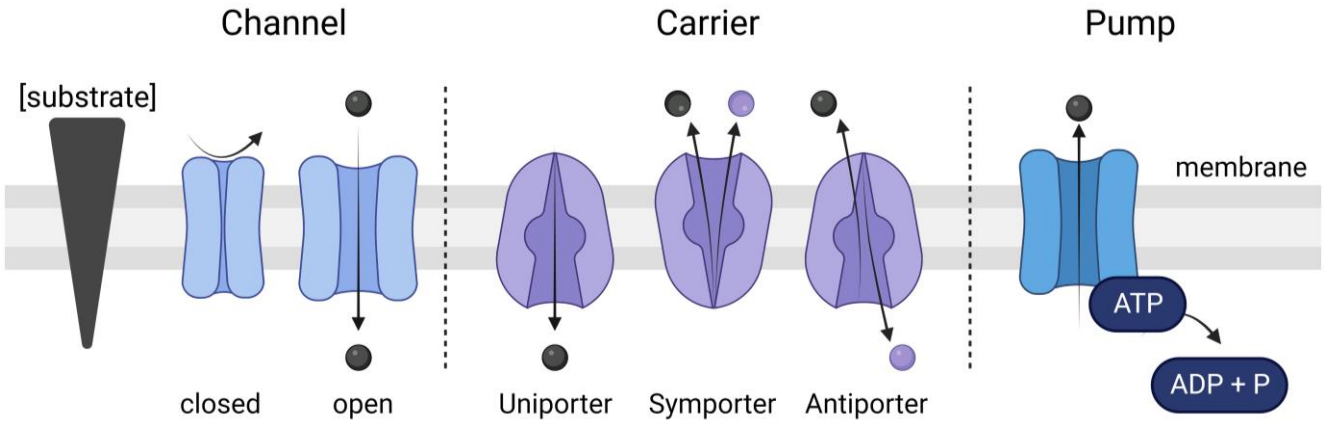


**Figure 1.3: Schematic representation of membrane transport protein classes.** MTPs facilitate the translocation of substrates across a membrane when passive diffusion is not possible. The three main classes of MTPs are channels, carriers, and pumps. Channels translocate molecules down their concentration gradient through an aqueous passage. Carriers conformationally change upon substrate binding prior to substrate translocation either with or against the substrate concentration gradient. These are classified as uniporters, symporters, or antiporters. ATP-powered pumps translocate molecules against the concentration gradient with the aid of ATP hydrolysis. The primary substrate (black circle) concentration gradient is represented by a black triangle, with the co-substrate represented by purple circles. ATP: adenosine triphosphate, ADP: adenosine diphosphate, P: inorganic phosphate.Created with BioRender.com.

Approximately 2.5 % of the *P. falciparum* genome encodes for MTPs, which is lower than the predicted MTP genome proportion in the vector, *Anopheles gambiae* (4.77 %), and the host, *Homo sapiens* (4.32 %) [50, 51], but similar in size to the transportome of other apicomplexan parasites. The reduced size of the transportome in these parasites highlights evolutionary adaptation in these organisms for streamlined nutrient acquisition [51]. Aside from nutrient transport, MTPs in these organisms are also frequent contributors to resistance mechanisms [52-54], with almost half of the *P. falciparum* MTPs forming part of its 'resistome' [52]. Polymorphisms in MTP genes aid in resistance phenotypes through direct transport of the drug away from its site of action, reducing MTP-drug interaction or compensating for the drug-mediated action via changes in MTP function. Two of the most common resistance determinants are the chloroquine resistance transporter gene (*crt*) and the multidrug resistance gene 1 (*mdr1*) [52, 55]. Both of these MTPs, located on the digestive vacuole (DV) were previously identified to confer chloroquine resistance as well as resistance towards other antimalarial drugs. Chloroquine exerts its activity by accumulating in the DV and inhibiting haem polymerisation, resulting in parasite death. However, CRT in resistant parasites exports chloroquine from the parasite DV, the drug site of action, to the cytoplasm, rendering the administered drug useless [54]. In addition to *crt* and *mdr1,* other MTPs have been linked to resistance determinants such as the acetyl-CoA transporter towards compounds such as imidazolopiperazines, the ATP-binding cassette transporter I family member towards multiple drugs, the vacuolar ATP synthase to triaminopyridines [56] and the aminophospholipid-

transporting P-ATPase (ATP2) towards the compounds MMV007224 and MMV665852 [52, 55].

MTPs may also be druggable targets with the PPM-localised sodium efflux transporter, PfATP4, a classical example. Multiple inhibitors (e.g. spiroindolones [57] or SJ733 [58]) exhibit potent nanomolar activity against the asexual stage by targeting PfATP4 [57]. This disrupts sodium homeostasis, causing osmotic fragility that leads to parasite and infected erythrocyte swelling [58, 59]. One spiroindolone, cipargamin, is a dual-active compound with asexual and transmission-blocking activity that is currently in the product development phase, emphasizing the potential of targeting MTPs in *P. falciparum* [60]. Furthermore, PfATP6, PfNCR1 (Niemann-Pick type C1-related protein), and PfNT1 (nucleoside transporter) are a few MTPs that are inhibited with atelorane [61], bafilomycin, MMV009108 an,d MMV028038 [62], respectively. Further investigations are needed into the parasite biology surrounding MTPs to identify possible druggable MTPs or MTPs that contribute to resistance mechanisms.

## 1.5 Central carbon metabolism of the intraerythrocytic *P. falciparum* parasite

Carbon metabolism is fundamental to sustaining physiological processes and, consequently, the survival of the parasite. It is characteristically composed of three central pathways (Figure 1.3); the cytosolic glycolytic pathway and two mitochondrial pathways, the tricarboxylic acid (TCA) cycle and oxidative phosphorylation, which produce ATP [63]. Although energy production is an obvious necessity, an organism's microenvironment and physiological needs will dictate which metabolic pathway is prioritised to maintain efficient cell function [64]. The metabolic framework of *P. falciparum* parasites is rearranged between the proliferative asexual stage and the transmissible gametocyte stage (Figure 1.3) [65, 66]. Both stages rely on glucose imported from the erythrocyte to fuel the respective metabolic needs [3]. Asexual parasites prioritise substrate-level phosphorylation from fermentative glycolysis to sustain this highly proliferative state, resulting in rapid ATP production. This is similar to the Warburg effect describing rapid energy metabolism in proliferating cancer cells [65, 66]. By contrast, gametocytes use a more energy-efficient production process that involves the TCA cycle and oxidative phosphorylation (Figure 1.3) [66].

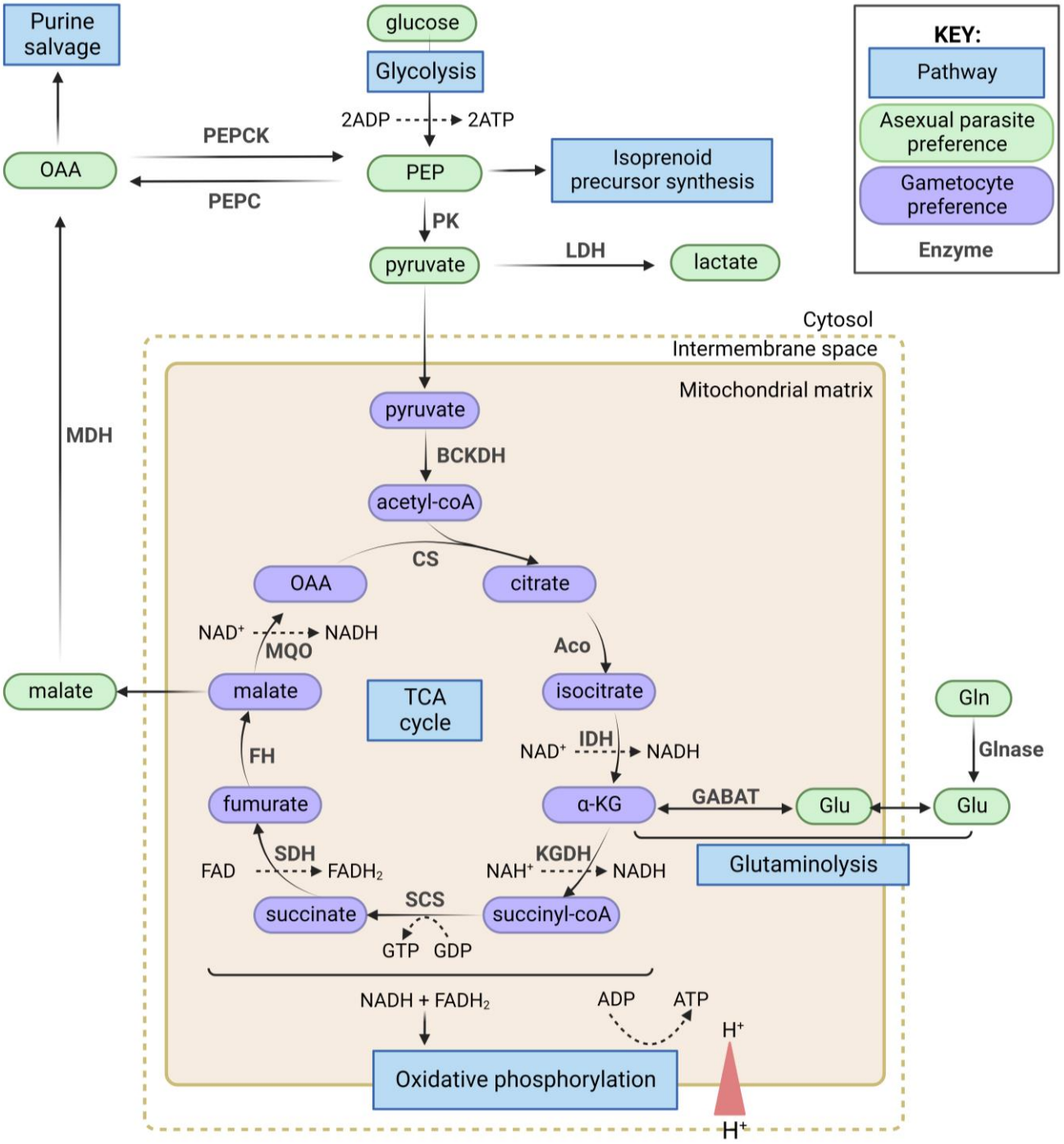


**Figure 1.4: Schematic diagram of *P. falciparum* central carbon metabolism.** Energy metabolism canonically involves glycolysis, the TCA cycle and oxidative phosphorylation. Asexual parasites rely on fermentative glycolysis as the main mechanism of energy production. The TCA cycle, predominately fuelled through glutaminolysis, is used to produce metabolites that supply alternative pathways such as purine salvage. Gametocytes rely on the canonical TCA cycle and oxidative phosphorylation to produce energy. Central carbon metabolism pathways are indicated in blue, with pathways favoured by asexual parasites indicated in green and those favoured by gametocytes indicated in purple. The proton concentration gradient is indicated by a red triangle. Abbreviations: α-KG: α-ketoglutarate, Aco: aconitase, ADP: adenosine diphosphate, ATP: adenosine triphosphate, BCKDH: branched-chain keto-acid dehydrogenase, CS: citrate synthase, FAD: flavin adenine dinucleotide, FH: fumarate hydratase, GABAT: GABA transaminase, GDP: guanosine diphosphate, Gln: glutamine, Glnase: glutaminase, Glu: glutamate, GTP: guanosine triphosphate, $H^+$: protons, IDH: isocitrate dehydrogenase**,** KGDH: α-ketoglutarate dehydrogenase, LDH: lactate dehydrogenase, MQO: malate-quinone oxidoreductase, $NAD^+$: nicotinamide adenine dinucleotide, OAA: oxaloacetate, PEP: phosphoenolpyruvate, PEPC: PEP carboxylase, PEPCK: PEP carboxykinase, PK: pyruvate kinase, SCS: succinyl-CoA synthetase, SDH: succinate dehydrogenase. Created with Biorender.com

Pyruvate is involved at a crucial branchpoint in carbon metabolism, and thus the prioritised pathway dictates the fate of pyruvate. In asexual parasites, due to the prioritised glycolytic pathway, pyruvate is primarily converted into lactate of which 93 % is exported [65]. However, glucose-derived phosphoenolpyruvate (PEP) feeds into mitochondrial metabolism contributing to the minor flux of the TCA cycle by producing malate [67-69]. Glutaminolysis, an anaplerotic pathway, contributes to the major flux of the TCA cycle by producing α-ketoglutarate, a metabolite able to enter the TCA, from glutamine (Figure 1.3) [65, 67]. Although mitochondrial metabolism is active in asexual parasites, its primary function is to produce intermediate metabolites for purine salvage, pyrimidine biosynthesis, redox balance and other biochemical pathways, instead of energy production [69, 70].

Central carbon metabolism shifts from glycolytic dependence in asexual parasites to TCA cycle and oxidative phosphorylation dependence during gametocytogenesis, most notably during stage III gametocyte formation (Figure 1.4) [65]. This allows the gametocyte to have a long-lasting lifespan as a result of the slower metabolism [71]. Additionally, this is evident in increased levels of transcripts for TCA cycle enzymes during gametocytogenesis [72, 73]. The genetic disruption of proteins involved in the TCA cycle caused gametocyte progression to halt [68, 74]. This highlights the importance of these TCA cycle proteins in gametocytes. In comparison to asexual parasites, the slow-maturing gametocyte contains a larger mitochondrion with greater cristae formation than its asexual counterpart to support this increased mitochondrial metabolism that leads to slow but efficient ATP production [75]. In gametocytes, the major metabolic flux through the TCA cycle is driven by the glycolytic end-product pyruvate, which is converted to acetyl-CoA by the mitochondrial-based branched-chain ketoacid dehydrogenase (BCKDH) [65, 67, 76]. BCKDH functions similarly to pyruvate dehydrogenase (PDH), which converts pyruvate to acetyl-CoA in eukaryotes. However, in apicomplexans, such as *P. falciparum*, PDH is solely found in the apicoplast [76].

To maintain the major and minor metabolic flux of the parasite, metabolite translocation, such as glucose, glutamine, or pyruvate, is important and possible with MTPs [77]. For instance, glucose, an important carbon source, is imported into the parasite cytoplasm from the erythrocyte via a hexose transporter located in the PPM [78]. Lactate, the end-product of glycolysis, is exported from the parasite through the PPM localised monocarboxylate transporter or the fumarate-lactate transporter [74, 79, 80]. Cytosolic pyruvate fuels the mitochondrial TCA cycle, particularly during gametocytogenesis [65]. However, the mechanism of pyruvate translocation is unknown in *P. falciparum* parasites, but it is speculated that an MTP, known as a mitochondrial pyruvate carrier, is responsible for this translocation.

## 1.6 Mitochondrial pyruvate carriers

Pyruvate is required to translocate from the cytosol into the mitochondrial matrix, crossing the outer and inner mitochondrial membranes (OMM and IMM). Pyruvate migrates across the OMM into the mitochondrial intermembrane space through non-selective voltage-dependent channels [81]. However, a specific transporter is required to transport the charged pyruvate molecule across the highly restrictive IMM [82, 83].

The mitochondrial pyruvate carrier (MPC) is a proton symporter that facilitates pyruvate translocation across the IMM into the mitochondrial matrix, against the proton concentration gradient and forms a critical link between glycolysis and the TCA cycle energy metabolic pathways. This 150 kDa heterocomplex consists of two small subunits, MPC1 (12 kDa) and MPC2 (15 kDa), located within the IMM [84, 85]. MPC1 and MPC2 proteins are highly conserved between humans, yeast, and other eukaryotic organisms. Although the structure of this MPC heterocomplex is unsolved, it appears to act as a functional heterodimer [84-86], as the genetic deletion of either MPC subunit resulted in complex destabilisation and degradation [87, 88]. MPC1 and MPC2 loss-of-function gene deletions in flies, humans, mice, yeast as well as the apicomplexan parasites *Trypanosoma brucei* and *Trypanosoma cruzi* results in pyruvate accumulation in the cytosol and impaired pyruvate-driven respiration [84, 85, 89-91]. However, whether this phenotype is detrimental to the organism is dependent on the preferred means of energy production by the organism. In *T. brucei* and *T. cruzi,* MPC1 and MPC2 are classified as essential MTPs for stages where pyruvate-driven respiration is important but dispensable in the stages reliant on aerobic fermentative glycolysis [90, 91]. In humans, abnormal MPC functioning has been implicated in many diseases such as inborne metabolic errors, hyperthyroidism, diabetes, neurodegenerative diseases, and cancer [92-94]. The Warburg effect has been associated with a complete or complete loss of MPC function in most cancers with poor MPC expression correlated with a poor tumour prognosis [98].

In addition to the genetic investigations of the MPC heterocomplex subunits, chemical perturbation is a complementary method of probing MPC heterocomplex function [84, 85, 89, 90, 95]. The two main classes of MPC inhibitors are the highly specific α-cyanocinnamate and the non-selective thiazolidinediones [96, 97]. The α-Cyano-4-hydroxycinnamate (CHC) and other cinnamate derivatives are analogues of the pyruvate enol form with an additional hydrophobic aromatic ring [98]. CHC and α-cyano-β-(1-phenylindol-3-yl)-acrylate (UK-5099) are mitochondrial pyruvate transporter inhibitors with nanomolar activity against isolated mitochondria [85, 99].

Two putative MPC proteins (MPC1 (PF3D7_1340800) and MPC2 (PF3D7_1470400)) have been identified in the *P. falciparum* genome [74, 99], based on sequence similarity to yeast and human MPCs. To date, there is limited research on these MPCs in *P. falciparum*, with a single article reporting the genetic manipulation of these putative genes in asexual parasites. A largescale mutagenesis project involving the random insertion of *piggyBac* transposons at tetranucleotide sequence was able to produce a loss-of-function and survival phenotype for genes that are essential to parasite survival [100]. The *mpc1* gene was found to be refractory to genetic manipulation, however, this result was tentatively labelled as *mpc1* is a small gene which could be misrepresented with this data, whilst *mpc2* was deemed dispensable [100]. Both genes were expected to be dispensable to the asexual stages because of the proven lack of importance mitochondrial pyruvate transport has on central carbon metabolism during proliferation [65, 66, 69]. Further investigation into the biological importance of MPC in *P. falciparum* at the different intraerythrocytic stages and validation of this whole-genome study is required. These studies would include alternative genetic manipulation tools alongside chemical validation with known MPC inhibitors.

## 1.7 *P. falciparum* genetic editing techniques

Genetic editing techniques are useful to elucidate antimalarial resistance genes, drug modes of action, individual gene importance and function as well as to validate genome-wide studies [101]. The genetic editing techniques discussed here are transfection-based and rely on the allelic exchange of the “foreign” introduced DNA with the parasite’s genome at a homology-based region. Various gene manipulation systems can modify at the DNA, RNA, or protein level (Table 1.1).

On the DNA level, the gene of interest (GOI) could be irreversibly disrupted through the traditional homologous-recombination system where the GOI is exchanged with a truncated version to produce a non-functional protein [102]. Alternatively, a CRISPR-Cas mediated system could introduce point mutations in the GOI to render it non-functional upon translation [103]. In the event the GOI is essential to parasite survival, the disruption will reduce parasite fitness and no integrants will be obtained. The latter is a downfall of genetic disruption systems since it prevents any functional evaluation of the gene’s role in parasite biology. Another DNA-level modification tool involves the irreversible knockout of the GOI at the naive loci with the inducible dimerisable Cre recombinase system, whereby the Cre recombinase excises a GOI that is flanked by loxP sites (recombinase recognition sites) [104]. Although the advantage of

this system is complete knockout that can be induced at any parasite stage, previous conditional knockouts have reported only an 80 % excision in parasite populations [105].

**Table 1.1: The advantages and disadvantages of genetic editing strategies used in *P. falciparum.*** Information compiled from [102-112].

| Level of editing | System | Advantages | Disadvantages |
|---|---|---|---|
| DNA | Gene disruption (homologous recombination approach) | • Investigates gene at native loci<br>• Determines which genes are essential and dispensable | • Non-inducible system<br>• Cannot retrieve integrant lines for essential genes |
| | Gene disruption (CRISPR/Cas) | • Investigates gene at native loci<br>• Introduces point mutations<br>• Determines which genes are essential and dispensable | • Non-inducible system<br>• Cannot retrieve integrant lines for essential genes |
| | Conditional gene deletion (Cre system) | • Investigates gene at native loci<br>• Inducible system<br>• Rapid system with minimal leakage<br>• Complete deletion of gene function if the gene is excised | • Irreversible system<br>• Dual plasmid transfection<br>• Cannot be used for large genes > 5Kb<br>• Gene excision does not occur in all parasites<br>• Requires a parental line expressing DiCre |
| | Bxb1 ectopic expression | • Investigates gene at an alternative locus<br>• Rapid site-specific GOI insertion into the genome<br>• Minimal copy number variation with drug pressure<br>• Multiple genes can be linked under a single or multiple promoters<br>• Increases expression of GOI | • GOI operates under a different promoter (no native locus investigation)<br>• Requires a parental line with the *attB* region<br>• Dual plasmid transfection |
| RNA | *glmS* ribozyme | • Investigates genes at native or alternative loci<br>• Conditional, reversible system<br>• Gene can be tagged for identification | • The inducer, glucosamine, is cytotoxic and lowers the growth mediums pH<br>• Knockdown is inefficient (50-90 %) |
| Protein | Destabilisation domain | • Rapid and reversible system | • Not possible on secreted proteins<br>• Proteins may have an inability to tolerate the DD tag<br>• Knockdown is inefficient (60-80 %)<br>• Shield1 ligand may be toxic |
| | Knock sideways | • Reversible system<br>• Rapid protein displacement | • Not possible on membrane proteins<br>• Requires a parental line with a localizer |

All of the above systems genetically manipulate the GOI at its native loci where it is expressed under its native promoter. This provides insight into the phenotype of reduced production of functional protein. As an alternative strategy, the Bxb1 ectopic expression system allows a GOI to be inserted into an alternative locus under a more active promoter to express the GOI above basal levels (Table 1.1). This is useful for a GOI expressed under a weak promoter that does not respond well to positive selection during transgenic line generation. This system uses the mycobacteriophage Bxb1 integrase to catalyse homology-specific recombination between the GOI-containing plasmid and a dispensable *cg6* gene in the *P. falciparum* genome to integrate the coding sequence of the GOI in a rapid manner [108].

To genetically modify the mRNA levels of a GOI, a *glmS* ribozyme system is used to conditional knockdown the GOI. The *glmS* ribozyme system incorporates a ribozyme (a catalysing RNA molecule) on the 3' end of a GOI. The *glmS* ribozyme is activated when glucosamine is added to the cell causing the transcribed mRNA of the GOI to self-cleave, preventing downstream protein expression [107]. The downfalls of this system are cytotoxicity and acidity of glucosamine [109] as well as the inefficiency in the knockdown of the GOI [110] (Table 1.1). However, the *glmS* ribozyme system is still used as a genetic editing tool for *P. falciparum* parasites due to its inducible nature.

For a post-translational effect on protein levels, the destabilisation domain (DD) system can be used in a reversible manner to prematurely degrade a protein of interest, in the absence of the stabilising ligand Shield-1, by adding an FK506-binding protein (FKBP)-based DD to the protein [113]. The DD is unstable and promotes the degradation of the protein, however, protein degradation is preventable through Shield-1 binding to the DD [106, 112]. This system can knock down <80 % of the protein of interest (Table 1.1) [111]. However, the downfalls of this system are that proteins synthesised via the secretory pathway cannot be DD tagged, proteins may lose their functionality from the DD tag, or the degradation may not produce a noticeable phenotype [112]. As an alternative to degradation, proteins can be post-translationally mislocalised (knocked sideways) to move the protein of interest from its native site of action (i.e. the nucleus) to another (i.e. the cytosol) [102]. This system relies on dimerisation between the target fused to FKBP and FKBP rapamycin binding (FRB) fused to a signal that mediates protein movement to a different cellular location when rapamycin or an analogue is introduced, directing the fused protein away from the native site of action [102]. However, the system does not work on MTPs as they may mislocalise to another cellular location such as the cytoplasm (Table 1.1). Although there are many choices for genetic editing tools, the best tool is dependent on the aim and gene/protein of interest of the study.

In addition to selecting the most optimal genetic editing tool, there are ways to improve the efficiency of generating transgenic lines. A selection-linked integration (SLI) system was developed as a more efficient approach to generate transgenic parasite lines because of its dual-selection process. In the first instance, the human dihydrofolate reductase gene (hDHFR) is expressed on the plasmid that can be selected for if it is episomally present by addition of the antifolate compound, WR99210. Secondly, homologous recombination mediated genomic integration would result in the presence of a neomycin resistance gene (neo-R), which is expressed under the integration site promotor [102]. This results in the selection of integrants by addition of a neomycin-derivative, G418. The Neo-R gene is separated from the GOI by a

skip peptide (T2A) that allows di-cistronic translation of the single mRNA into separate proteins [102].

This study aims to initiate investigations into the biological importance of the putative *mpc1* (PF3D7_1340800) and *mpc2* (PF3D7_1470400) genes in *P. falciparum* parasites. A two-pronged approach involving chemical perturbation of parasites with a known MPC inhibitor and the genetic manipulation of *mpc* genes was attempted to establish systems to interrogate MPC biology in the parasite. The genetic manipulation approaches used are the SLI-TGD based genetic disruption and a conditional knockdown approach with SLI-*glmS* to study the essentiality of MPC at basal levels. Additionally, to evaluate biology upon increased MPC expression, the BXB2 ectopic expression system was established.

# Aim

To determine the function and essentiality of putative mitochondrial pyruvate carriers in *P. falciparum* parasites

# Hypothesis

The putative mitochondrial pyruvate carriers are biologically important to the transmissible, gametocyte stage of the parasite.

# Objectives

a) Determine the effect a known MPC inhibitor has on parasite proliferation and differentiation
b) Generate a targeted *mpc1* and *mpc2* gene disruption parasite line
c) Generate a conditional *mpc1* and *mpc2* knockdown line
d) Ectopically express the *mpc* genes with a generated *mpc* ectopic expression transgenic line

**Research outputs:**

da Rocha, S., Mugo, E., Birkholtz, LM., Niemand, J. The functional evaluation of putative mitochondrial pyruvate carriers in *Plasmodium falciparum* parasites. *6th South African Malaria Research Conference.* Oral presentation. Pretoria. August 2021

da Rocha, S., Birkholtz, LM., Niemand, J. The biological interrogation of *Plasmodium falciparum's* putative mitochondrial pyruvate carriers. *South African Society of Biochemistry and Molecular Biology.* Oral presentation. Pretoria. January 2022

da Rocha, S., Mugo, E., Birkholtz, LM., Niemand, J. Towards overexpression of the putative mitochondrial pyruvate carrier in *Plasmodium* falciparum parasites. *7th South African Malaria Research Conference.* Poster presentation. Pretoria. August 2022

# 2. Materials and Methods

## 2.1 *In silico* analyses of putative MPCs

Two putative *P. falciparum mpc* genes, *mpc1* (PF3D7_1340800) and *mpc2* (PF3D7_1470400), were analysed with *in silico* tools to confirm existing annotations and identify structural characteristics. The *P. falciparum* amino acid sequences of MPC1 and MPC2, obtained from the *Plasmodium* database (PlasmoDB: https://plasmodb.org/plasmo/app), were used in the NCBI Protein Basic Local Alignment Search (BLASTP: https://blast.ncbi.nlm.nih.gov/Blast.cgi?PAGE=Proteins) tool to identify MPC homologs. Amino acid sequences of MPC1 and MPC2 proteins from different organisms used were obtained from the UniProt consortium database (https://www.uniprot.org/) (Table 2.1) [114]. To evaluate the evolutionary relationship between the MPC proteins of different organisms, these sequences were used in the Molecular Evolutionary Genetics Analysis (MEGA) software version 11.0.10 (USA) to perform a MUSCLE multiple sequence alignment (MSA) (default parameters) between the MPC orthologues. A maximum likelihood phylogeny tree was generated from these MSA data using the Bootstrap phylogeny test (500 replicates) according to the following parameters: LG substitution model, gamma distributed rate with invariant sites (G+I) with an estimated 4 gamma categories and the Nearest-Neighbour-Interchange tree interface [90, 115, 116].

**Table 2.1: UniProt accession codes for MPC1 and MPC2 amino acid sequences for various organisms.**

| Organism | Accession codes | |
|---|---|---|
| | MPC1 | MPC2 |
| *Arabidopsis thaliana* | Q949R9 | Q8L7H8 |
| *Drosophila melanogaster* | Q7KSC4 | Q9VHB1 |
| *H. sapiens* | Q9Y5U8 | O95563 |
| *Leishmania braziliensis* | A4H359 | A4H7W6 |
| *Mus musculus* | P63030 | Q9D023 |
| *Plasmodium berghei* | A0A0Y9ZKK1 | A0A0Y9ZX96 |
| *Saccharomyces cerevisiae* | P53157 | P38857 |
| *T. brucei* | Q38FF5 | Q57WG7 |
| *T. cruzi* | A0A2V2VGT4 | A0A2V2V3R9 |

Additionally, the MPC1 and MPC2 amino acid sequences were used in a MUSCLE MSA (default parameters) performed in MEGA with known MPC homologs from *S. cerevisiae, H. sapiens* and *D. melanogaster* to identify common sequence regions. The MSA was edited with BioEdit sequence alignment editor version 7.2.5 [117]. Membrane topology of MPC1 and MPC2 was investigated with deepTMHMM (https://dtu.biolib.com/DeepTMHMM/) [118],

PHOBIUS data from InterPro (https://www.ebi.ac.uk/interpro/) [119] and TOPCONS (https://topcons.cbr.su.se/) [120]. The Uniprot, Pfam and InterProFamily information from InterPro was used to identify which protein family MPC1 and MPC2 are classified under. MitoProt (https://ihg.helmholtz-muenchen.de/ihg/mitoprot.html) was used to predict the proteins' subcellular location [121].

## 2.2 *In vitro P. falciparum* parasite cultivation

### 2.2.1 Ethical clearance statement

All experiments requiring the use of *P. falciparum* parasites were performed in the Malaria Parasite Molecular Laboratory ($M^2PL$), a certified biosafety level 2 (BSL2) facility (registration number: 39.2/University of Pretoria-19/160). *In vitro* parasite cultivation is covered by an umbrella ethical clearance for the SARChI program provided to Professor Birkholtz (reference: 180000094) by the Faculty of Natural and Agricultural Science. The use of human erythrocytes is approved by the Research Ethics Committee, Health Sciences Faculty (reference: 506/2018) by the Faculty of Health Science to Professor Birkholtz.

### 2.2.2 *In vitro* asexual parasite cultivation

A drug-sensitive strain of *P. falciparum* parasites, NF54 (MRA-1000, BEI resources) was cultivated in human erythrocytes at 5 % haematocrit and maintained in a hypoxic environment consisting of 90 % $N_2$, 5 % $CO_2$ and 5 % $O_2$ (Afrox, South Africa) in complete culture medium [RPMI-1640 culture medium (Sigma-Aldrich, USA), supplemented with 25 mM HEPES pH 7.5 (Sigma-Aldrich, USA), 23.81 mM sodium bicarbonate (Sigma-Aldrich, USA), 200 µM hypoxanthine (Sigma-Aldrich, USA), an additional 0.2 % (w/v) glucose (Merck, Germany), 0.024 mg/mL gentamycin (HyClone, USA) and completed with 5 g/L Albumax II (Life technologies, USA)]. To ensure maximal merozoite invasion of erythrocytes, the parasite cultures were incubated at 37 °C on a rotary platform at 60 rpm [122]. Parasitaemia (the percentage of parasite-infected erythrocytes) and parasite morphology was determined by staining methanol fixed, thin smears of parasite samples with RapiDiff stain and visualised using oil immersion at 1000x magnification with light microscopy using a YS2-H Nikon microscope (Nikon, Japan). Parasite images were taken with a Nikon Eclipse 50i microscope with Nikon Digital sight (Nikon, Japan) and analysed on NIS-Elements software F package version 3.0 (Nikon, Japan).

### 2.2.3 Sorbitol synchronisation of asexual *P. falciparum* parasites

Intraerythrocytic *P. falciparum* parasite cultures consisting predominately of ring stages with a parasitaemia >2 %, were synchronised using isosmotic 5% (w/v) D-sorbitol solution (Sigma-Aldrich, USA). Sorbitol selectively lyses trophozoite- and schizont-stage parasites due to the increased permeability of these stages due to the formation of new permeability pathways [123]. Parasite cultures were incubated in pre-warmed sorbitol for 15 min at 37 °C followed by centrifugation for 5 min at 1800 x*g*. Following this, parasite cultures were washed twice with incomplete culture medium [RPMI-1640 culture medium (Sigma-Aldrich, USA), supplemented with 25 mM HEPES pH 7.5 (Sigma-Aldrich, USA), 23.81 mM sodium bicarbonate (Sigma-Aldrich, USA), 200 μM hypoxanthine (Sigma-Aldrich, USA), an additional 0.2 % (w/v) glucose (Merck, Germany), 0.024 mg/mL gentamycin (HyClone, USA)] to remove the residual sorbitol and lysed parasite debris. Thereafter, the washed parasite pellet was reconstituted to a 5 % haematocrit culture in complete culture medium and maintained as described in section 2.2.2.

### 2.2.4 *In vitro P. falciparum* early gametocyte cultivation

Gametocytes were produced from *P. falciparum* NF54 parasites by exposing parasites to two environmental stress factors, namely: haematocrit reduction and nutrient starvation [124]. Gametocytogenesis was initiated from synchronised asexual parasites (>90 % ring population) by adjusting the culture to a 0.5 % parasitaemia at a 6 % haematocrit in gametocyte medium (complete culture medium without the additional 0.2 % glucose). The culture was maintained in a hypoxic environment at 37 °C without agitation. After 72 h (designated as day 0), the parasite culture's haematocrit was reduced to 4 % in gametocyte medium and incubated as before. From day 1-4, the culture was maintained in complete culture medium supplemented with 50 mM N-acetyl glucosamine (NAG), which prevents erythrocyte invasion by merozoites to halt further asexual parasite proliferation [125]. This ensures the production of a homogenous gametocyte population. Gametocytes were monitored daily with RapiDiff-stained samples using light microscopy and images were taken as stated in section 2.2.2. On Day 5, the predominately stage III gametocyte culture was harvested for experiments requiring early stage gametocytes.

## 2.3 Evaluating asexual proliferation using a SYBR Green I fluorescence assay

The anti-plasmodial activity of the known MPC inhibitor, UK-5099 (MedChemExpress, USA), was determined using a SYBR Green I fluorescence-based assay. The fluorophore, SYBR Green I, intercalates into the minor grove of double-stranded DNA (dsDNA), whereupon its

fluorescent intensity increases. Therefore, the emitted fluorescence is used as a measure of relative nucleic acid levels and consequently of parasite proliferation. This fluorophore specifically detects parasite dsDNA as erythrocytes do not contain nuclear material [126].

To characterise the activity of UK-5099, a 2-fold serial dilution was created in complete culture medium in technical triplicates in 96-well plates. Chloroquine (0.5 µM) was used as a background control with 2.5 % (v/v) dimethyl sulfoxide (DMSO) as a vehicle control and untreated parasites as the live parasite control. To each well, a 1:1 ratio of synchronised asexual parasite culture (>95 % ring population) at 1 % parasitaemia was added to the drug solution, with a final haematocrit of 1 %. Assay plates were incubated in a hypoxic environment in a stationary incubator at 37 °C for 96 h. After incubation, a 1:1 ratio of sample to SYBR Green I lysis buffer (20 mM Tris, pH 7.5; 5 mM EDTA; 0.008 % (w/v) saponin and 0.08 % (v/v) Triton X-100) supplemented with 0.002 % SYBR Green I (Invitrogen, USA) was incubated for 1 h at room temperature in a 96-well plate. Fluorescent intensity was determined with the Fluoroskan Ascent FL microplate reader (Thermo Scientific, USA; excitation at 490 nm and emission at 520 nm). The background control was subtracted from the data and the data normalised to the viable parasite population. Data from three independent experiments, each performed in technical triplicate were analysed using Microsoft Excel and graphically represented using GraphPad Prism 9 (GraphPad Software, USA) with the standard-error-of-the-mean (S.E.) indicated. Statistical significance was determined using the unpaired students T-test with the online software from GraphPad by Dotmatics (GraphPad, USA) (https://www.graphpad.com/quickcalcs/ttest1.cfm).

## 2.4 Evaluating gametocyte viability using the lactate dehydrogenase assay

To investigate the gametocytocidal activity of a compound, the viability of maturing gametocyte populations was measured via parasite lactate dehydrogenase (pLDH) activity as this reflects the active glycolytic state of a gametocyte. In the presence of the cofactor 3-acetylpyridine adenine dinucleotide (APAD), an analogue of NAD, pLDH will enzymatically convert lactate into pyruvate at a higher efficiency compared to the human LDH. During this conversion, APAD is reduced to APADH. Concurrently, nitroblue tetrazolium chloride (NBT) is reduced to form a blue formazan product that is spectrophotometrically detectable [127, 128].

A gametocyte suspension (1.5 % gametocytaemia, > 75% stage II gametocyte population at 1 % haematocrit) was added to a 2-fold serial dilution series of UK-5099 in technical triplicates in a 96-well plate, with equivalent DMSO concentrations included as a vehicle control and 5 µM methylene blue as a positive inhibition control. A 1 % haematocrit erythrocyte suspension

was co-cultured to serve as the background LDH control. Samples were statically incubated at 37 °C for 72 h in a hypoxic environment. After 72 h, 80 % of the medium per sample was aspirated and replaced with complete culture medium and incubated for a further 72 h. After the total 144 h incubation period, 20 µL of each sample was resuspended in 100 µL of Malstat reagent (54.5 mM Tris, pH 9.0; 0.166 mM APAD; 222 mM lithium lactate and 0.2 % v/v Triton X-100), followed by the addition of 25 µL of NBT/PES solution (1.96 mM NBT; 0.239 mM phenazine ethosulphate) and incubated for 20-60 min at room temperature Absorbance was spectrophotometrically determined at 620 nm using a Paradigm plate reader (Molecular Devices, USA). The background LDH control was subtracted from each datapoint and normalised to the methylene blue-treated positive inhibition control and averaged for three independent experiments performed in technical triplicate. Data analysis was performed using Microsoft Excel and data were graphically represented using a grouped bar-graph with GraphPad Prism 6 (GraphPad Software, USA) with the standard-error-of-the-mean (S.E.) indicated. Statistical significance was determined using the unpaired students T-test with the online software from GraphPad by Dotmatics (GraphPad, USA) (https://www.graphpad.com/quickcalcs/ttest1.cfm).

## 2.5 Generation of SLI-TGD and SLI-*glmS* transgenic parasite lines

The biological importance and function of putative *mpc1* (PF3D7_1340800) and *mpc2* (PF3D7_1470400) genes in *P. falciparum* were investigated with two SLI-based genetic disruption and conditional knockdown systems (Figure 2.1). These systems contain similar features in the SLI plasmid backbone including a 3' green fluorescent protein (GFP) tag intended for localisation studies, two transgenic parasite selection features (a human dihydrofolate reductase gene (hDHFR) and a neomycin resistance gene (neo-R)), as well as restriction enzyme cut sites, *NotI* (5' GCGGCCGC 3') and *MluI* (5' ACGCGT 3'), flanking the 5' and 3' regions of the gene of interest, respectively (GOI) (Figure 2.1).

The SLI-TGD system incorporates a shortened 5' fragment of the GOI into the plasmid to genetically disrupt the GOI by producing a non-functional protein after genomic integration [102]. The SLI-*glmS* system requires a 3' fragment to be cloned into the plasmid containing either a *glms* or *glms-mutant* ribozyme gene. This is to ensure a functional protein is produced upon integration. Subsequently, the GOI expression can be knocked down with glucosamine when a functional *glmS* ribozyme is present. The mutant *glmS* ribozyme functions as a conditional knockdown control that cannot induce self-cleavage in the presence of glucosamine [107].

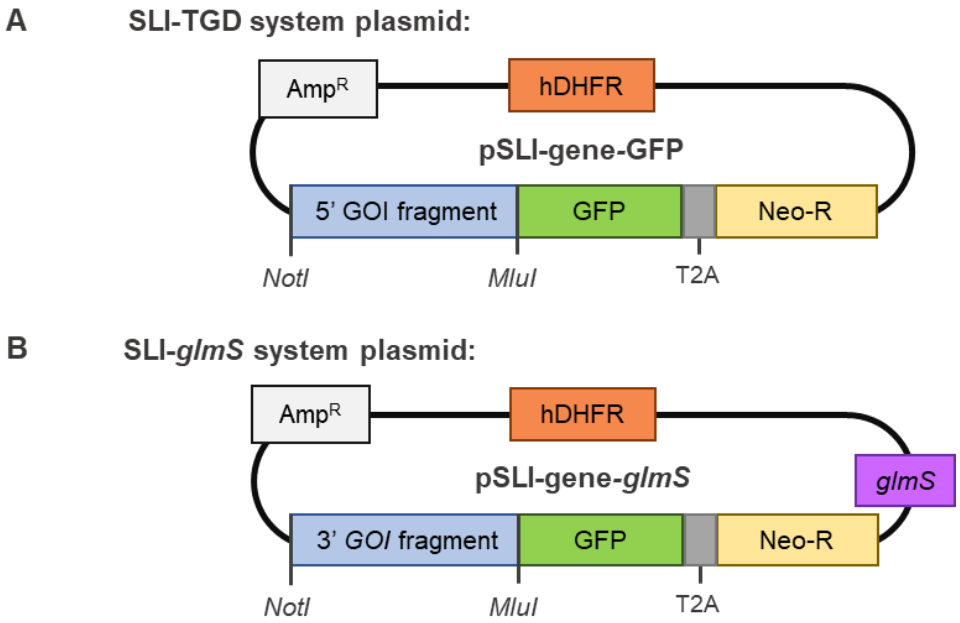


**Figure 2.1: Plasmid representation of the SLI-based systems.** SLI-based systems use a plasmid backbone consisting of an ampicillin resistant ($Amp^R$) gene to aid in bacterial cloning and hDHFR gene necessary for episomal plasmid selection within the parasite. The GOI fragment is cloned into a cassette flanked by the 5' and 3' located restriction cut sites: *NotI* and *MluI* respectively. Additionally, the cassette consists of a 3' located GFP tag to localise the GOI, a T2A skip peptide ensuring the protein produced from the GOI is not linked to the remainder of the cassette and a Neo-R gene used to select for transgenic parasites that integrate the GOI fragment. The genetic disruption **(A)** SLI-TGD system incorporates a short 5' GOI homology region to produce a non-function truncated protein upon integration. The conditional knockdown **(B)** SLI-*glmS* system includes a *glmS* riboswitch gene that can be activated with glucosamine to induce self mRNA cleavage as well as a 3' GOI homology region to produce a functional protein upon integration and translation of the protein.

The SLI plasmids containing the relevant *mpc1* and *mpc2* regions for the genetic disruption and conditional knockdown systems were previously developed by our laboratory as part of my BSc (Honours) degree (Table 2.2). The constructs were used in this study to generate the transgenic parasite lines for downstream interrogation of the biological function of putative MPCs. Primers used in the amplification of each *mpc* homology region are listed in Supplementary Table 1.

**Table 2.2: SLI-TGD and SLI-*glmS* construct information.**

| Genetic manipulation system | Plasmid name | Plasmid backbone | Gene insert | Homology region (bp) |
|---|---|---|---|---|
| Gene disruption | pSLI-*mpc1*-GFP | pSLI-TGD | *mpc1* | 219 |
| Gene disruption | pSLI-*mpc2*-GFP | pSLI-TGD | *mpc2* | 324 |
| Conditional knockdown | pSLI-*mpc1-glmS* | pSLI-*glmS* | *mpc1* | 399 |
| Conditional knockdown (negative knockdown control) | pSLI-*mpc1-glmS*-mut | pSLI-*glmS* | *mpc1* | 399 |
| Conditional knockdown | pSLI-*mpc2-glmS* | pSLI-*glmS* | *mpc2* | 561 |
| Conditional knockdown (negative knockdown control) | pSLI-*mpc2-glmS*-mut | pSLI-*glmS* | *mpc2* | 561 |

### 2.5.1 Preparation of SLI constructs for transfection

In preparation for transfection, *Escherichia coli* DH5α bacterial glycerol stocks containing plasmids constructed previously, listed in Table 2.2, were used to inoculate Luria Bertani broth (LB: pH 7.5, 1 % (w/v) tryptone, 1 % (w/v) sodium chloride and 0.5 % (w/v) yeast extract) supplemented with 50 mg/mL ampicillin (Roche Diagnostics, Switzerland) (LB-ampicillin) and incubated at 37 °C with agitation at 200 rpm for 16 h in an MRC LM-570 incubator (MRC, Israel). Bacterial cultures were diluted 1/100 into 200 mL of LB-ampicillin and incubated at 37 °C with agitation at 200 rpm for 12-16 h, until an optical density reading at 600 nm ($OD_{600}$), as a measure of turbidity of 2.5-3.0 was reached. $OD_{600}$ readings were determined with a NanoDrop One$^{C}$ spectrophotometer (Thermo Fisher Scientific, USA). Plasmid DNA was isolated from the saturated cultures with NucleoBond Xtra Midi purification kits (Machery Nagel, Germany) as per manufacturer's instructions. This isolation was performed based on DNA denaturation in an alkaline environment, with subsequent purification by adsorption of the DNA to a silica matrix.

Eluted plasmid DNA was concentrated and purified by precipitation with 3.5 mL of ice-cold 100 % (v/v) isopropanol, followed by collection of the pellet with centrifugation at 15 000 x*g* for 30 min at 4 °C. Ice-cold 70 % (v/v) ethanol (2mL), was added to the pellet and centrifuged as above for 5 min. The pellet was subsequently air-dried and reconstituted in sterile double distilled water. The concentration and quality of the plasmid DNA pellet was measured spectrophotometrically with the NanoDrop One$^{C}$ (Thermo Fisher Scientific, USA). DNA quality was determined based on the presence of proteins and chaotropic salts, indicated by the absorbance ratios $A_{260}/A_{280}$ and $A_{260}/A_{230}$, respectively. The isolated plasmid was stored at -20 °C.

The identity of the SLI constructs was confirmed with restriction enzyme digestion. The isolated SLI constructs (1 µg) were digested using 6 units of *NotI* and *MluI* restriction enzymes (New England Biolabs, USA) in 1x CutSmart buffer (20 mM Tris-acetate pH 7.9, 10 mM $Mg(CH_3CHOO)_2$, 50 mM $CH_3COOK$, 100 µg/mL bovine serum albumin (New England Biolabs, USA)) for 3 h at 37 °C. The *NotI* and *MluI* restriction cut sites flank the *mpc* insert in the pSLI-*mpc1*-GFP, pSLI-*mpc2*-GFP, pSLI-*mpc1-glmS* or *glmS-mut* and pSLI-*mpc2-glmS or glmS-mut* plasmids. The digested constructs were visualised alongside a 1 Kb molecular marker (Promega, USA) on a 1.5 % (w/v) agarose (Promega, USA) /Tris-acetate-EDTA (TAE: 0.04 M Tris-acetate pH 8, 1 mM EDTA) gel, in 1x TAE buffer and stained with 0.5 µg/mL ethidium bromide (EtBr) after electrophoresis. The agarose/TAE gel was viewed with a Bio-Rad Molecular Imager (Bio-Rad, USA) at 300 nm. Images were captured using the Gel Doc XR+ imaging system and analysed using Image Lab software, version 4.1 (Bio-Rad, USA).

Subsequently, approximately 100-250 µg of isolated plasmid DNA was further purified prior to transfection. Plasmid DNA was incubated in 3x the volume of 96 % (v/v) ethanol and 0.1x the volume of sodium acetate (3 M) at 4 °C for 15 min, after which the sample was centrifuged at 11 000 x*g* for 30 min at 4 °C. The pelleted plasmid DNA was washed twice with 250 µL of 70 % (v/v) ethanol followed by 1 mL 96 % (v/v) ethanol and centrifuged as above for 15 min. The pellet was dried in a sterile BSL2 flow hood and reconstituted with cytomix (25 mM HEPES pH 7.6, 120 mM KCl, 0.15 mM $CaCl_2$, 2 mM EGTA, 5 mM $MgCl_2$, 10 mM $K_2HPO_4$) to a final concentration of 400-600 ng/µL and stored at 4 °C for a maximum of three days prior to use.

### 2.5.2 Transfection of SLI constructs into NF54 parasites

Transfection introduces foreign DNA into a cell for transgenic line generation when parasite membrane permeability increases with electroporation [129, 130]. To this end, the predominantly ring stage parasite culture (>5 % parasitaemia, >75 % ring population at 5 % haematocrit) medium was replaced with fresh complete culture medium 3 h prior to the start of the transfection process and the ring stage culture was incubated as described in section 2.2.2. Thereafter, asexual parasites were harvested by centrifugation at 3500 x*g* for 3 min. Cytomix was used to wash the parasite-containing pellet in a 1:1 ratio and centrifuged as above. The parasite pellet, ~200 µL at 100 % haematocrit, was resuspended with the cytomix-plasmid DNA mixture (~400-600 ng/µL) mentioned in section 2.5.1 to a final volume of 450 µL. This mixture was electroporated in a pre-cooled 2 mm cuvette (Bio-Rad, USA) in a Gene Pulser Xcell Electroporation system (Bio-Rad, USA) programmed at a voltage of 310 V and capacitance of 950 µF with maximum resistance to produce a time constant between 10-20 ms. The electroporated mixture was added to 5 mL of complete culture medium and incubated in a hypoxic environment in a stationary incubator for 2 h at 37 °C. After 2 h, lysed erythrocytes were aspirated from the parasite suspension after centrifugation at 3500 x*g* for 3 min. Parasites were resuspended in complete culture medium to a final volume of 5 mL and incubated in the stationary environment described above.

### 2.5.3 Drug selection and screening of transgenic parasites

The SLI based genetic disruption and conditional knockdown transgenic parasite lines were created as outlined in Figure 2.2. Daily drug pressure using 4 nM of WR99210 (Jacobus Pharmaceutical Company, USA) was applied to parasites 24 h post-transfection for a 10 day period to select for episomal uptake of SLI-constructs. WR99210, an antifolate drug, is a potent inhibitor of the parasite dihydrofolate reductase (DHFR) [131]. However, the SLI-constructs

selection marker, the human DHFR (hDHFR), negates the action of WR99210 allowing proliferation of transfected parasites [102]. Parasitaemia was monitored daily with RapidDiff-stained samples using light microscopy as described in section 2.2.2. This was followed by a 3–4 week recovery period with fresh erythrocytes added weekly to maintain a 5 % haematocrit and complete culture media was exchanged every 3-4 days. During this period, parasite cultures were incubated without agitation at 37 °C in a hypoxic environment.

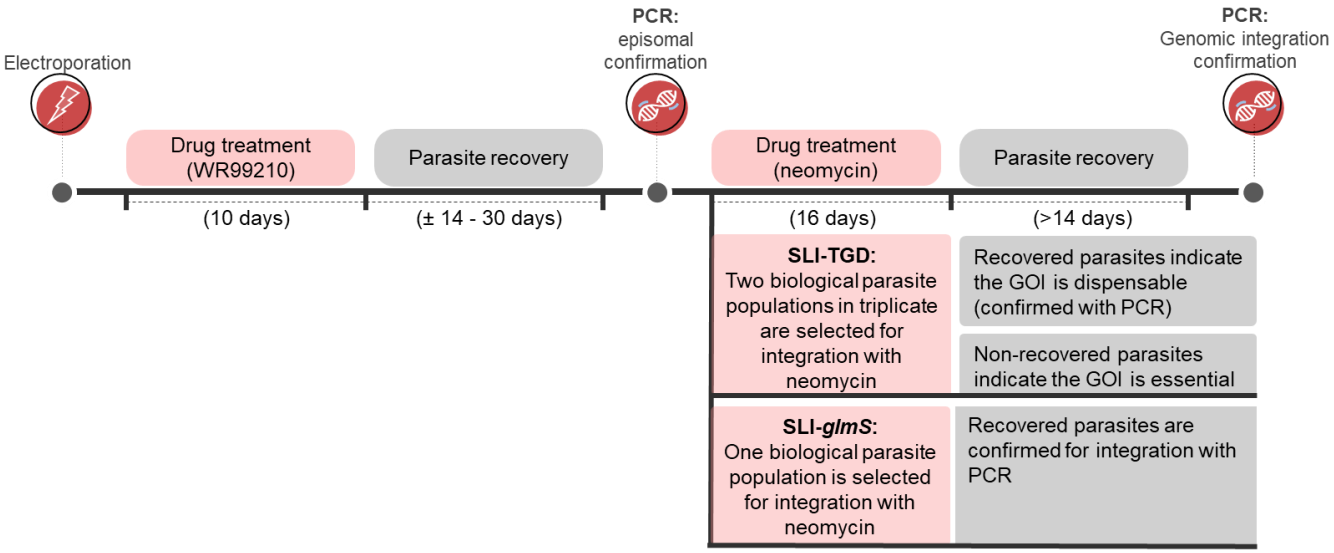


**Figure 2.2: Schematic representation of transgenic parasite line generation using the SLI-systems.** After transfection of the respective plasmids into NF54 parasites, parasites were subjected to daily WR99210 drug pressure to select for a parasite population that has taken up the plasmid episomally. After parasite recovery, the population was screened with PCR to confirm episomal uptake of the plasmid. This was followed by G418 drug selection to obtain transgenic parasites that have undergone allelic exchange with the plasmid, which was confirmed with PCR. The G418 drug event for the SLI-TGD system was performed on two parasite populations (n=2) in triplicate to confirm the results

After parasite resurgence, parasites were cultured routinely, as described in section 2.2.2, to a >2 % parasitaemia. The episomal presence of the SLI-constructs was determined via PCR with genomic and plasmid DNA extracted from a predominantly trophozoite culture as per manufacturer's instructions with the Quick-DNA Miniprep kit (Zymo Research, USA). The PCR used primers flanking the upstream and downstream GOI region within the SLI-construct (Figure 2.3). The PCR mixture consisted of: 1x KAPA Taq polymerase (Sigma-Aldrich, USA), 5 pmol of the forward and reverse primer (Table 2.3) and 30-80 ng of extracted DNA. The thermocycler was programmed with the following conditions: initial denaturation at 95 °C for 3 min followed by 30 cycles of denaturation at 95 °C for 30s, annealing at 58 °C for 30s, and extension at 68 °C for 1 min, with a final extension at 68 °C for 2 min. The PCR product was visualised on a 1.5 % (w/v) agarose/TAE gel, stained, and imaged as outlined in section 2.5.1.

**Table 2.3: Primers used for screening the episomal presence of SLI constructs and the allelic exchange at the *mpc* loci in *P. falciparum* NF54 parasites.**

| Parasite line | Detection region | Primer code | Orientation | Primer sequence (5'-3') | Expected amplified size (bp) |
|---|---|---|---|---|---|
| NF54 parasites transfected with pSLI-*mpc1* or *mpc2*-GFP and pSLI-*mpc1* or *mpc2- glmS* or *glmS-mut* | Plasmid (episomal detection) | P1 | forward | AGCGGATAACAATTTCAC ACAGGA | pSLI-*mpc1*-GFP: 381<br>pSLI-*mpc2*-GFP: 485<br><br>pSLI-*mpc1-glmS* or *glmS-mut*: 576<br>pSLI-*mpc2-glmS* or *glmS-mut*: 738 |
| | | P2 | reverse | ACAAGAATTGGGACAAC TCCAGTGA | |
| NF54-epi(pSLI-*mpc1- glmS/glmS-mut*) | 5' integrated locus | P3 | forward | TCTAATGTAGGATCATTT TTTCATAATG | 641 |
| | | P2 | reverse | ACAAGAATTGGGACAAC TCCAGTGA | |
| | 3' integrated locus | P1 | forward | AGCGGATAACAATTTCAC ACAGGA | 460 |
| | | P4 | reverse | GCCTTCCCTATACGTCCT GTTC | |
| | Wild-type Locus | P3 | forward | TCTAATGTAGGATCATTT TTTCATAATG | 492 |
| | | P4 | reverse | GCCTTCCCTATACGTCCT GTTC | |
| NF54-epi(pSLI-*mpc2-glmS/glmS-mut*) | 5' integrated locus | P5 | forward | TGAAAGTTTAAAAAAAGT GCTTGG | 874 |
| | | P2 | reverse | ACAAGAATTGGGACAAC TCCAGTGA | |
| | 3' integrated locus | P1 | forward | AGCGGATAACAATTTCAC ACAGGA | 1331 |
| | | P6 | reverse | GCAGAATACGCAAAACA GTTCG | |
| | Wild-type Locus | P5 | forward | TGAAAGTTTAAAAAAAGT GCTTGG | 1467 |
| | | P6 | reverse | GCAGAATACGCAAAACA GTTCG | |

*P. falciparum* cultures with confirmed episomal uptake were named as follows: NF54-epi(pSLI-*mpc1* or *mpc2*-GFP), NF54-epi(pSLI-*mpc1* or *mpc2-glmS*) and NF54-epi(pSLI-*mpc1* or *mpc2-glmS-mut).* These parasite populations (>3 % parasitaemia, >75 % ring population) were cryogenically preserved in liquid nitrogen using a 1:1 ratio of 100 % haematocrit parasite pellet

to specialised-freezing media [(28 % (v/v) glycerol (Sigma-Aldrich, USA), 3 % (w/v) D-sorbitol (Sigma-Aldrich, USA), 0.65 % (w/v) sodium chloride (Glentham, USA)].

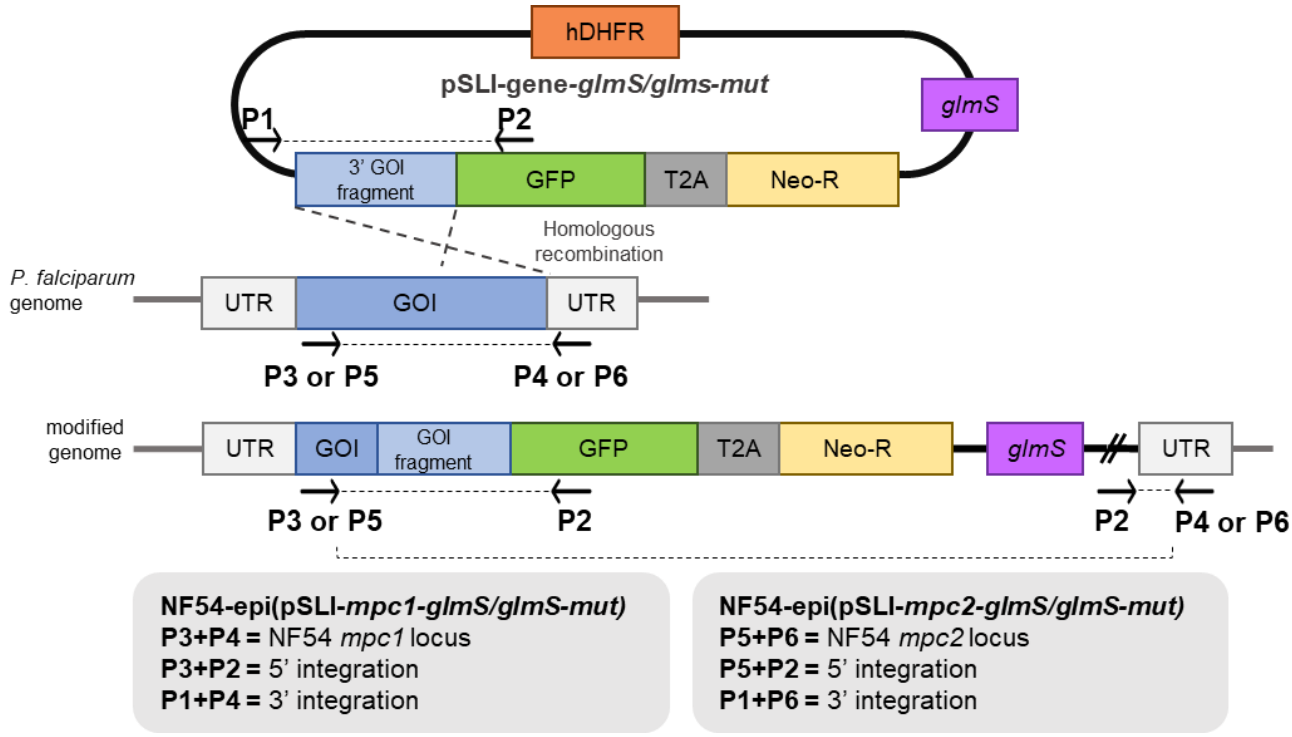


**Figure 2.3: Schematic representation of the primer combinations used in screening the SLI-transgenic parasite lines.** To confirm genomic integration in suspected transgenic lines, PCR screening of the entire locus, 5' region and 3' region of the native loci of the GOI was performed to confirm the presence of the SLI-GOI plasmid in the original locus. This schematic visually represents the primer code, location and pair used in screening suspected transgenic parasite lines containing the pSLI-*mpc1* or *mpc2-glmS/glmS-mut* plasmids.

Two biological NF54-epi(pSLI-*mpc1* or *mpc2*-GFP) populations in technical triplicate as well as four biological NF54-epi(pSLI-*mpc1* or *mpc2-glmS*) and NF54-epi(pSLI-*mpc1* or *mpc2-glmS-mut)* populations were subjected to a second period of drug pressure with the neomycin-derivative, G418. G418 prevents polypeptide synthesis in wild-type NF54 parasites. However, transgenic parasites will be unaffected by this selection pressure if allelic exchange with the SLI-plasmid has occurred as the neomycin resistance gene is expressed under the GOI endogenous promoter [102]. All parasite lines were subjected to a second period of drug pressure using G418 (ThermoFisher Scientific, USA) for a 10 day period with daily replacement of complete culture media containing 400 µg/mL G418. Subsequently, the complete culture medium containing 400 µg/mL G418 was replaced every second day for a further 6 day period, unless specified otherwise. Parasitaemia was monitored every second day over the 16 day period with RapiDiff-stained samples using light microscopy as described in section 2.2.2.

Parasite populations were routinely cultured, described in section 2.2.2, with fresh erythrocytes and complete culture medium without G418 replaced every 3-4 days for a minimum 30 day

period following G418 selection to allow for parasite recovery, as indicated by an increase in parasitaemia. Recovered parasite populations were screened for integration by amplifying the 5' and 3' region of the native locus with the PCR conditions described for episomal confirmation using the primer pairs described in Table 2.3 and schematically represented in Figure 2.3. Allelic exchange will result in a change in amplicon size when amplifying the same segment from the wild type genome versus the modified *P. falciparum* genome.

## 2.6 Generation of a transgenic ectopic expression line

The *mpc1* and *mpc2* genes were cloned into an inducible Bxb1 ectopic expression system resulting in the MPC heterocomplex falling under the control of the constitutive calmodulin promoter (Figure 2.4) [132]. The aim was to co-express the *mpc1* and *mpc2* genes above basal levels to observe the biological effect constitutive expression of the MPC heterocomplex has on *P. falciparum* parasites. The inducible portion of this system allows for activation of the inducible *glmS* ribozyme with glucosamine to reduce the ectopic expression of the MPC heterocomplex back to basal levels.

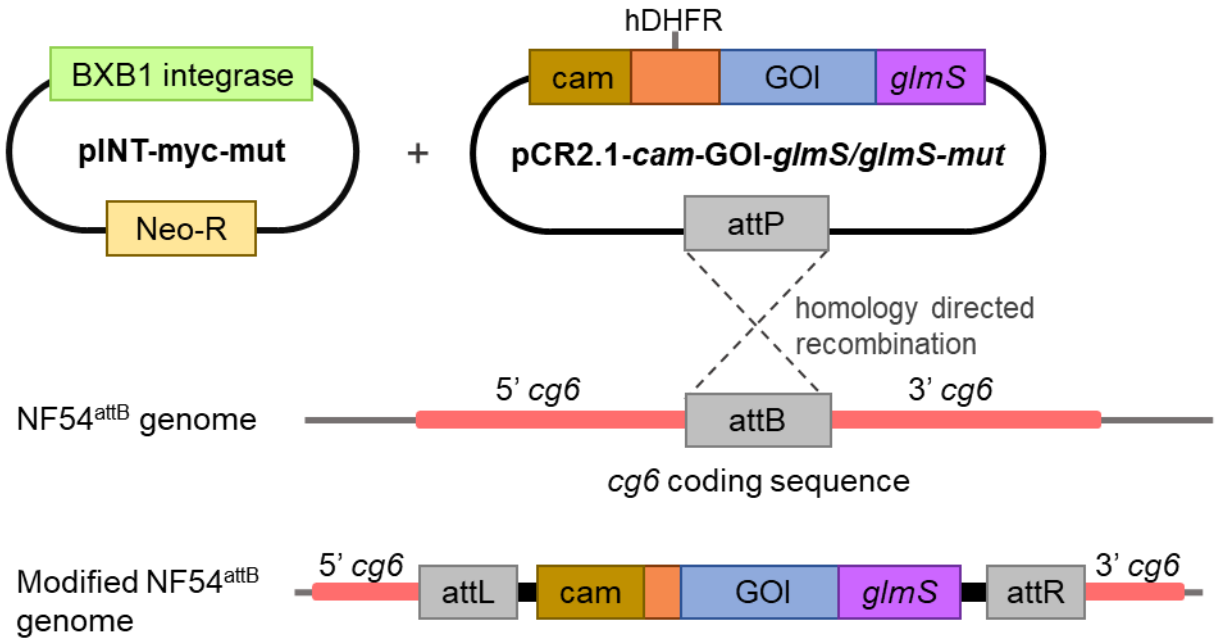


**Figure 2.4: Schematic representation of the BXB1 ectopic expression system.** This dual plasmid system expresses the GOI ectopically and constitutively in the *cg6* locus under the control of the calmodulin (cam) promoter above the basal expression of the GOI. The pCR2.1-cam-GOI-*glmS* plasmid contains the coding sequence of the GOI alongside the cam promoter, a *glmS* ribozyme allows the system/GOI to be conditionally knocked down to its basal level upon glucosamine activation and a hDHFR gene for episomal section. The pINT plasmid contains the *neo-R* gene for transgenic parasite selection and a *bxb1* integrase gene which instigates the allelic exchange between the two homology sites, the *attP* and *attB* sites, located in the plasmid and *cg6* gene, respectively. For this reason, the two plasmids, pCR2.1-cam-GOI-*glmS* and pINT, are transfected together to generate a transgenic parasite line.

Transgenic parasites are generated using a dual plasmid system that integrates the GOI in a site-specific manner into the dispensable *cg6* gene of the NF54-*cg6-attB* parasite line ($NF54^{attB}$) provided by Pietro Alano and Giulia Siciliano from the Istituto Superiore di Sanita in Italy. The mycobacteriophage Bxb1 integrase, expressed in pINT-*myc-mut*, mediates this integration by catalysing the allelic exchange between two nonidentical sites, the plasmid *attP* and chromosomal *attB* sites, located in the pCR2.1-*attP-cam-glmS* or pCR2.1-*attP-cam-glmS-mut* plasmids and *cg6-attB* gene, respectively (Figure 2.4) [108, 133]. Upon allelic exchange, two asymmetrical *attL* and *attR* sites flanking the integrated transgene are produced, stabilising this integrant which is non-excisable by the Bxb1 integrase [108]. The pINT-*myc-mut*, pCR2.1-*attP-cam-glmS,* pCR2.1-*attP-cam-glmS-mut* plasmids were produced by Dr Elisha Mugo and Doré Joubert from the Malaria Parasite Molecular Laboratory, University of Pretoria, South Africa. The *glmS* and *glmS-mut* ribozymes function similarly as mentioned in section 2.5.

### 2.6.1 *In silico* design of *mpc1-myc-mpc2-HA* fragment

The coding nucleotide sequences of *mpc1* and *mpc2* were obtained from PlasmoDB and used to design an oligonucleotide fragment *in silico* with the Benchling software (https://benchling.com/). A single myc tag (5' GAGCAGAAGCTGATCTCGGAGGAGGATCTG 3') and hemagglutinin (HA) tag (5' TACCCATACGATGTTCCAGATTACGCT 3') was added to the 3' sequence of the *mpc1* and *mpc2* genes, respectively, for downstream localisation studies (Figure 2.5). Additionally, a skip peptide (T2A) was inserted before the start of each gene to ensure both genes will be translated as two separate proteins with the appropriate tags. The 5' and 3' ends of the fragment were flanked by the restriction cut sites *SalI* (5' AGGCCT 3') and *StuI* (5' GTCGAC 3'), respectively, to allow directional cloning of the fragment into the pCR2.1-*attP-cam-glmS* or pCR2.1-*attP-cam-glmS-mut* plasmids. This *in silico* designed fragment was commercially synthesised (GeneUniversal, USA) and provided as an insert in the pU57- *mpc1-myc-mpc2-HA* plasmid.

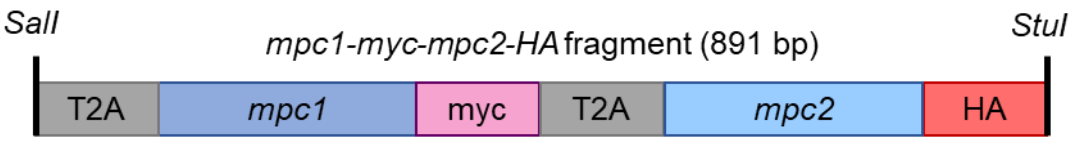


**Figure 2.5: Schematic representation of the *mpc1-myc-mpc2-HA* fragment.** A fragment with the coding sequences of *mpc1* and *mpc2* was designed *in silico* to co-express these genes above basal *mpc* expression with an ectopic expression system. The fragment includes a myc and HA tag after *mpc1* and *mpc2* sequences, respectively, to enable downstream co-localisation of these proteins. Additionally, a skip peptide (T2A) was added prior to each gene to ensure the proteins are translated as two separate proteins. The flanking restriction enzyme cut sites for *SalI* and *StuI* restriction enzymes were added to directionally clone this fragment into the ectopic expression plasmids.

### 2.6.2 Cloning of the *mpc1-myc-mpc2-HA* fused fragment into pCR2.1-*cam*

Competent cells were produced by inoculating 5 mL of LB with *E. coli* DH5α cells followed by incubation for 16 h at 37 °C with agitation at 200 rpm in an MRC LM-570 incubator (MRC, Israel). This culture was transferred to 50 mL of LB, incubated with agitation at 37 °C until an $OD_{600}$ reading of 0.5 was reached. This bacterial culture was incubated on ice for 20 min and centrifuged at 1870 x*g* for 30 min in a centrifuge pre-cooled to 4 °C. The bacterial pellet was resuspended in cold 0.1 M $CaCl_2$ (25 mL) and centrifuged as above. Following this, 0.1 M $CaCl_2$ (2.5 mL) and 100 % glycerol (375 µL) was used to resuspend the pellet. After a 1 h incubation on ice, 100 µL aliquots of competent cells were stored at -80 °C until use.

The pUC57-*mpc1-myc-mpc2-HA,* pINT-*myc-mut*, pCR2.1-*cam-glmS* and pCR2.1-*cam-glmS-mut* plasmids were transformed with a heat-shock based method into chemically competent *E. coli* DH5α cells. Cells were incubated with 100 ng of plasmid on ice for 30 min prior to being heat-shocked at 42 °C for 90 s. After heat-shock, the cells were immediately transferred to ice for 2 min. Subsequently, 900 µL of LB supplemented with 20 mM glucose was added to transformed cells and incubated at 37 °C for 45 min with agitation at 200 rpm in an MRC LM-570 incubator (Israel). The cell suspension (100 µL) was spread-plated onto LB-agar plates (1 % (w/v) agar in LB-ampicillin) and incubated for 16 h at 37 °C. Bacterial colonies were selected from each plate and inoculated into LB-ampicillin incubated with agitation at 200 rpm for 16 h at 37 °C. Plasmid DNA was isolated from the bacterial cultures with a NucleoBond Xtra Mini purification kit (Machery Nagel, Germany) as per manufacturer's instructions. Plasmid DNA purity was assessed as described in section 2.5.1. Isolated pCR2.1-*cam-glmS*, pCR2.1-*cam-glmS-mut* and pUC57-*mpc1-myc-mpc2-HA* plasmids (1-2 µg) were enzymatically digested with 6 units of the two restriction enzymes, *SalI* and *StuI* (NewEngland Biolabs, USA), at the 5' and 3' flanking restriction sites surround the cloning site and fragment, respectively. All digestion reactions were performed and visualized on a 1.5 % (w/v) TAE/agarose gel as mentioned in section 2.5.1.

The *mpc1-myc-mpc2-HA* fragment and pCR2.1-*cam-glms/glms-mut* plasmid backbone was isolated from the gel using the silica matrix technique of the NucleoSpin PCR and Gel Clean-up kit (Machery-Nagel, Germany) as per manufacturer's instructions and stored at 20 °C. The isolated fragment and plasmid backbone concentration and purity was determined with the NanoDrop One$^C$ (Thermo Fisher Scientific, USA) as mentioned in section 2.5.1. The purified digested vectors and *mpc1-myc-mpc2-HA* fragment were ligated with T4 DNA ligase (NewEngland Biolabs, USA) with a vector to insert ratio of 5:1. The required *mpc1-myc-mpc2-HA* fragment amount was calculated according to the equation below.

$$\text{ng of insert} = \frac{\text{ng of vector x kb size of insert}}{k\text{b size of vector}} \text{ x } (\text{insert: vector molar ratio})$$

The ligation reaction comprised of T4 DNA ligase, 1 x ligase reaction buffer (50 mM Tris-HCl pH 7.5, 10 mM $MgCl_2$, 1 mM ATP, 10 mM DTT), 50 ng of pCR2.1-*cam-glms/glms-mut* plasmid backbone and the calculated amount of *mpc1-myc-mpc2-HA* fragment. The ligation reaction was incubated at 4 °C for 16 h prior to heat-shock transformation into competent *E. coli* DH5α cells as described previously.

### 2.6.3 Putative recombinant colony screening

Recombinant pCR2.1-*cam-mpc1-myc-mpc2-HA-glmS* and pCR2.1-*cam-mpc1-myc-mpc2-HA-glmS-mut* plasmids were screened with bacterial colony-screening PCR, restriction enzyme digestion and Sanger sequencing to confirm that the *mpc1-myc-mpc2-HA* fragment was inserted correctly into the respective plasmids and no mutations had occurred.

#### 2.6.3.1 Bacterial colony-screening PCR

Individually chosen bacterial colonies, from the previously transformed and plated *E. coli* DH5α cells with recombinant pCR2.1-*cam-mpc1-myc-mpc2-HA-glmS/glmS-mut* plasmids, were inoculated into 100 µL of LB-ampicillin and incubated with agitation at 200 rpm for 3 h at 37 °C in an MRC LM-570 incubator (MRC, Israel). Following incubation, a PCR reaction containing 1 x Kapa Taq Ready Mix (Kapa Biosystems, USA), 5 pmol of plasmid specific forward and reverse primer (Table 2.4) and 1 µL of bacterial culture was prepared. The thermocycler was programmed with the following conditions: initial denaturation at 95 °C for 3 min followed by 30 cycles of denaturation at 95 °C for 30s, annealing at 60 °C for 30s, and extension at 68 °C for 2 min, with a final extension at 68 °C for 2 min. The PCR product was visualised on a 1.5 % (w/v) agarose/TAE as described in section 2.5.1.

**Table 2.4: Primers used to identify bacterial clones containing the ectopic expression plasmids.**

| Primer code | Orientation | Primer sequence (5'-3') | Homologous to: |
|---|---|---|---|
| P7 | Forward | AGAATACCCAGGTGTTCTCTCTGA | pCR2.1-*cam-glmS/glmS-mut* |
| P8 | Reverse | TGAACAAAGAGAAATCACATGATCT | |

Colonies with the correct insert size were used to inoculate LB-ampicillin and incubated with agitation at 200 rpm for 16 h at 37 °C. Plasmid DNA was isolated from the bacterial cultures with a NucleoBond Xtra Mini purification kit (Machery Nagel, Germany) as per manufacturer's

instructions. Plasmid DNA quantity and purity was assessed as described in section 2.5.1. Isolated plasmid DNA was used in further recombinant plasmid screening experiments, restriction enzyme digestion and Sanger sequencing.

#### 2.6.3.2 Restriction enzyme digestion of putative recombinant plasmid

Isolated recombinant pCR2.1-*cam-mpc1-myc-mpc2-HA-glmS*/*glmS-mut* plasmids (1-2 µg) were enzymatically digested with 6 units of the two restriction enzymes, *SalI* and *StuI* (NewEngland Biolabs, USA), at the 5' and 3' flanking restriction sites, respectively. Digestion was preformed and visualised as described in section 2.5.1.

#### 2.6.3.3 Sanger sequencing of putative recombinant plasmid

Individual sequencing reactions consisted of 0.5x BigDye reaction mix (Applied Biosystems, Foster City, USA), 2x BigDye buffer (Applied Biosystems, Foster City, USA), 5 pmol of the P7 or P8 primers (Table 2.3) and 60-200 ng of plasmid DNA. The 2720 Thermocycler (Applied Biosystems, USA) was programmed with the following conditions: initial denaturation at 95 °C for 1 min followed by 25 cycles of denaturation at 95 °C for 10s, annealing at 58 °C for 5s, and extension at 60 °C for 4 min. The sequencing product was purified with ethanol precipitation in a 0.6 µL Eppendorf tube by incubating the reaction in 3x the volume of 96 % (v/v) ethanol and 0.1x the volume of sodium acetate (3 M) at -20 °C for 15 min. After incubation, the reaction was centrifuged at 11 000 x *g* for 30 min in a pre-cooled (4 °C) centrifuge. Ice-cold 70 % ethanol/$H_2O$ (250 µL) was added to the pellet and centrifuged as mentioned above for 10 min. The supernatant was removed, and the pellet was dried under vacuum for 10 min prior to sequencing. Plasmid sequences were determined using the ABI PRISM Genetic Analyser (Applied Biosystems, USA) available at the sequencing facility at the University of Pretoria. Sequences were analysed with the Benchling software (https://benchling.com) and Snapgene software version 5.3 for base calling from chromatograms and sequence alignments.

### 2.6.4 Recombinant ectopic expression system plasmid preparation

The pINT-*myc-mut*, recombinant pCR2.1-*cam-mpc1-myc-mpc2-HA-glmS* and pCR2.1-*cam-mpc1-myc-mpc2-HA-glmS-mut* plasmids were isolated and purified to obtain >1 µg/µL of each plasmid as outlined in section 2.5.1. These purified plasmids were digested with 6 units of *SalI* and *StuI* restriction enzymes (New England Biolabs, USA), which flank the *mpc1-myc-mpc2-HA* fragment and visualised according to the method outlined in section 2.5.1. Lastly,

100-250 µg of each plasmid was further purified and resuspended in cytomix (25 mM HEPES pH 7.6, 120 mM KCl, 0.15 mM $CaCl_2$, 2 mM EGTA, 5 mM $MgCl_2$, 10 mM $K_2HPO_4$) to a final concentration of 400-600 ng/µL in preparation for transfection as per the method in section 2.5.1.

### 2.6.5 Transfection of ectopic expression system plasmids

This ectopic expression system relies on a dual-plasmid transfection with the recombinant pCR2.1-*cam-mpc1-myc-mpc2-glmS/glmS*-mut and the pINT-*myc-mut* to produce an integrated line where the *mpc1-myc-mpc2-glmS/glmS*-mut fragment integrates into the *cg6* gene. A *P. falciparum* NF54$^{attB}$ parasite culture ( >5 % parasitaemia, >75 % ring population at 5 % haematocrit) was transfected with two plasmids simultaneously: 100 µg of pCR2.1-*cam-mpc1-myc-mpc2-glmS* or pCR2.1-*cam-mpc1-myc-mpc2-glmS*-mut (125 µL) and 100 µg of pINT-*myc-mut* (125 µL). Transfection was performed as outlined in section 2.5.2.

### 2.6.6 Drug selection and transgenic parasite screening

Twenty-four hours after transfection, dual drug pressure with 2 nM WR99210, and 250 µg/mL G418 was added daily for a 6 day period to the parasite culture. This is followed by a further daily 4 day treatment with only 250 µg/mL G418 amounting to a total of 10 days of drug pressure. Dual drug pressure was needed to select for the episomal presence of both transfected plasmids, as well as transgenic parasites that have undergone allelic exchange. Parasitaemia was monitored daily with light microscopy and RapidDiff stained samples as described in section 2.2.2. This was followed by a month-long recovery period with fresh erythrocytes and complete culture media added every 3-4 days to maintain a 5 % haematocrit.

Once parasites recovered, cultures were maintained at a >2 % parasitaemia and 5 % haematocrit, as described in section 2.2.2. Genomic integration was determined via PCR with genomic and plasmid DNA isolated from a predominantly trophozoite culture (>3 % parasitaemia and 5 % haematocrit) as per manufacturer's instructions with the Quick-DNA Miniprep kit (Zymo Research, USA). The PCR used primers flanking the GOI region located in the 5' and 3' coding sequence of the *cg6* gene (Figure 2.6). The PCR mixture consisted of: 1x KAPA Taq polymerase (Sigma-Aldrich, USA), 5 pmol of the forward and reverse primer (Table 2.5) and 30-80 ng of extracted DNA. The thermocycler was programmed with the following conditions: initial denaturation at 95 °C for 5 min followed by a 35-cycle two-step PCR

programme with denaturation at 95 °C for 30s and a combined annealing/extension step at 60 °C for 2 min. The final extension was programmed to 60 °C for 4 min.

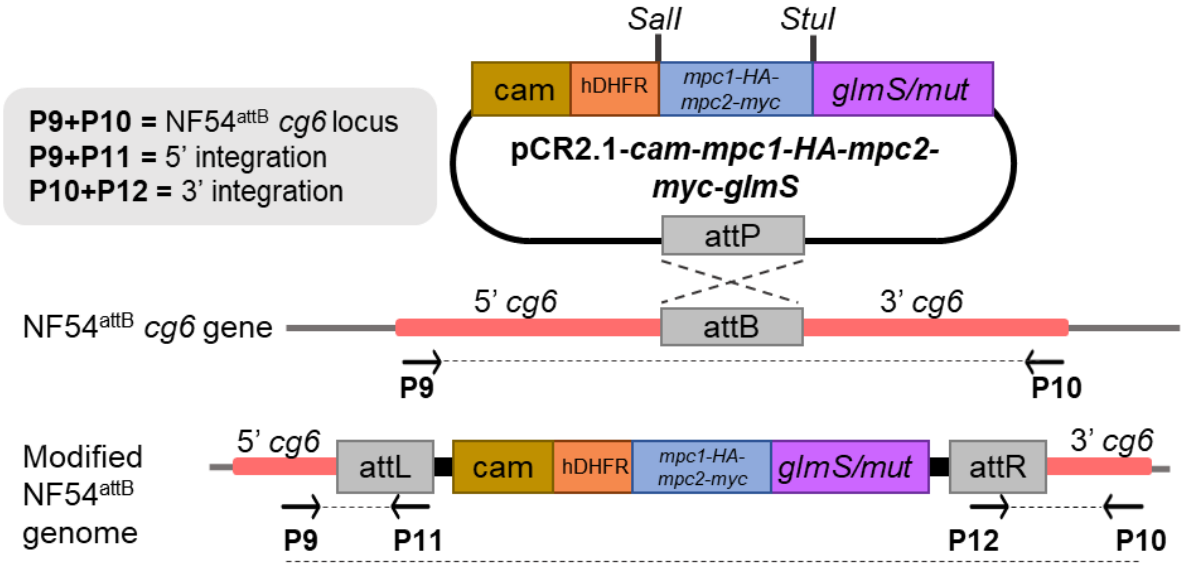


**Figure 2.6: Schematic representation of screening the ectopic transgenic parasite lines generated with the ectopic expression system.** To confirm genomic integration in suspected transgenic lines, PCR screening of the entire locus, 5' region and 3' region of the *cg6* gene was performed to confirm the insertion of the *mpc1-HA-mpc2-myc* fragment. This schematic visually represents the primer code, location and pair used in screening suspected transgenic parasite lines transfected with the pINT and pCR2.1-*cam-mpc1-HA-mpc2-myc-glmS* or pCR2.1-*cam-mpc1-HA-mpc2-myc-glmS-mut* plasmids.

The PCR product was visualised as mentioned in section 2.5.1. *P. falciparum* cultures with confirmed genomic integration were named as follows: NF54$^{attB}$-*cam-mpc1-myc-mpc2-HA-glmS* or *-glmS-mut*. This integrated parasite population was cryogenically preserved as described in section 2.5.3.

**Table 2.5: Primers used for identifying transgenic *P. falciparum* parasites with genomic integration into NF54$^{attB}$ parasites.**

| Parasite line | Detection region | Primer code | Orientation | Primer sequence (5'-3') | Expected amplified size (bp) |
|---|---|---|---|---|---|
| NF54$^{attB}$-*cg6* | Wild-type locus | P9 | Forward | CATCCTGTGAAGTTACCCAGGATCCA | 681 |
| | | P10 | Reverse | CATAGACAAGTTGCAAGAATTGCATG | |
| NF54$^{attB}$-cg6(*mpc1-myc-mpc2-HA-glmS/glmS-mut)* | 5' integrated locus | P9 | Forward | CATCCTGTGAAGTTACCCAGGATCCA | 653 |
| | | P11 | Reverse | GATTACTTTGATTAACAAAGGCACGC | |
| | 3' integrated locus | P12 | Forward | TGCTCACATGTTCTTTCCTGCG | 863 |
| | | P10 | Reverse | CATAGACAAGTTGCAAGAATTGCATG | |

# 3. Results

## 3.1. *In silico* analyses of putative MPC proteins

The two genes, MPC1 (PF3D7_1340800) and MPC2 (PF3D7_1470400), were previously only putatively annotated to encode MPC proteins based on high-level general gene annotation strategies within PlasmoDB (www.plasmodb.org). To confirm this annotation and expand on the classification of these genes, several parallel *in silico* evaluations were performed. The evolutionary relationship of the putative *P. falciparum* MPC proteins was investigated in comparison to 20 other putative and well-characterised MPCs in different eukaryotic organisms (Figure 3.1).

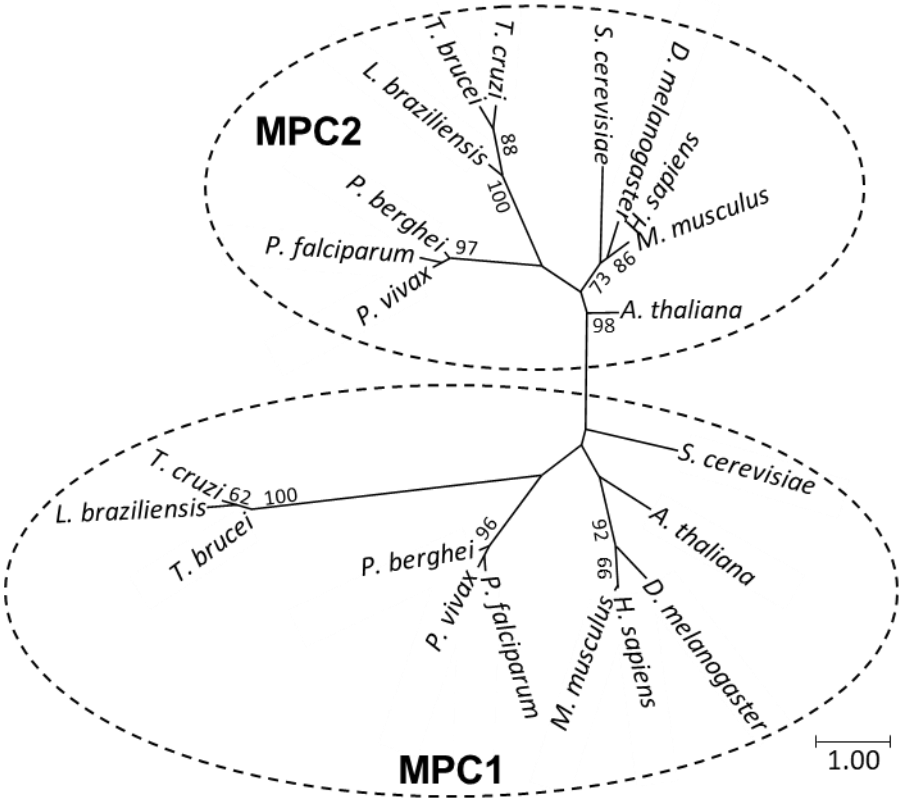


**Figure 3.1: Evolutionary analysis of putative MPC1 and MPC2 proteins.** The highest likelihood evolutionary history between 22 selected known and predicted MPC orthologs of MPC1 and MPC2 was inferred by using the Maximum Likelihood method and LG model displayed on an unrooted phylogenetic tree. The initial tree for the heuristic search were obtained automatically by applying the Maximum Parsimony method. A discrete Gamma distribution was used to model evolutionary rate differences among sites (4 categories (+G, parameter = 1.8213)). The rate variation model allowed for some sites to be evolutionarily invariable ([+*I*], 0.92% sites). Nodal values next to its corresponding branch represent bootstrap values for 500 replicates above 65 %. The tree is drawn to scale, with branch lengths measured in the number of substitutions per site indicated by the scale bar. Evolutionary analyses were conducted in MEGA11.

An unrooted phylogenetic tree inferring MPC1 and MPC2 evolutionary history was generated by using the Maximum Likelihood method and LG model with discrete Gamma distribution to model the evolutionary rate differences among sites (4 categories (+G, parameter = 1.8213)) (Figure 3.1). *P. falciparum* MPC1 and MPC2 proteins cluster with MPC1 and MPC2 orthologs

into two clades (Figure 3.1). Within these two clades, the apicomplexan MPC1 and MPC2 proteins from *Plasmodia spp.*, *Leishmania spp.* and *Trypanosoma spp.* are the most closely related to each other with high statistical support but separated from multicellular organisms such as *H. sapiens, M. musculus,* and *D. melanogaster.* However, *P. falciparum* MPC1 and MPC2 shared low sequence similarity with *S. cerevisiae* and *A. thaliana*, respectively.

To expand on the functional and structural annotations of MPC1 and MPC2, common amino acid residues and shared membrane topology was identified between *P. falciparum* putative MPC protein sequences and three experimentally characterised MPC proteins of *H. sapiens, S. cerevisiae,* and *D. melanogaster* (Figure 3.2). MPC1 and MPC2 are predicated to have three transmembrane spanning helices within the MPC family domain (InterPro: IPR005336 and Pfam: PF03650) (Figure 3.2). Conserved amino acid residues are identified between the MPC1 and MPC2 sequences of four organisms (Figure 3.2) with the majority of the conserved residues positioned within the transmembrane regions. Transmembrane region conservation within the predicted MPC family domain most likely provides the characteristic features of the MPC heterocomplex resulting from ancestral lineages previously noted in Figure 3.1. A previous computational simulation of *de novo* human MPC heterocomplexes identified residues that could define the transport pathway of pyruvate/pyruvic acid [134]. In MPC1, Asn33, His84, and Asn87 were conserved between all four species (Figure 3.2). Upon analysis of the MSA in Figure 3.2, there was conservative amino acid replacement from the human Leu36, to Ile in *S. cerevisiae,* and *D. melanogaster*. By contrast, the aliphatic Leu36 in the *H. sapiens* sequence was replaced with an aromatic Phe in the *P. falciparum* MPC1 sequence. In MPC2, only Ala55 and Asn100 were conserved between all four species (Figure 3.2). Leu52 and Leu75 were conservatively replaced with Ile in the *P. falciparum* sequence, and Trp82 with Phe. Val103 was conservatively replaced with Leu in *S. cerevisiae*, but the *P. falciparum* MPC2 sequence contains a Met at this position. All of the amino acid replacements between *H. sapiens* and *P. falciparum* MPC1 and MPC2 amino acid sequences are with non-polar residues to maintain the hydrophobic property of the predicted transmembrane regions. However, the non-conservative amino acid substitutions (Leu→Phe; Val→ Met) in MPC1 and MPC2 could result in structural differences between the human and *P. falciparum* MPC heterocomplexes.

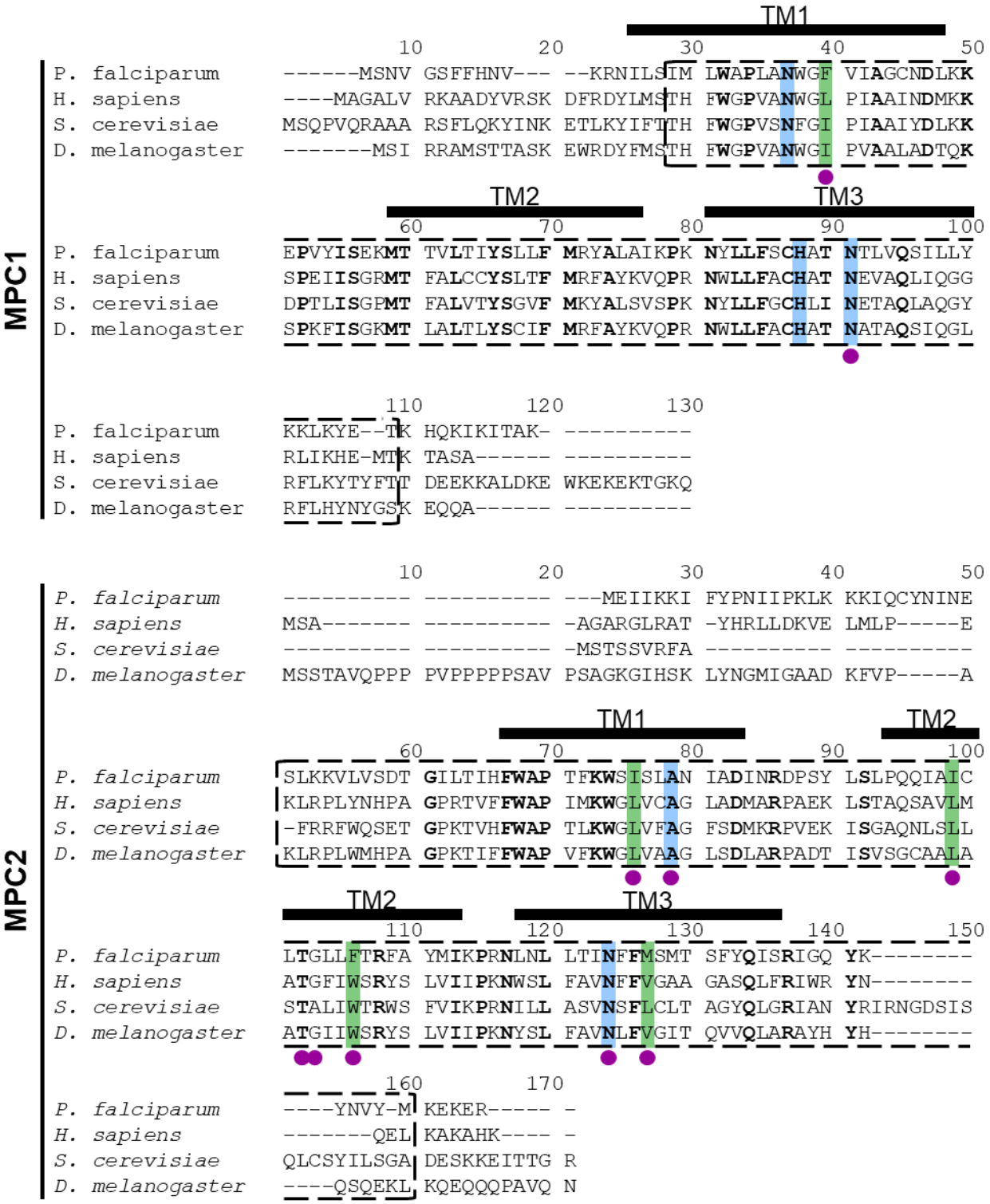


**Figure 3.2: Protein sequence alignment of *P. falciparum* MPC1 and MPC2 to MPC orthologues with experimentally confirmed function. (A)** MPC1 and **(B)** MPC2 protein sequences were MUSCLE sequence aligned in MEGA11 to corresponding MPC protein sequences in *H. sapiens, S. cerevisiae* and *D. melanogaster.* Amino acid residues with 100 % conservation are bolded. The MPC family domain predicted by InterPro and Pfam is highlighted by a black dotted box. The predicted transmembrane spanning region (deepTMHMM, PHOBIUS and TOPCONS) are highlighted by a black line. TM1-3: Transmembrane spanning region 1-3. Amino acids predicted to be in involved in pyruvate transport are indicated with blue blocks for conserved amino acids and green blocks for substituted amino acids. Predicted sites of UK-5099 are indicated with plum circles (142).

The topological features of MPC1 and MPC2 that were predicted with deepTMHMM, PHOBIUS and TOPCONS were used to generate a schematic representation of the MPC1 and MPC2 subunits (Figure 3.3). The N-terminus of MPC1 and MPC2 are predicted to be located in the mitochondrial matrix, whereas the C-terminus of these proteins are located in the intermembrane space. These N- and C-terminal predictions confirm the human MPC computational simulations, which found that the positively charged N-terminus would be located in the negatively charged mitochondrial matrix and the C-terminus to reside in the intermembrane space [134].

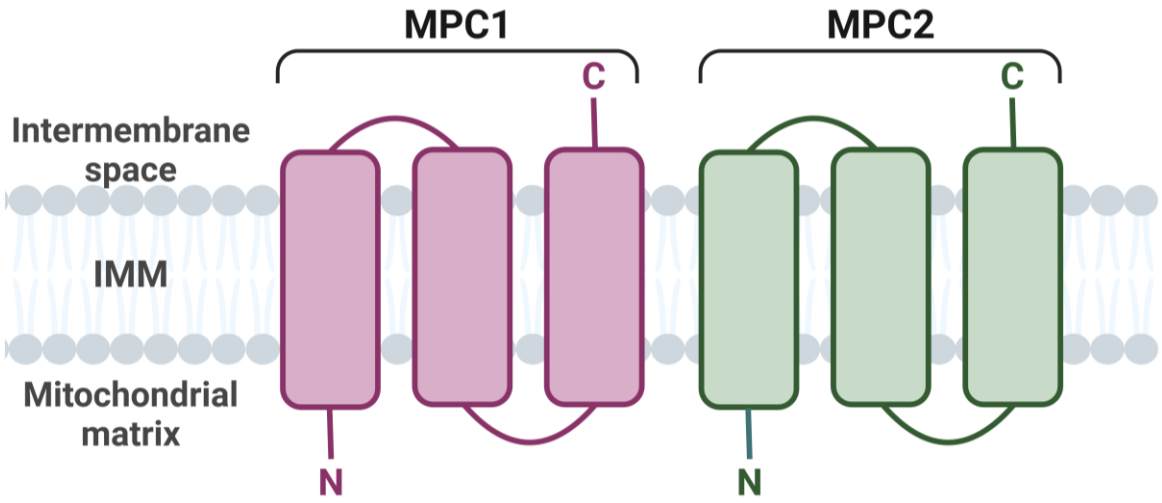


**Figure 3.3: Schematic representation of the predicted MPC1 and MPC2 protein topology.** MPC1 and MPC2 membrane topology was determined with deepTMHMM, PHOBIUS and TOPCONS to predict the terminal location and transmembrane spanning regions across the inner mitochondrial membrane (IMM). Image generated on Biorender.com.

In addition to these features, the probability of *P. falciparum* MPC1 and MPC2 proteins being exported to the mitochondria was predicted with MitoProtI to be 0.89 and 0.43, respectively (Table 3.1). This indicates there is a high likelihood of mitochondrial localisation for MPC1 similar to the prediction values of other organisms with known MPC1 localisation. However, *P. falciparum* MPC2 has a lower prediction score compared to MPC2 from other organisms (Table 3.1). This predictive score indicates it is less likely that *P. falciparum* MPC2 is exported to the mitochondria compared to other organisms. However, *D. melanogaster* MPC2 had a 0.50 probability of mitochondrion localisation, but experiments showed mitochondrial localization. This is likely the case with *P. falciparum* MPC2, where the prediction score is lower than expected but the protein is localized to the mitochondria as part of the MPC heterocomplex. The lower prediction score for MPC2 may be a result of MitoProtI program limitations. The program predicts whether the N-terminus of a sequence can support a

mitochondrial targeting sequence and cleavage, however, the lack of information on mitochondrial targeting sequences in *P. falciparum* could skew these predictions [135].

**Table 3.1: Likelihood prediction of MPC1 and MPC2 export to the mitochondria in eukaryotic organisms.**

| Eukaryotic organism | Probability of protein export to the mitochondria (0-1 scale) | |
|---|---|---|
| | MPC1 | MPC2 |
| *H. sapiens* | 0.72 | 0.78 |
| *S. cerevisiae* | 0.91 | 0.97 |
| *D. melanogaster* | 0.80 | 0.50 |
| *T. cruzi* | 0.70 | 1.00 |
| *T. brucei* | 0.86 | 0.83 |
| *P. falciparum* | 0.89 | 0.43 |

## 3.2. *In vitro* cultivation of *P. falciparum* parasites

Asexual *P. falciparum* NF54 parasites were cultivated for multiple purposes such as transfection, genomic DNA isolation, SYBR green proliferation and pLDH viability assays. Asexual parasites successfully progressed through the 48 h cycle with ring stage parasites present at 1-16 h post invasion (hpi) of the erythrocyte (Figure 3.1A), noted by the thin chromatin ring surrounding the digestive vacuole. Trophozoites developed from 18-30 hpi, respectively, and as haemoglobin digestion occurs, the parasite's size increased and a dense hemozoin crystal became visible (Figure 3.1A). Schizonts formed between 36-48 hpi indicated by the multi-nucleated regions within the erythrocyte (Figure 3.1A) [136].

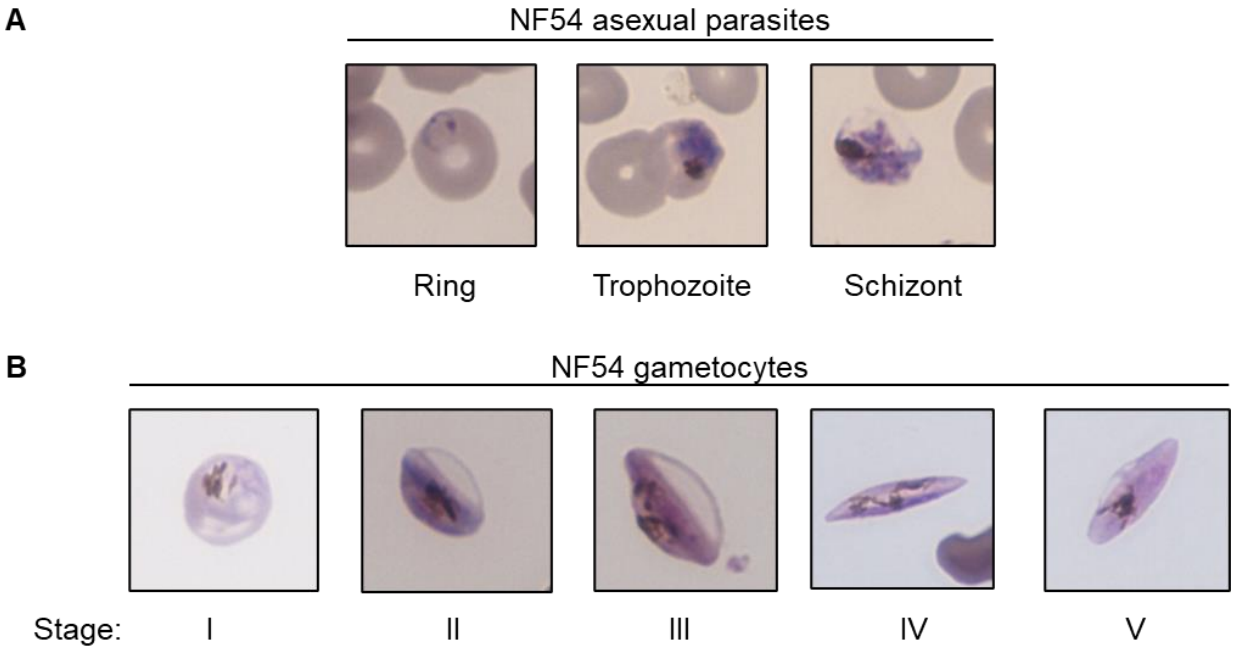


**Figure 3.4: *P. falciparum* NF54 parasite morphology. (A)** Asexual and **(B)** gametocyte NF54 parasites were routinely cultivated over the 48-h proliferation and 10-14 day growth period, respectively.

Immature gametocytes developed as expected from stage I, which are morphologically similar to trophozoites, to the lemon-shaped stage II to the more elongated D-shaped stage III and lastly to the maximally elongated stage IV with tapered ends (Figure 3.1B). Mature stage V gametocytes developed by day 10-12 of gametocytogenesis indicated by the distinct elongated and rounded edge form (Figure 3.1B) [20]. In conclusion, *P. falciparum* asexual and gametocyte parasites were successfully cultivated.

## 3.3. MPC inhibitor effect on *P. falciparum* parasites

The known MPC inhibitor, UK-5099 (Figure 3.5), was used as a chemical probe to interrogate its effect on *P. falciparum* NF54 parasite proliferation and viability. Previous, human MPC heterocomplex computational simulations with UK5099 suggest that this compound could prevent pyruvate transport across the IMM by occupying the predicted amino acid residues important for pyruvate binding (Figure 3.2) [134].

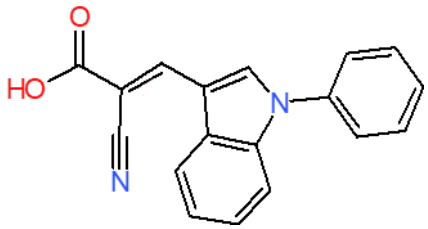


**Figure 3.5: The chemical structure of the MPC inhibitor, UK-5099.** UK-5099 was used to treat *P. falciparum* NF54 parasites to determine its effect on asexual proliferation and gametocyte viability.

The $IC_{50}$ of UK-5099 (inhibitory concentration needed to effectively inhibit 50 % of asexual parasite proliferation or early stage gametocyte viability) was determined, whilst controlling for the toxic effects of the solvent, DMSO on *P. falciparum* parasites at <0.1 % (w/v) [137]. UK-5099 treatment did not affect *P. falciparum* asexual proliferation below this vehicle threshold. The inhibitory effect of UK-5099 and DMSO was subsequently evaluated above the 0.1 % threshold and although UK-5099 treatment consistently resulted in inhibition of proliferation at both 62.5 µM and 125 µM compared to the respective 0.62 % and 1.25 % DMSO control, this difference was not statistically significant ($P > 0.05$, n=3, unpaired student t-test) (Figure 3.6). DMSO was found to be highly toxic to asexual parasites at >1.25 % and masked any potential inhibitory effect the compound would have on parasite proliferation. Therefore, due to the insolubility of the compound and limitations on the use of DMSO, this compound would be unsuitable for further biological interrogations against asexual parasites.

Similarly, UK-5099 was used to treat early stage gametocytes to evaluate its inhibitory effect on gametocyte viability. Early stage gametocyte viability was not affected below 100 µM UK-5099 treatment. Early stage gametocytes were more tolerable of DMSO compared to asexual parasites at higher concentrations as only an ~18 % and ~50 % gametocyte inhibition was noted at 1 % and 8 % DMSO treatment, respectively (Figure 3.6B). There was a statistically significant difference ($P \leq 0.05$, n=3, unpaired student t-test) between gametocyte inhibition at 1 % DMSO and 100 µM of UK-5099 with approximately double the inhibition noted in the inhibitor treated sample (Figure 3.6B). However, there was no significant differences ($P > 0.05$, n=3, unpaired student t-test) between the 8 % DMSO and 800 µM of UK-5099 treatment. The inhibitory effect of DMSO was most likely too great at 8 %, therefore, masking the inhibitory effect of UK-5099 on early stage gametocytes. Although UK-5099 inhibits gametocyte viability (~30 % inhibition) at 100 µM, this inhibitor would be unsuitable for gametocyte chemical interrogation studies due to the high concentration of UK-5099 needed to elicit an effect and DMSO toxicity.

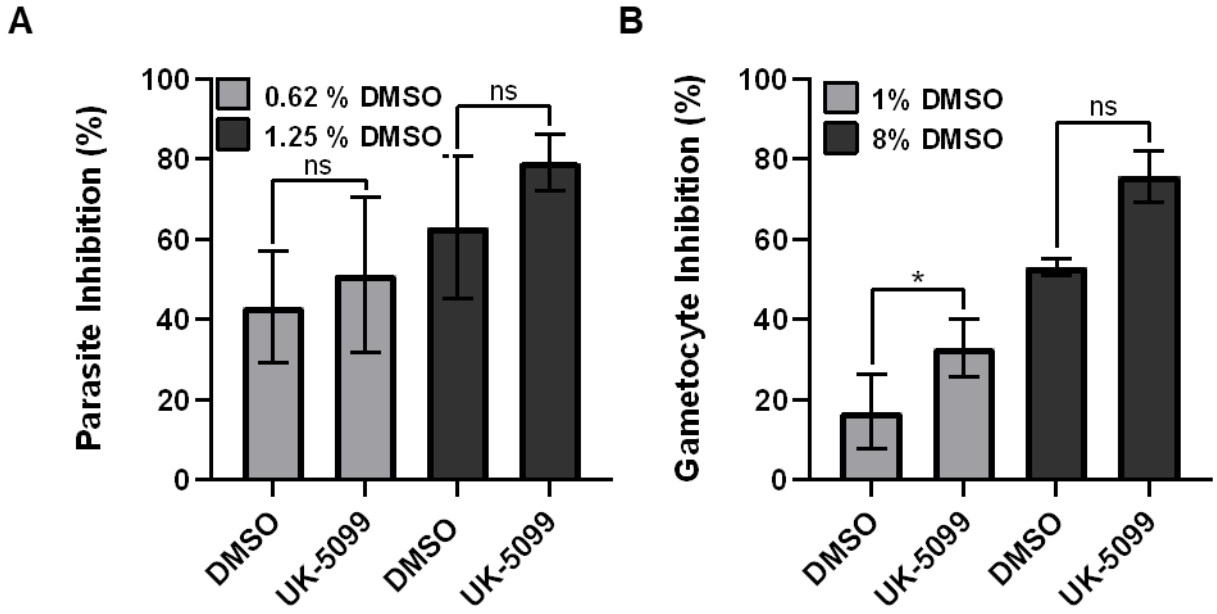


**Figure 3.6: The inhibitory effect of UK-5099 and DMSO on asexual parasites and early stage gametocytes.** **(A)** Asexual parasites (initiated treatment on ring stage parasites, 1 % parasitaemia, 1 % haematocrit, 96 h incubation) and **(B)** early stage gametocytes (initiated treatment on a stage II and III gametocyte culture, 1 % parasitaemia, 1 % haematocrit, 144 h incubation) were treated with of UK-5099 and DMSO to determine if an inhibitory effect above the vehicle control could be established. Data shown for n=3 independent biological repeats, performed in technical triplicates with error bars indicating ± S.E from an unpaired student t-test: ns: non-significant ($P>0.05$), * significant ($P<0.05$).

Given that we currently cannot determine the drug effect below the toxicity of the vehicle control, we cannot evaluate if the observed lack of effect is due to the experimental barrier created by the drug solubility, or whether there is a biological reason that prevents activity. Therefore, a MPC specific inhibitor with increased aqueous solubility would be required in

future studies to determine if MPC inhibition has an effect on asexual proliferation, gametocyte viability.

## 3.4. Genetic manipulation of putative MPCs to evaluate biological function

Two SLI-based genetic modification systems, SLI-TGD and SLI-*glmS*, were used to generate transgenic parasite lines with the aim to modify the native loci of *mpc1* and *mpc2* with a truncated tagged gene or insert a 3' tag to the 3' end of the gene, respectfully.

### 3.4.1. Investigation of MPC essentiality in asexual stage parasites using SLI-TGD

To generate a transgenic *P. falciparum* NF54 parasite line where the native *mpc1* and *mpc2* genes are replaced with a 3' GFP tagged truncated version, previously constructed pSLI-*mpc1*-GFP and pSLI-*mpc2*-GFP plasmids were used in this study (Figure 3.7 A). In summary, a 5' fragment of each *mpc* gene, *mpc1* (~194 bp) and *mpc2* (~298 bp), was successfully amplified and cloned into the pSLI-GFP plasmid (Figure 3.7 B). The plasmids were validated here with restriction enzyme digestion using the restriction enzymes *NotI* and *MluI*, which flank the 5' and 3' GOI region. The digestion of pSLI-*mpc1*-GFP and pSLI-*mpc2*-GFP yielded two distinct bands representative of the SLI-plasmid backbone (~6760 bp) and the *mpc* insert, *mpc1* (~194 bp) or *mpc2* (~298 bp), respectfully (Figure 3.7 C). The pSLI-*mpc1*-GFP (>50 µg with an $A_{260}/A_{280}$ ratio of 1.8) and pSLI-*mpc2*-GFP (>50 µg with an $A_{260}/A_{280}$ ratio of 1.9) recombinant plasmids were subsequently used in downstream experiments.

Recombinant pSLI-*mpc1*-GFP and pSLI-*mpc2*-GFP plasmids were transfected into a *P. falciparum* NF54 asexual parasite population (5% parasitaemia of >75 % ring stage parasites at a 5 % haematocrit). This was followed by a 10 day drug selection process with the antifolate drug, WR99210, to select for parasites that contain the plasmids episomally (Figure 3.8). After the selection period, parasite cultures were maintained under normal culturing conditions.

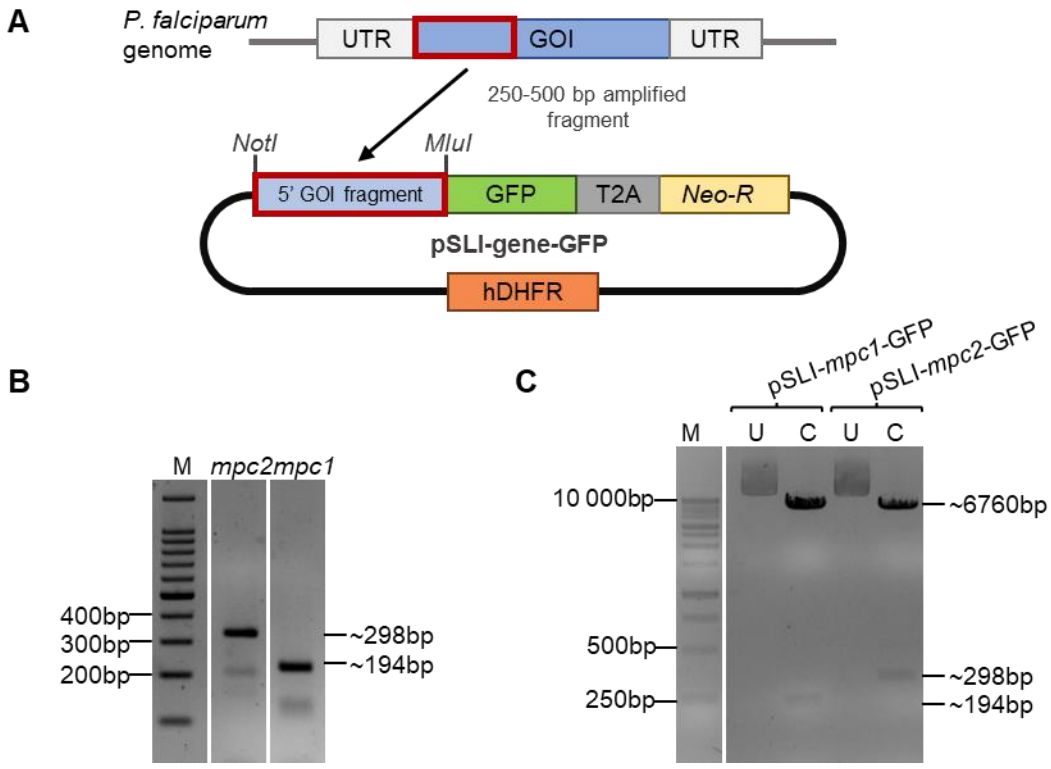


**Figure 3.7: Summary of pSLI-*mpc1*-GFP and pSLI-*mpc2*-GFP cloning and validation process.** Previously constructed pSLI-*mpc1*-GFP and pSLI-*mpc2*-GFP plasmids contain the necessary 5' *mpc* fragment to genetically disrupt the native *mpc* loci upon integration. **(A)** Schematic representation of the *mpc* fragment cloned into pSLI-GFP plasmids. **(B)** PCR amplification of the 5' fragments of *mpc1* and *mpc2* for incorporation into the pSLI-GFP plasmid. **(C)** Restriction enzyme digestion of the recombinant constructs with *NotI* and *MluI* validated the presence of respective *mpc* fragment inserts in each plasmid. U: undigested recombinant plasmid control and C: digested recombinant plasmid sample. All samples **(B and C)** were visualised on a 1.5 % (w/v) agarose/TAE gel with the 100 bp Promega (USA) molecular marker (M), stained in 0.5 µg/mL EtBr after electrophoresis. Complete gels for B and C are located in Supplementary Figure 1 and 2, respectively.

The electroporation process exerted a large amount of stress on the parasite and erythrocyte, often leading to some degree of erythrocyte lysis and parasite death. This was evident with the >3% parasitaemia drop from day 0 to day 2 of the selection process (Figure 3.8). WR99210 treatment had further reduced the parasitaemia to 0-0.5% by the end of the 10 day selection period (Figure 3.8). Approximately 22-26 days post-selection (32-36 days post-transfection), parasites were detected within each transfected culture that proliferated as expected over a 48 h period. Samples from the recovered parasite populations (>2 % parasitaemia, 5 % haematocrit) were used to isolate DNA to screen for the episomal presence of the respective plasmids using PCR (Figure 3.9). The SLI plasmids, pSLI-*mpc1*-GFP and pSLI-*mpc2*-GFP, transfected into NF54-epi(pSLI-*mpc1*-GFP) and NF54-epi(pSLI-*mpc2*-GFP) parasite lines were successfully detected with SLI-plasmid specific primers represented by the single bands at ~381 bp and ~486 bp found in Figure 3.9 B, respectively. This successful episomal detection indicated that the parasite lines could progress to the next drug selection cycle in an attempt to integrate the plasmid into the parasite genome.

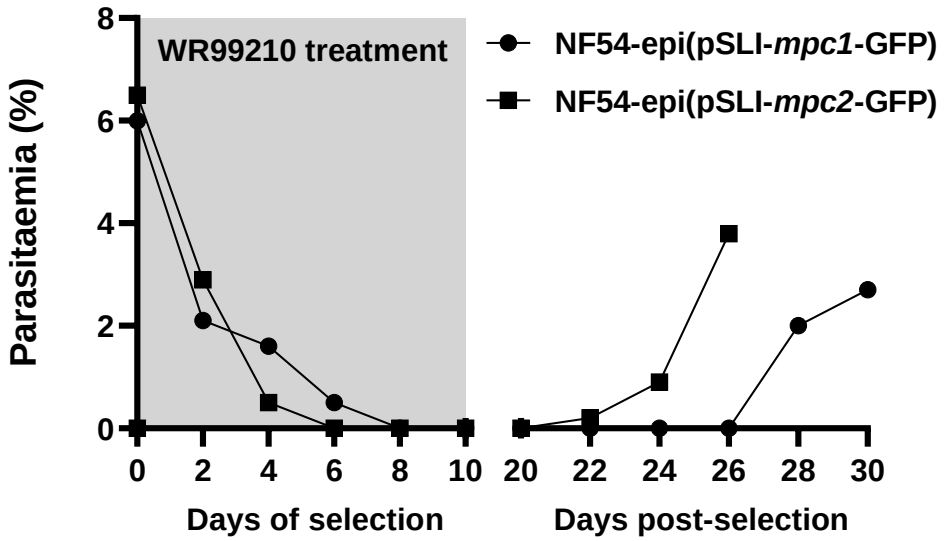


**Figure 3.8: Parasitaemia of *P. falciparum* NF54 parasites transfected with pSLI-*mpc1*-GFP and pSLI-*mpc2*-GFP during episomal selection and recovery.** *P. falciparum* NF54 parasites were transfected with pSLI-*mpc1*-GFP and pSLI-*mpc2*-GFP plasmids (day 0), followed by a 10 day WR99210 selection process (grey box) to select for parasites containing the plasmids episomally. Parasitaemia was monitored every second day post-transfection (selection period) and post-selection period with RapidDiff stained samples.

The final step to create parasite lines that can be used to determine the essentiality or dispensability of the *mpc1* or *mpc2* genes in *P. falciparum* parasites was to attempt to integrate each plasmid into the parasite's genome with a second cycle of drug selection for neomycin resistance. NF54-epi(pSLI-*mpc1*-GFP) and NF54-epi(pSLI-*mpc2*-GFP) parasite lines were treated with G418 for a 16 day period (Figure 3.10). The neomycin phosphotransferase protein conferring neomycin resistance will only be expressed following integration into the genome, under the control of GOI promoter. This drug selection cycle was performed on two independent biological parasite populations in triplicate for each line to ensure the outcome was a consequence of the drug cycling event and subsequently homologous region integration into the parasite genome.

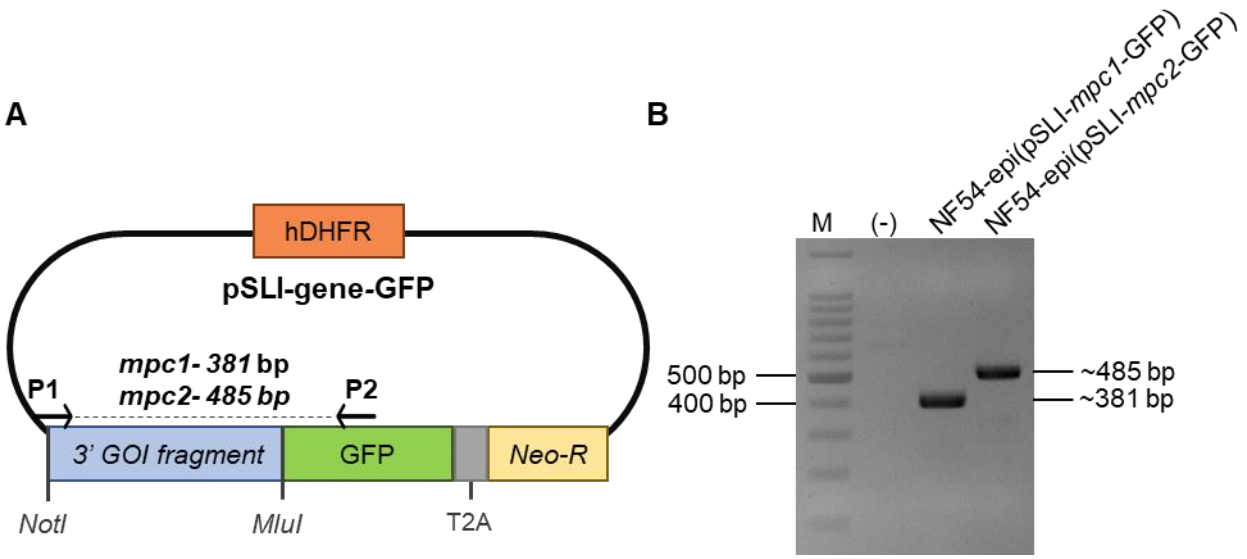


**Figure 3.9: PCR screening for episomal plasmid presence in NF54 parasites transfected with pSLI-*mpc1*-GFP and pSLI-*mpc2*-GFP plasmids. (A)** Schematic representation describing the primer location and amplified size for episomal confirmation of pSLI-*mpc1*-GFP and pSLI-*mpc2*-GFP plasmids in NF54 transfected parasites. **(B)** PCR amplification of the pSLI-*mpc1*-GFP (~381 bp) and pSLI-*mpc2*-GFP (~485 bp) plasmid to confirm the episomal presence each plasmid in the respective NF54 parasite lines. PCR products were visualised on an 1.5 % (w/v) agarose/TAE gel stained with EtBr (0.5 µg/mL) after electrophoresis. M: 100 bp molecular marker (Promega, USA), (-): PCR amplification with water as a substitute for the DNA template.

Parasite cultures showed a consistent and expected reduction in parasitaemia over the first 10 days of the drug selection with minimal to no parasites detected from day 10-16. After the 16 day selection period, parasite cultures were cultured without selection pressure under standard culturing conditions. After 30 days post-selection, no viable parasites reappeared in the two biological repeats of the two lines (Figure 3.10), NF54-epi(pSLI-*mpc1*-GFP) and NF54-epi(pSLI-*mpc2*-GFP), indicating that *mpc1* and *mpc2* are possibly essential to asexual parasite survival [102], since the presence of a truncated, non-functional protein would lead to parasite death. A further 10 days of recovery (40 days post-selection) still did not result in any parasite recovery. Alternatively, homologous recombination did not occur possibly due to the lack of a random double stranded break that occurred in the DNA near the *mpc1* and *mpc2* locus or integration did occur, but the native promoter was too weak to overcome G418 selection. Given that a transgenic parasite line with truncated MPC proteins could not be established, an alternative inducible system, the SLI-*glmS* system, was investigated to generate an inducible transgenic line. This was to confirm the possibility that these genes are essential to the parasite and to study these genes at specific stages in the parasite's life cycle.

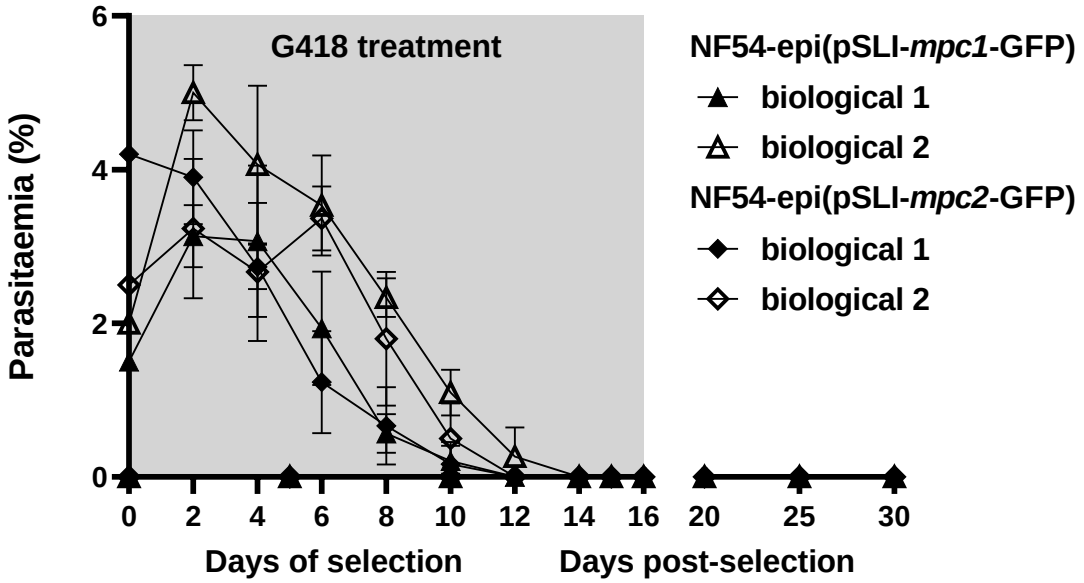


**Figure 3.10: Parasitaemia of *P. falciparum* NF54-epi(pSLI-*mpc1*-GFP) and NF54-epi(pSLI-*mpc2*-GFP) parasite lines during G418 selection and recovery.** NF54-epi(pSLI-*mpc1*-GFP) and NF54-epi(pSLI-*mpc2*-GFP) lines were treated with G418 for a 16 day period (grey box) followed by a recovery period. The parasitaemia of the parasite lines were monitored every second day with light microscopy. Data shows two biological repeats per episomal parasite line performed in triplicate and error bars are indicative of the standard deviation between triplicates.

### 3.4.2. Generation of conditional knockdown lines with the SLI-*glmS* system

The SLI-*glmS* conditional knockdown system allows on-demand reduction of *mpc1* and *mpc2* expression to evaluate the phenotypic effect this has on the parasite. Previously constructed pSLI-*mpc1-glmS*, pSLI-*mpc2-glmS*, pSLI-*mpc1-glmS-mut*, pSLI-*mpc2-glmS-mut* recombinant plasmids were used to generate these conditional knockdown lines (Figure 3.11A). The respective plasmids contained a 3' *mpc* gene fragment of *mpc1* (~389 bp) or *mpc2* (~551 bp) upstream to the GFP tag. The 3' *mpc* fragments were successfully amplified and cloned into pSLI-*glmS/glmS-mut* plasmids (Figure 3.11B). Digestion of pSLI-*mpc1-glmS/glmS-mut* and pSLI-*mpc2-glmS/glmS-mut* plasmids using *NotI* and *MluI* restriction enzymes indicated two bands as expected of the linear plasmid backbone (~6760 bp) and the *mpc* insert, *mpc1* (~389 bp) and *mpc2* (~551 bp) (Figure 3.11C). The recombinant plasmids, pSLI-*mpc1-glmS/glmS-mut* (>100 µg with an A260/A280 ratio of 1.7) and pSLI-*mpc2-glmS/glmS-mut* (>150 µg with an A260/A280 ratio of 1.9), were used in subsequent experiments

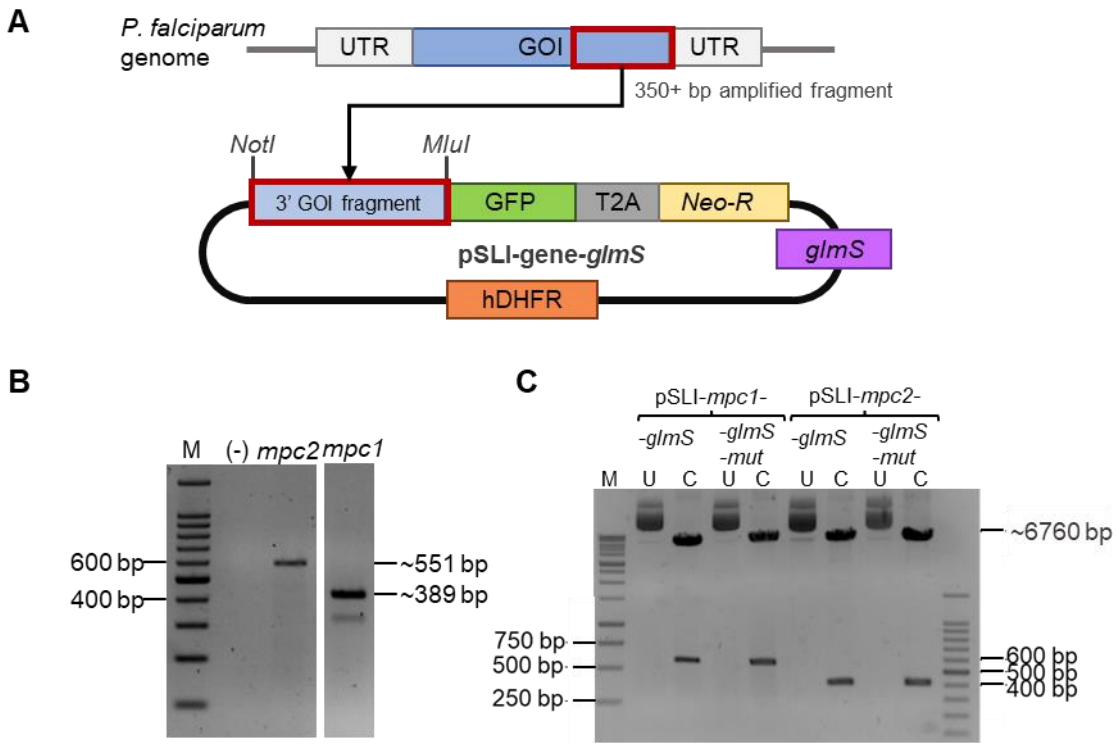


**Figure 3.11: Summary of pSLI-*mpc1-glmS/glmS-mut* and pSLI-*mpc2-glmS/glmS-mut* cloning and validation process.** Previously constructed pSLI-*mpc1-glmS/glmS-mut* and pSLI-*mpc2-glmS/glmS-mut* plasmids contain a 3' *mpc* gene fragment to conditionally knockdown the native mpc loci upon integration. **(A)** Schematic representation of the *mpc* fragment cloned into pSLI-*glmS/glmS-mut* plasmids. **(B)** PCR amplification with plasmid specific primers of the 3' fragments of *mpc1* and *mpc2* represented on an 1.5 % (w/v) agarose/TAE gel with the 100 bp Promega (USA) molecular marker (M). Complete gel located. **(C)** Recombinant constructs were restriction enzyme digested with *NotI* and *MluI* validated the presence of respective mpc fragment inserts in each plasmid. PCR products and digested constructs visualised on 1.5 % (w/v) agarose/TAE gel with the **(B)** 100 bp (M) and **(C)** 1 Kb Promega (USA) (M) molecular marker, respectively. U: undigested plasmid sample, C: digested plasmid samples. All agarose gels were stained with 0.5 µg/mL EtBr after electrophoresis. Complete gel for B is located in supplementary Figure 1.

Recombinant pSLI-*mpc1-glmS/glmS-mut* or pSLI-*mpc2-glmS/glmS-mut* plasmids were transfected into a *P. falciparum* NF54 parasite culture (>6 % parasitaemia of >75 % ring stage parasites at 5 % haematocrit) with electroporation. The transfected cultures placed under drug selection with WR99210 in the same manner as the SLI-TGD system. During the first four days of the selection cycle, the parasitaemia reduced by 2-4 % every second day due to the combined stress of electroporation and selection pressure. From day four to ten of the selection pressure, the parasitaemia reduced until minimal to no parasites were detected with light microscopy (Figure 3.12).

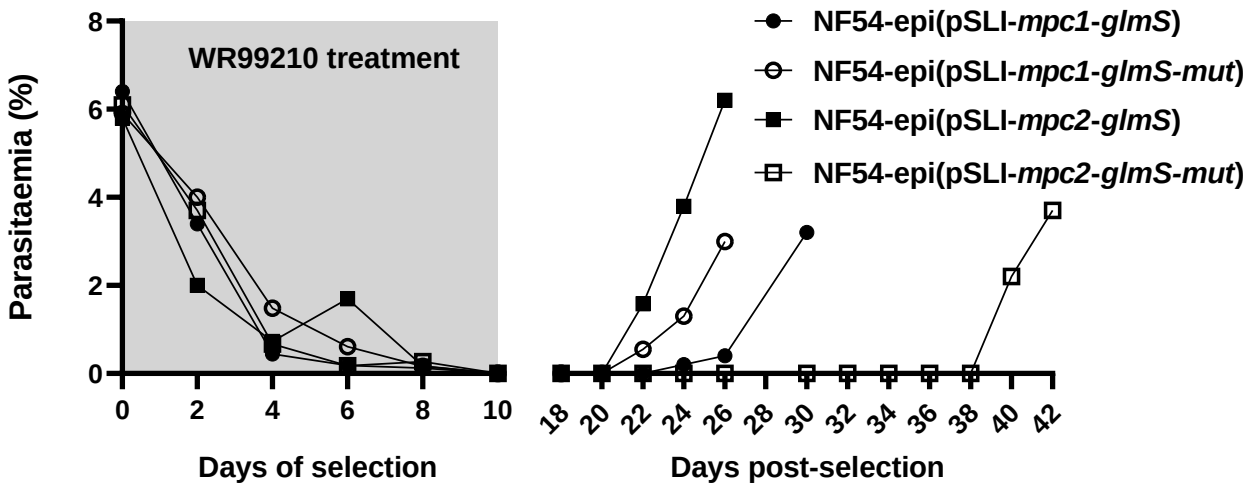


**Figure 3.12: Parasitaemia of *P. falciparum* NF54 parasites transfected with pSLI-*mpc1-glmS/glmS-mut* and pSLI-*mpc2-glmS/glmS-mut* during episomal selection and recovery.***P. falciparum* NF54 parasites were transfected with pSLI-*mpc1-glmS/glmS-mut* and pSLI-*mpc2-glmS/glmS-mut* plasmids (day 0). Electroporation was followed by a 10 day WR99210 selection process (grey box) to select for parasites with episomally present plasmids. Parasitaemia was monitored every second day post-transfection (selection period) and post-selection period with RapidDiff stained samples.

Parasites re-emerged from day 20-38 post-selection period (30-48 days post-transfection) proliferating as expected through the parasite life cycle. Recovered parasite cultures, with a parasitaemia >2 %, were used to isolate genomic and plasmid DNA to screen the population for the episomal presence of the pSLI-*mpc1-glmS/glmS-mut* or pSLI-*mpc2-glmS/glmS-mut* plasmids. PCR amplification of *mpc1* (~576 bp) and *mpc2* (~738 bp) 3' gene fragments confirmed that the plasmids were taken up into the parasite's cytosol (Figure 3.13B).

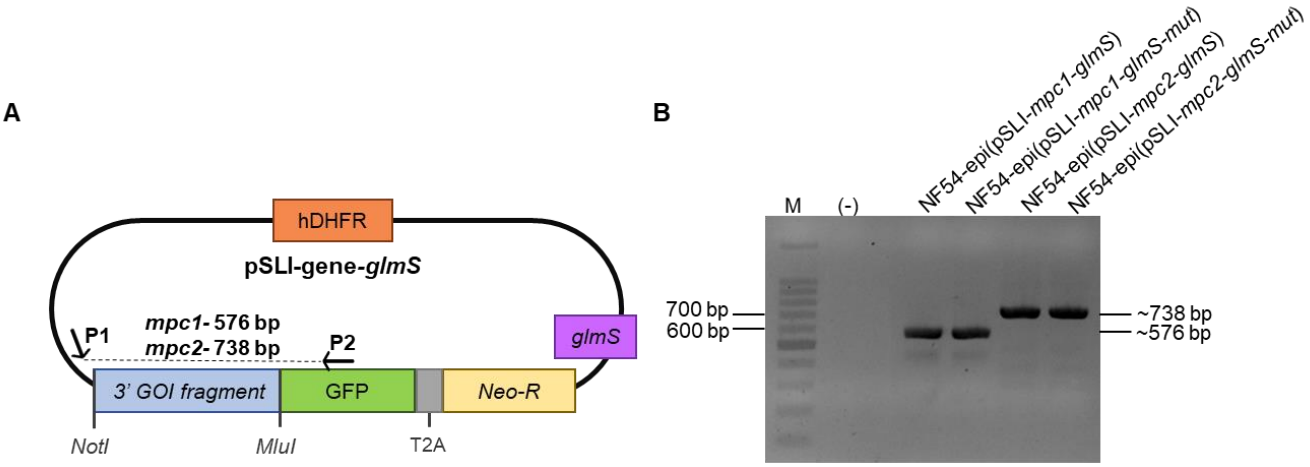


**Figure 3.13: PCR confirmation of the episomal uptake into NF54 parasites transfected with pSLI-*glmS/glmS-mut*.(A)** Schematic representation of the region of interest amplified by plasmid specific primers to confirm episomal uptake within the parasite. **(B)** PCR amplification of the pSLI-*mpc1-glmS* (~576 bp) and pSLI-*mpc2-glms-mut* (~738 bp) plasmid backbone confirming the episomal presence each plasmid in NF54 parasites. PCR products were visualised on an 1.5 % (w/v) agarose/TAE gel stained with EtBr (0.5 µg/mL) after electrophoresis.

The NF54-epi(pSLI-*mpc1-glmS/glmS-mut)* and NF54-epi(pSLI-*mpc2-glmS/glmS-mut)* parasite lines were exposed to a second drug pressure with G418 (400 µg/mL) similarly to the SLI-TGD system to force genomic integration of the SLI-*mpc1* or *mpc2-glmS/glmS-mut* plasmids. During this period, the parasitaemia slowly declined over the 16 day drug period until no parasites were detected with microscopy (Figure 3.14). During the recovery period, the parasite cultures were cultured under standard conditions. Unexpectedly, the SLI technique did not generate integrated conditional knockdown lines, with complete *P. falciparum* death observed after 30 days post-selection. A second integration attempt with G418 (400 µg/mL) had the same results (Suppletory Figure 3). This could not be as a result of truncated versions of MPC1 and MPC2 being produced as above but could indicate there is no homologous recombination occurring with the genome possible due to the lack of random breaks in the DNA. Alternatively, the *mpc* native promoter is incapable of overcoming G418 selection.

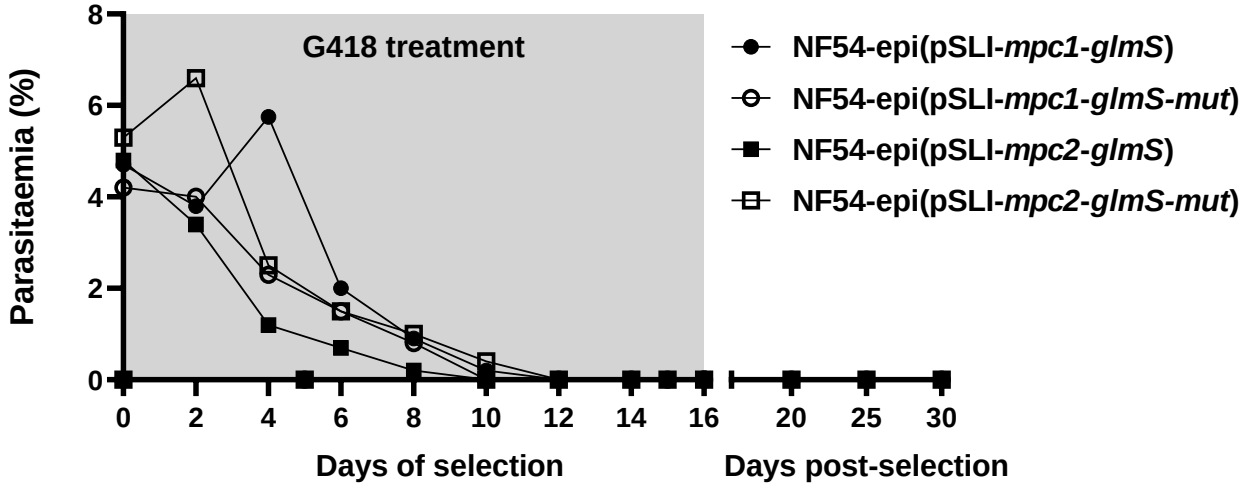


**Figure 3.14: Parasitaemia of *P. falciparum* NF54-epi(pSLI-*mpc1-glmS/glmS-mut*) and NF54-epi(pSLI-*mpc2-glmS/glmS-mut*) parasite lines during G418 selection and recovery.** NF54-epi(pSLI-*mpc1- glmS/glmS-mut*) and NF54-epi(pSLI-*mpc2- glmS/glmS-mut*) parasite lines were treated with G418 (400 µg/mL) for a 16 day period (grey box) followed by a recovery period. The parasitaemia of each line was monitored every second day with light microscopy.

In an attempt to circumvent premature parasite death from G418 pressure, the selection pressure was repeated on NF54-epi(pSLI-*mpc1-glmS/glmS-mut)* and NF54-epi(pSLI-*mpc2-glmS/glmS-mut)* for a 16 day period with reduced G418 concentrations of 300 µg/mL and 200 µg/mL to overcome the unexpected parasite sensitivity towards G418. Despite these efforts, an integrated line could not be established after the G418 selection period as either parasites did not re-emerge or only the wild type parasite was present (Supplementary Figure 3 and 4). Therefore, it was decided to establish an ectopic expression system where the effect of simultaneous expression of *mpc1* and *mpc2* could be investigated.

### 3.4.3. Generation of an MPC ectopic expression line

The previous genetic disruption and knockdown strategies that were tested relied on reducing *mpc* gene expression at the native loci under the control of the native promoter. These strategies focused on a single component of the MPC heterocomplex since the removal of a subunit should be sufficient to abrogate MPC heterocomplex function. This would have had the additional advantage of investigating the individual contribution of MPC1 or MPC2. However, these were unsuccessful at generating an integrated line that could be used to investigate MPC biology. An alternative strategy using the Bxb1 ectopic expression system was investigated where both *mpc1* and *mpc2* genes were inserted at an alternative locus under the calmodulin promoter. This would enable the simultaneous ectopic expression of *mpc1* and *mpc2* for increased MPC heterocomplex production.

#### 3.4.3.1. Cloning the *mpc1-myc-mpc2-HA* fragment into Bxb1 ectopic expression system

To develop this ectopic expression line, the *in silico* designed *mpc1-myc-mpc2-HA* fragment (Figure 2.5) was commercially synthesised for subsequent cloning into the pCR2.1-*cam-glmS/glmS-mut* plasmids. The synthesised fragment was enzymatically digested from the pUC57-*mpc1-myc-mpc2-HA* plasmid with the restriction enzymes, *SalI* and *StuI*, which yielded three bands at approximately 4000, 3000 and 891 bp (Figure 3.15). These bands were indicative of a linearised pUC57-*mpc1-myc-mpc2-HA* (4000 bp), the linearised pUC57 backbone without the insert (3000 bp) and the *mpc1-myc-mpc2-HA* insert (891 bp).

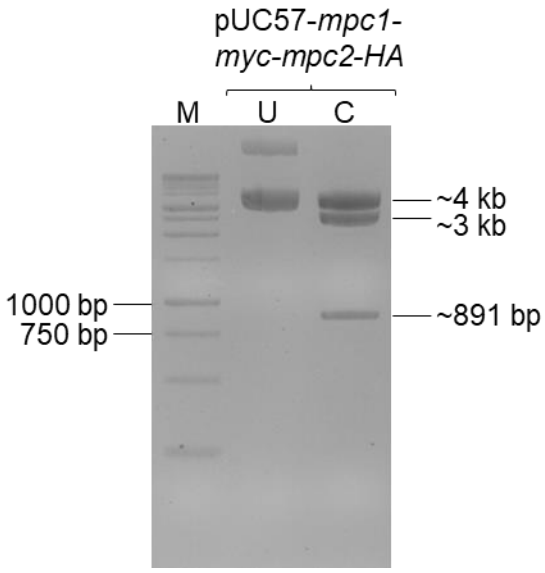


**Figure 3.15: Restriction enzyme digest of pUC57-*mpc1-myc-mpc2-HA*.** The pUC57-*mpc1-myc-mpc2-HA* plasmid was digested with *SalI* and *StuI* restriction enzymes and visualised on a 1.5 % (w/v) agarose/TAE gel with the 1Kb Promega (USA) molecular marker (M), stained with 0.5 µg/mL EtBr after electrophoresis, to separate the synthesized *mpc1-myc-mpc2-HA* fragment (~891 bp) from the plasmid backbone (~3000 bp). U: undigested plasmid sample, C: digested plasmid sample.

In preparation of producing the pCR2.1-*cam-mpc1-myc-mpc2-HA-glmS* and pCR2.1-*cam-mpc1-myc-mpc2-HA-glmS-mut* constructs, the pCR2.1-*cam-glmS* (584 ng/µL with an $A_{260}/A_{280}$ ratio of 1.8) and pCR2.1-*cam-glmS-mut* (289 ng/µL with an $A_{260}/A_{280}$ ratio of 1.9) plasmids were enzymatically digested with *SalI* and *StuI* similarly to pUC57-*mpc1-myc-mpc2-HA* to confirm plasmid identity as well as to isolate the plasmid backbone needed for downstream ligation experiments. The two plasmids were successfully digested indicated by the two distinctive bands at approximately 10 Kb and 1100 bp representative of the plasmid backbone and insert, respectively (Figure 3.16).

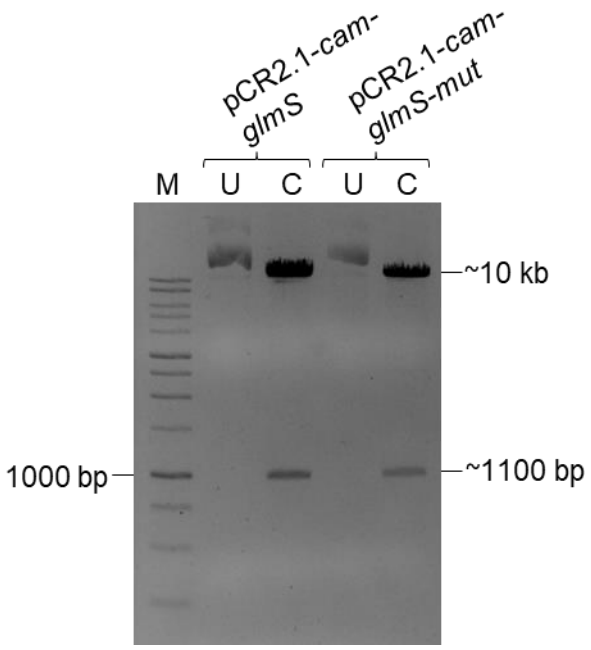


**Figure 3.16: Restriction enzyme digest of pCR2.1-*cam-glmS* and pCR2.1-*cam-glmS-mut*.** Plasmids, pCR2.1-*cam-glmS* and pCR2.1-*cam-glmS-mut* were digested with *SalI* and *StuI* restriction enzymes in preparation for cloning the *mpc1-myc-mpc2-HA* insert into these plasmid backbones. Digested plasmids were visualised on a 1.5 % (w/v) agarose/TAE gel stained with EtBR 0.5 µg/mL after electrophoresis. M: 1Kb molecular marker (Promega, USA), U: undigested plasmid, C: digested plasmid sample.

The purified *mpc1-myc-mpc2-HA* insert (6.1 ng/µL with an $A_{260}/A_{280}$ ratio of 2.0) was ligated to the purified plasmid backbones of pCR2.1-*cam-glmS* (21 ng/µL with an $A_{260}/A_{280}$ ratio of 1.9) and pCR2.1-*cam-glmS-mut* (12 ng/µL with an $A_{260}/A_{280}$ ratio of 1.7) and subsequently transformed into competent *E. coli* DH5α cells. Randomly selected bacterial colonies were PCR screened for the presence of the *mpc1-myc-mpc2-HA* insert with plasmid specific primers to confirm the success of the cloning process (Figure 3.17A). Recombinant pCR2.1-*cam-mpc1-myc-mpc2-HA-glmS* and pCR2.1-*cam-mpc1-myc-mpc2-HA-glmS*-mut plasmids were successfully detected, indicated by the approximate 1012 bp band visualised on the agarose/TAE gel representative of the *mpc1-myc-mpc2-HA* insert and flanking plasmid regions (Figure 3.17B).

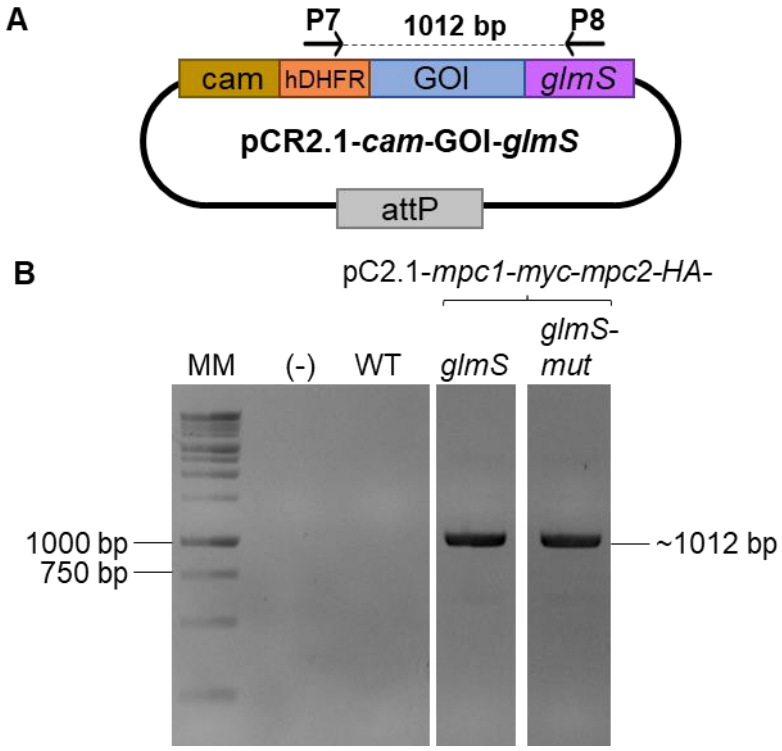


**Figure 3.17: Bacterial colony screening for a recombinant pCR2.1-*cam-glmS* and *pCR*2.1-*cam-glmS* plasmid. (A)** Schematic representation of the 1012 bp region amplified by the plasmid specific primers to confirm the presence of a recombinant pCR2.1-*cam-mpc1-myc-mpc2-HA-glmS/glmS-mut* plasmids. **(B)** Bacterial colonies were screened for recombinant pCR2.1 plasmids with the *mpc1-myc-mpc2-HA* insert indicated by the 1012 bp band. PCR products were visualised on a 1.5 % (w/v) agarose/TAE gel stained with 0.5 µg/mL EtBr after electrophoresis. M: 1Kb molecular marker (Promega, USA), (-): no template control and (WT): LB-broth inoculated with water to indicate a negative screen. Complete gel located in Supplementary Figure 5.

These recombinant plasmids were further screened with restriction enzyme digestion to confirm the insert size and that the *SalI* and *StuI* cloning sites flanking the *mpc1-myc-mpc2-HA* insert were not disrupted. Two bands of the expected ~10 Kb and ~891 bp sizes were visualized on the agarose/TAE gel representing the recombinant pCR2.1-*cam-glmS/glmS-mut* backbone and *mpc1-myc-mpc2-HA* insert, respectfully (Figure 3.18A). Lastly, the insert identity was evaluated on the nucleotide level through Sanger sequencing. The combination of the chromatogram data and consensus sequence, produced from the overlapping forward and reverse sequences, allowed evaluation of the *mpc1-myc-mpc2-HA* insert, flanking cut sites and plasmid regions which indicate there were no discrepancies on the nucleotide level of the recombinant pCR2.1-*cam-mpc1-myc-mpc2-HA-glmS* and *-glmS-mut* plasmids (Figure 3.18B). Therefore, the *mpc1-myc-mpc2-HA* insert was successfully cloned into the pCR2.1-*cam-glmS/glmS-mut* plasmids and was used in the development of an ectopically expressed *mpc* line.

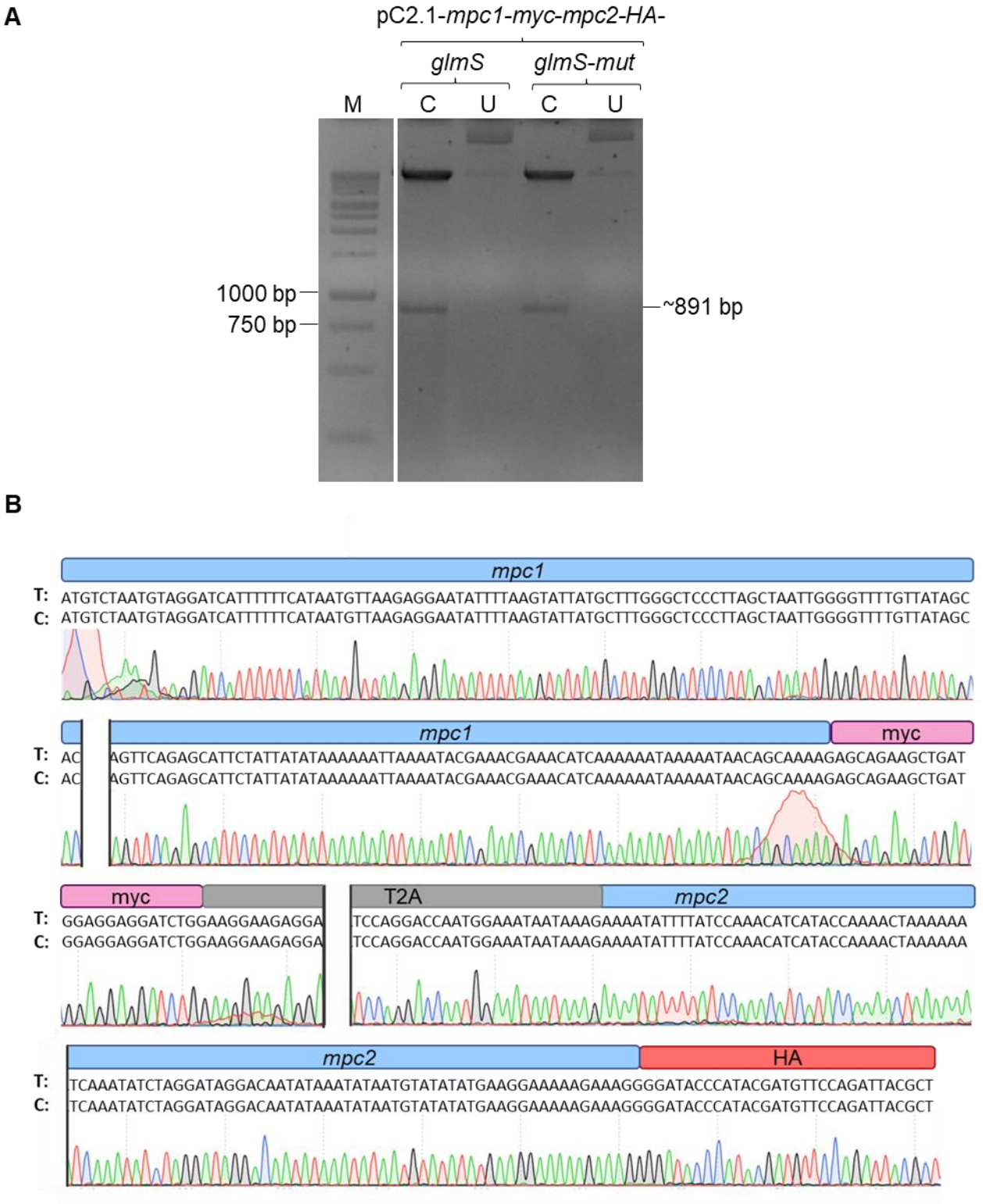


**Figure 3.18: Validation of recombinant pCR2.1-*cam-mpc1-myc-mpc2-HA-glmS* and pCR2.1-*cam-mpc1-myc-mpc2-HA-glmS-mut* plasmids. (A)** Restriction enzyme mapping of the recombinant pCR2.1-*cam-mpc1-myc-mpc2-HA-glmS* and pCR2.1-*cam-mpc1-myc-mpc2-HA-glmS-mut* plasmids with the *SalI* and *StuI* restriction enzymes. Digested constructs were visualized on a 1.5 % (w/v) agarose/TAE gel stained with EtBr 0.5 µg/mL. M: 1Kb molecular marker (Promega, USA), U: undigested plasmid sample and C: digested plasmid sample. Complete gel located in Supplementary Figure 6. **(B)** Sequence alignments of the recombinant plasmids to confirm the insert nucleotide identity. Partial consensus sequence of the insert cloned into the pCR2.1- pCR2.1-*cam-mpc1-myc-mpc2-HA-glmS* was indicated with the associated chromatogram, representative of the pCR2.1- pCR2.1-*cam-mpc1-myc-mpc2-HA-glmS-mut* sequence. T: template sequence, C: consensus sequence, white gaps indicates where sequences are not shown.

### 3.4.3.2. Generation of ectopic expression lines in *P. falciparum*

To produce a *P. falciparum* line capable of expressing the *mpc* genes above the basal level of expression, the recombinant pCR2.1-*cam-mpc1-myc-mpc2-HA-glmS* and pCR2.1-*cam-mpc1-myc-mpc2-HA-glmS*-mut plasmids must integrate into the *cg6* gene at the attB site, in an NF54$^{attB}$ parasite population, homologous to the attP site facilitated by the Bxb1 integrase found in the pINT-myc-mut plasmid. This is possible through a dual-plasmid transfection with pINT-myc-mut and either pCR2.1-*cam-mpc1-myc-mpc2-HA-glmS* and pCR2.1-*cam-mpc1-myc-mpc2-HA-glmS*-mut plasmids.

A 1:1 ratio of the pINT-myc-mut and either pCR2.1-*cam-mpc1-myc-mpc2-HA-glmS* or pCR2.1-*cam-mpc1-myc-mpc2-HA-glmS*-mut plasmids were transfected into a *P. falciparum* NF54$^{attB}$ parasite culture (>5 % parasitaemia, >75 % ring stage parasite culture at 5 % haematocrit) with electroporation. The transfected cultures were dual-drug pressured with G418 and WR99210 for a 6 day period followed by a final 4 day drug period with WR99210 only. Over the 10 day drug cycle, the parasitaemia reduced drastically with minimal to no parasites detected with light microscopy by the end of the selection pressure (Figure 3.19). During the post-selection period, the parasite cultures were maintained under standard culturing conditions and monitored weekly for parasite re-emergence. Parasites re-emerged 20 days post-selection (30 days post-transfection) in the culture transfected with the pCR2.1-*cam-mpc1-myc-mpc2-HA-glmS* plasmid. From this point, this parasite line was referred to as NF54-*cam-mpc1-myc-mpc2-HA-glmS.* Parasites transfected with pCR2.1-*cam-mpc1-myc-mpc2-HA-glmS-mut* did not re-emerge during the post-selection period. Therefore, the NF54-*cam-mpc1-myc-mpc2-HA-glmS-mut* ectopic expression line could not be generated.

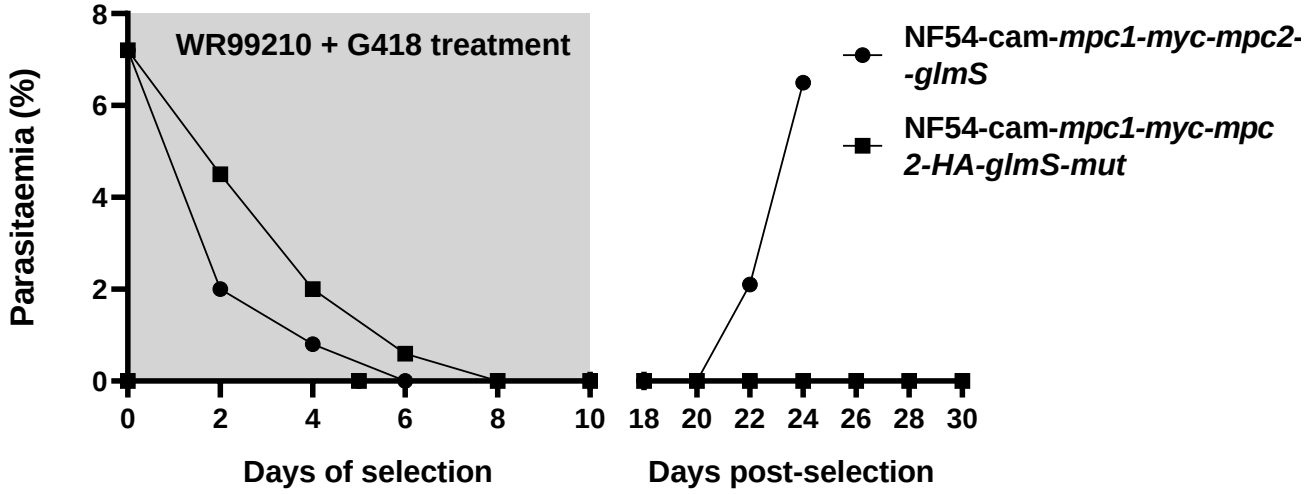


**Figure 3.19 Parasitaemia of *P. falciparum* transfected *P. falciparum* NF54$^{attB}$ parasites during G418 and WR99210 selection and recovery.** Parasites were transfected with pCR2.1-*cam-mpc1-myc-mpc2-HA-glmS* and *glmS-mut*, after which, the culture underwent a dual-drug cycle with WR99210 and G418 to simultaneously select for parasites containing the plasmid of interest as well as for integrated parasites, respectively.

Genomic integration in the suspected transgenic NF54-*cam-mpc1-myc-mpc2-HA-glmS* parasite line (>2% parasitaemia) was assessed with a PCR screen using *cg6* gene specific primers to flank the 5' and 3' surrounding regions to the site of integration (Figure 3.20A).

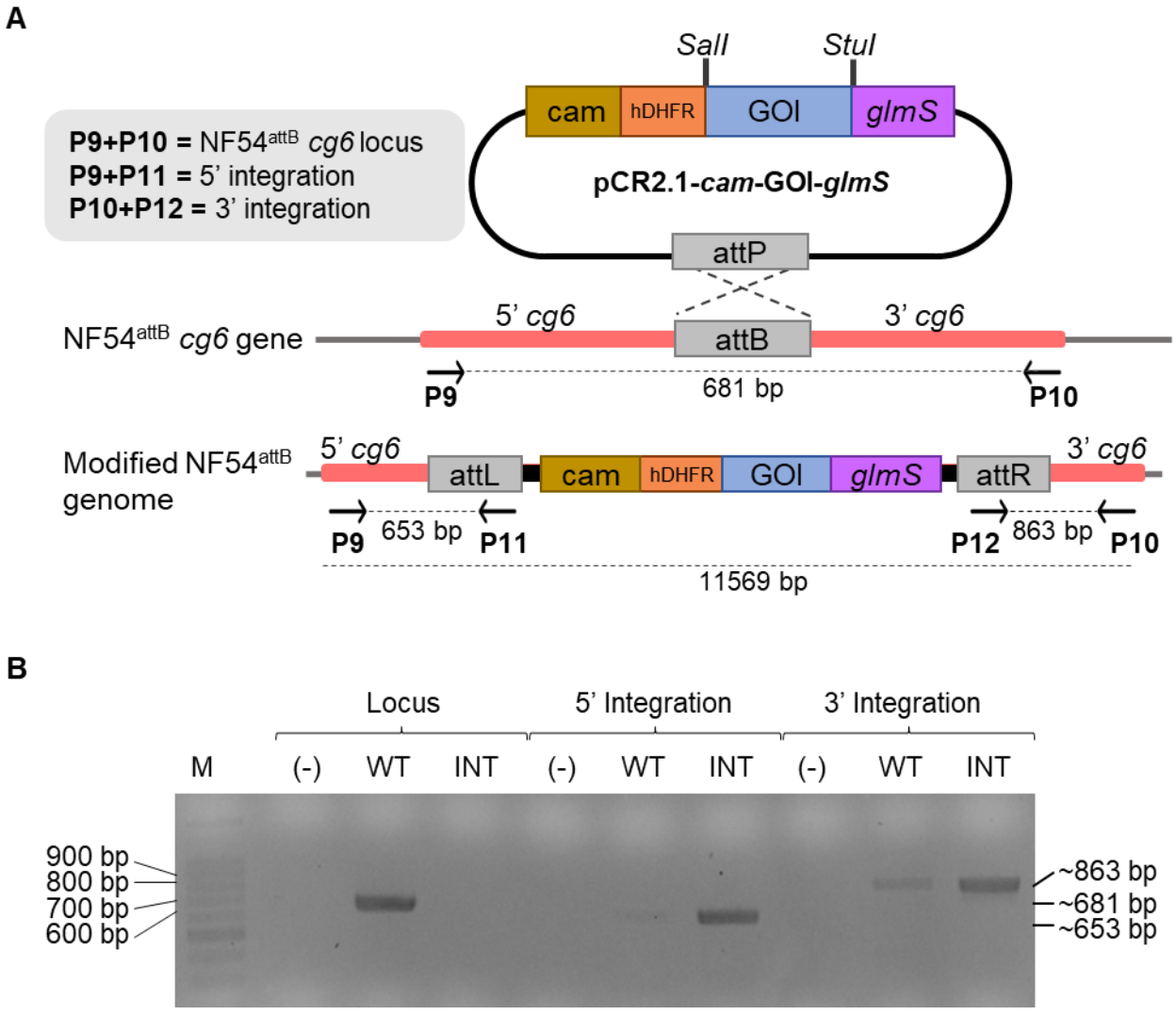


**Figure 3.20: Genomic integration confirmation of the NF54-*cam-mpc1-myc-mpc2-HA-glmS* parasite line. (A)** Schematic representation of the primer pair location and amplified region to detect genomic integration in NF54$^{attB}$ parasites transfected with recombinant pCR2.1-*cam-glmS*. **(B)** Parasite population suspected of integrating the cammpc1-myc-mpc2-HA cassette were PCR screened for the presence of the 5' and 3' amplified region as well as the absence of the locus region. The NF54-*cam-mpc1-myc-mpc2-HA-glmS* parasite line was successfully integrated with visible 5' (653 bp) and 3' (863 bp) fragments and the lack of a loci detected in the parasite line under investigation. PCR products were visualised on a 1.5 % (w/v) agarose/TAE gel stained with 0.5 µg/mL EtBr after electrophoresis. M: 100 bp molecular marker (Promega, USA). (-): negative control without template DNA in PCR, WT: NF54$^{attB}$ wildtype parasite template DNA, INT: NF54-*cam-mpc1-myc-mpc2-HA-glmS* parasite line template DNA.

The NF54-*cam-mpc1-myc-mpc2-HA-glmS* parasite line was partially integrated as the population retained some wild type parasite populations indicated through PCR amplification of the original *cg6* gene fragment (Supplementary Figure 7). The parasite line was subjected to a second round of drug pressure with only WR99210 for 6 days to clear the parasite populations that do not have genomic integration at the *cg6* gene (Supplementary Figure 8).

The parasitaemia of the NF54-*cam-mpc1-myc-mpc2-HA-glmS* parasite line had reduced over a 10 day selection and recovery period to <1 %. However, parasites were successfully proliferating by 8 days post-selection (Supplementary Figure 8). The NF54-*cam-mpc1-myc-mpc2-HA-glmS* parasite line was tested with PCR for pure genomic integration as above. A pure integrated transgenic line was obtained with the 5' and 3' region detectable at ~653 bp and ~863 bp (Figure 3.20B) only in the transgenic line, respectfully. Additionally, this was further validated by the lack of amplification of the ~681 bp locus band detectable in NF54$^{attB}$ wild-type parasite sample. This integrated NF54$^{attB}$ -*cam-mpc1-myc-mpc2-HA-glmS* parasite line can be used in future studies to co-localise the MPC proteins as well as to determine the biological effect an increased *mpc* gene expression would have on the asexual *P. falciparum* parasite proliferation, as well as sexual gametocyte differentiation.

# 4. Discussion

The *P. falciparum* parasite has distinct energy production dynamics that differ between the intraerythrocytic stages: the proliferative asexual stage and the slow-maturing gametocyte stage. Asexual parasites rapidly proliferate within a 48 h cycle in which multiple processes occur seamlessly, partially as a result of rapid energy production with anaerobic glycolysis [65]. Anaerobic glycolysis metabolises the extracellularly sourced glucose to produce pyruvate, that is converted to lactate and subsequently exported from the cytosol. The abnormal energy production of an asexual parasite closely resembles that of a cancerous cell, which is predominantly focused on proliferating [64]. However, the slower developing gametocyte, over a 10–14 day period, has a less rapid demand for energy production allowing the cell to revert back to a canonical means of energy production using the efficient mitochondrial-based processes: the TCA cycle and oxidative phosphorylation [65, 138]. Pyruvate produced from glycolysis is shuttled into the mitochondria for further metabolising by the TCA cycle and oxidative phosphorylation. Although these intraerythrocytic stages rely on the metabolism of extracellular glucose, the metabolic path of pyruvate differs in that gametocytes require the shuttling of pyruvate across mitochondrial membranes, unlike asexual parasites. These defined energy production dynamics highlighted the incomplete understanding surrounding the metabolic path of pyruvate, in particular, the biology of its transport across the mitochondria and whether this biology is specific to gametocytes. Mitochondrial pyruvate translocation had remained elusive until the molecular identification of a two-subunit pyruvate specific symporter, the MPC heterocomplex, in humans, yeast and other organisms [84, 85]. However, an MPC heterocomplex and the associated proteins, MPC1 and MPC2, have not yet been characterised in *P. falciparum* apart from the putative annotations of the *mpc1 and mpc2* genes.

This study was focused on investigating the function and essentiality of putative mitochondrial pyruvate carriers suspected of forming an MPC heterocomplex in the intraerythrocytic *P. falciparum* parasites. For this study, a chemical and genetic approach was investigated to interrogate MPC-related parasite biology. For the chemical approach, an MPC inhibitor was used to chemically interrogate the parasite's proliferative and viability response through biochemical assays to determine the inhibitors usefulness as a future chemical interrogator for parasite MPC biology. The genetic approach involved the attempt to generate transgenic parasite lines which could genetically disrupt and conditionally knockdown the putative *mpc1* and *mpc2* genes as well as an alternative Bxb1 ectopic expression system to overexpress *mpc1* and *mpc2* genes. Multiple genetic editing techniques were employed in hopes that these transgenic parasite lines in combination with a chemical interrogator would aid in gaining a full

perspective surrounding absent and excess MPC phenotypes at different intraerythrocytic stages.

UK-5099 dissolved in DMSO, is a commonly used chemical interrogator of MPC biology in other eukaryotes. UK-5099 inhibition toward *P. falciparum* asexual parasite proliferation and gametocyte viability was evaluated using whole-cell biochemical assays. However, whole-cell parasite treatment with UK-5099 did not yield nanomolar activity similar to the isolated mammalian mitochondrial treatments found in literature [99]. Although mitochondrial isolation was not logistically viable on a <5 µm sized asexual parasite, the whole-cell treatment does pose additional difficulties for inhibitor uptake as the inhibitor would be required to pass through four membranes to reach the parasites cytosol prior to acting on the putative MPC heterocomplex. These obstacles could reduce the free inhibitor concentration which reaches the complex. UK-5099 whole-cell treatment on the larger apicomplexan extracellular parasite, *T. brucei*, was able to significantly reduce oxygen respiration rates and increase intracellular pH by preventing pyruvate translocation across the plasma membrane from >200 µM [139]. It was proposed that the high concentration of UK-5099 needed to impose an effect on pyruvate uptake or efflux from the parasite indirectly indicated that the pyruvate carrier has a low affinity toward UK-5099 [139]. However, a lower concentration of UK-5099 (10 µM) was needed to elicit an effect on isolated mitochondria and subsequent MPC-related pyruvate transport [90]. *P. falciparum* whole-cell treatment at this concentration range (>200 µM) could not be achieved due to solubility and toxicity issues with UK-5099. Additionally, there are reports that UK-5099 availability could also be reduced by albumin and other serum protein binding to the hydrophobic regions of this inhibitor [99]. However, removal of these proteins from culture media is not viable as they are a necessity to parasite survival and a *T. brucei* study indicated they did not observe a significant difference in UK-5099 activity when these proteins were removed [139]. Lastly, there are both conservative (Leu→ Ile; Trp→Phe) and non-conservative (Leu→Phe; Val→ Met) amino acid substitutions when comparing the amino acids involved in pyruvate transport as well as UK-5099 binding in humans to the MPC complex in *P. falciparum* parasites. These substitutions could result in sufficient structural differences that human and *P. falciparum* MPC heterocomplexes are inhibited by compounds with different structure activity relationships. While protein differences between the human and *P. falciparum* parasite is encouraging for possible future selective inhibition, it may affect chemical interrogation using known inhibitors. It is unclear which of the possible availability, uptake, specificity, and solubility hindrances with UK-5099 treatment led to inefficient parasite inhibition. Regardless, UK-5099 is not an effective chemical interrogator for putative parasite MPC activity. Other UK-5099

derivatives or new MPC inhibitors should be tested for better solubility, uptake, and parasite inhibition profiles.

Although a MPC chemical interrogator could not be established in this study, the alternative MPC interrogation approach relied on the genetic modification of putative *mpc* genes with different systems to evaluate the phenotypic changes to the parasite. Bioinformatic predictive tools indicated a spread of three transmembrane helices in MPC1 and MPC2 amino acid sequences. Therefore, the genetic disruption of the *mpc* genes with the SLI-TGD system near the N-terminus of each gene at its native loci should produce a non-functional truncated MPC protein without the majority of the transmembrane helices present, preventing a functional MPC heterocomplex from forming and subsequent pyruvate translocation. The lack of integrants obtained from this genetic disruption SLI-TGD system was indicative of *mpc1* and *mpc2* gene essentiality to asexual parasite proliferation according to literature [102]. This contradicted a previous large-scale mutagenesis study in *P. falciparum* parasites indicating *mpc2* as a mutable and therefore a dispensable gene [100]. A limitation of this large-scale study was that small gene essentiality could not be predicted, therefore, *mpc1* data was inconclusive [100]. *Mpc* gene essentiality in asexual parasites also biochemically contradicted metabolic flux analysis indicating a minimal flux through pyruvate into the TCA cycle during IDC [67, 69] unless the MPC heterocomplex is important for another biochemical process. These contradictions question whether *mpc* genes in *P. falciparum* parasites have a secondary unknown function or if the SLI-TGD system accurately predicts essentiality for MTPs.

To validate the SLI-TGD results, the SLI-*glmS* system was used in an attempt to generate a conditional *mpc1* and *mpc2* knockdown transgenic line which would produce a fully functional MPC protein until the knockdown is induced with the *glmS* ribozyme. However, after multiple integration attempts with varying G418 (neomycin-derivative) concentrations, the integration selection drug, no integrants were obtained for the SLI-*glmS* system similarly to the SLI-TGD system. This disproves the initial data from SLI-TGD indicating *mpc1* and *mpc2* essentiality but proves that the SLI-TGD and SLI-*glmS* systems were unsuccessful at genetically modifying the *mpc* genes at the native loci. Both systems were able to generate episomal lines, however, integration could not be obtained. This could be due to both systems being reliant on a random double stranded break in the *mpc* genes to allow for homologous recombination, which may have not occurred. Alternatively, homologous recombination did occur but the native promoter for each modified *mpc* gene could have been too weak to counteract G418 integration selection despite the lower ranges of G418 treatment that resulted in successful integration for other *P. falciparum* proteins [102]. In future, a system which uses a more targeted integration approach instead of random homologous recombination should be used, such as a

CRISPR/Cas system with specific guide RNAs, to generate a transgenic line that produces a reduced MPC expression phenotype.

Although transgenic lines which reduce *mpc* expression at the native loci could not be produced, an alternative genetic modification tool was used whereby the native locus expression is not affected. A successfully generated *mpc1* and *mpc2* ectopic expression line, NF54$^{attB}$-*cam-mpc1-myc-mpc2-HA-glmS*, in principle will allow equal constitutive expression of tagged *mpc1* and *mpc2* under the control of the calmodulin promoter and the subsequent increase MPC heterocomplexes. Although the *mpc* genes were not characterised in this study, this ectopic *mpc1* and *mpc2* expression transgenic line will yield useful information after the validation of this transgenic lines ability to overexpress the *mpc* genes with quantitate PCR and western blots.

Future studies should determine the subcellular and co-localisation of MPC1 and MPC2 and energy dynamic/metabolic flux changes in the IDC and gametocytogenesis with the NF54$^{attB}$-*cam-mpc1-myc-mpc2-HA-glmS* ectopic expression line to understand how the parasite responds to this phenotype. An MPC genetic knockout/knockdown line with the CRISPR/Cas system should be generated to view how the parasite responds to a reduced *mpc* expression phenotype in a similar manner to the ectopic expression line. The parasite's energy dynamics of these transgenic lines could reveal changes similar to what is seen when *mpc* gene expression is reduced or overexpressed in mammalian cells. For instance, the asexual parasite and cancerous cells share a common energy metabolic phenotype with glycolytic reliance related to reduced or absent MPC1 and MPC2 expression in cancer cells, similarly seen during the IDC [65, 140]. As the parasite transitions through gametocytogenesis, *mpc* genes are constitutively expressed from stage II, which highlights the parasites transition to a canonical cell state where MPCs are needed to support the TCA cycle [72, 73, 138]. This calls into question whether ectopically expressing *mpc1* and *mpc2* genes will affect the energy dynamics of the IDC towards operating more similarly to a canonical cell or gametocyte or will there be a higher gametocyte conversion rate with the increase energy available. Alternatively, will reduced MPC expression in gametocyte's cause gametocytogenesis to halt as a result of reduced ATP production or will a cancerous phenotype take over with glycolysis or glutaminolysis compensation. Further investigations into these phenotypes with transgenic lines, to be established in future, as well as better chemical MPC inhibitors would add to the comprehensive determination of the molecular identity of the putative *mpc* genes. Additionally, this future work would highlight the degree to which the *P. falciparum* parasite and cancerous cell phenotypes are similar and how strongly energy dynamics will compensate to maintain a certain phenotype or alternatively change.

# 5. Conclusion

Malaria eradication and elimination strategies need to evolve with the growing resistance toward current frontline antimalarials. To aid this drive in finding new antimalarials for disease treatment and transmission-blocking activity, the nuances in parasite biology needs to be investigated. This study was directed towards investigating the nuance in pyruvate translocation, particularly involving two putatively annotated *mpc* genes, between the IDC and gametocytes with a two-pronged approach involving chemical and genetic interrogation of putative *P. falciparum mpc* genes.

A known MPC inhibitor, UK-5099, was unsuitable as a chemical interrogator for *P. falciparum* parasites as an inhibitory effect could not be obtained for asexual parasites and gametocytes. Different MPC inhibitors should be identified as chemical interrogators for future MPC research. Additionally, genetic modification of *mpc* genes at the native loci to genetically disrupt and conditionally knockdown the genes was unable to produce a useable transgenic parasite line. However, different genetic modification systems that reduce *mpc* expression should be further investigated to study this phenotype. An ectopic expression line capable of constitutively overexpressing *mpc1* and *mpc2* genes was successfully produced and can be used in future to investigate parasite response to the overexpressed MPC phenotype to characterise these putative *mpc* genes.

# 6. References


1 World Health Organization. (2021) World malaria report 2021. 1-322

2 GBD 2019 Universal Health Coverage Collaborators. (2020) Measuring universal health coverage based on an index of effective coverage of health services in 204 countries and territories, 1990-2019: a systematic analysis for the Global Burden of Disease Study 2019. Lancet. **396**, 1250-1284

3 Sherman, I. W. (1979) Biochemistry of *Plasmodium* (malarial parasites). Microbiological reviews. **43**, 453-495

4 Antinori, S., Galimberti, L., Milazzo, L. and Corbellino, M. (2013) *Plasmodium knowlesi:* the emerging zoonotic malaria parasite. Acta tropica. **125**, 191-201

5 Ansari, H. R., Templeton, T. J., Subudhi, A. K., Ramaprasad, A., Tang, J., Lu, F., Naeem, R., Hashish, Y., Oguike, M. C. and Benavente, E. D. (2016) Genome-scale comparison of expanded gene families in *Plasmodium ovale wallikeri* and *Plasmodium ovale curtisi* with *Plasmodium malariae* and with other *Plasmodium* species. International journal for parasitology. **46**, 685-696

6 Trampuz, A., Jereb, M., Muzlovic, I. and Prabhu, R. M. (2003) Clinical review: Severe malaria. Critical care. **7**, 1-9

7 Mota, M. M., Pradel, G., Vanderberg, J. P., Hafalla, J. C., Frevert, U., Nussenzweig, R. S., Nussenzweig, V. and Rodríguez, A. (2001) Migration of *Plasmodium* sporozoites through cells before infection. Science. **291**, 141-144

8 Weiss, G. E., Gilson, P. R., Taechalertpaisarn, T., Tham, W.-H., de Jong, N. W., Harvey, K. L., Fowkes, F. J., Barlow, P. N., Rayner, J. C. and Wright, G. J. (2015) Revealing the sequence and resulting cellular morphology of receptor-ligand interactions during *Plasmodium falciparum* invasion of erythrocytes. PLoS pathogens. **11**, e1004670

9 Miller, L. H., Ackerman, H. C., Su, X.-z. and Wellems, T. E. (2013) Malaria biology and disease pathogenesis: insights for new treatments. Nature medicine. **19**, 156-167

10 Cowman, A. F. and Crabb, B. S. (2006) Invasion of red blood cells by malaria parasites. Cell. **124**, 755-766

11 Bannister, L. and Mitchell, G. (2003) The ins, outs and roundabouts of malaria. Trends in parasitology. **19**, 209-213

12 Chugh, M., Sundararaman, V., Kumar, S., Reddy, V. S., Siddiqui, W. A., Stuart, K. D. and Malhotra, P. (2013) Protein complex directs hemoglobin-to-hemozoin formation in *Plasmodium falciparum*. Proceedings of the National Academy of Sciences. **110**, 5392-5397

13 Josling, G. A., Williamson, K. C. and Llinás, M. (2018) Regulation of sexual commitment and gametocytogenesis in malaria parasites. Annual Review of Microbiology. **72**, 501-519

14 Meibalan, E. and Marti, M. (2017) Biology of malaria transmission. Cold Spring Harbor perspectives in medicine. **7**, 27-41

15 Talman, A. M., Domarle, O., McKenzie, F. E., Ariey, F. and Robert, V. (2004) Gametocytogenesis: the puberty of *Plasmodium falciparum*. Malaria journal. **3**, 24

16 Hawking, F., Wilson, M. E. and Gammage, K. (1971) Evidence for cyclic development and short-lived maturity in the gametocytes of *Plasmodium falciparum*. Transactions of the Royal Society of tropical Medicine and Hygiene. **65**, 549-559

17 Brancucci, N. M., Gerdt, J. P., Wang, C., De Niz, M., Philip, N., Adapa, S. R., Zhang, M., Hitz, E., Niederwieser, I. and Boltryk, S. D. (2017) Lysophosphatidylcholine regulates sexual stage differentiation in the human malaria parasite *Plasmodium falciparum*. Cell. **171**, 1532-1544. e1515

18 Dixon, M. W. and Tilley, L. (2021) *Plasmodium falciparum* goes bananas for sex. Molecular and Biochemical Parasitology. **244**, 111385

19 Parkyn Schneider, M., Liu, B., Glock, P., Suttie, A., McHugh, E., Andrew, D., Batinovic, S., Williamson, N., Hanssen, E. and McMillan, P. (2017) Disrupting assembly of the inner membrane complex blocks *Plasmodium falciparum* sexual stage development. PLoS pathogens. **13**, e1006659

20 Dearnley, M. K., Yeoman, J. A., Hanssen, E., Kenny, S., Turnbull, L., Whitchurch, C. B., Tilley, L. and Dixon, M. W. (2012) Origin, composition, organization and function of the inner membrane complex of *Plasmodium falciparum* gametocytes. Journal of cell science. **125**, 2053-2063
21 Smalley, M., Abdalla, S. and Brown, J. (1981) The distribution of *Plasmodium falciparum* in the peripheral blood and bone marrow of Gambian children. Transactions of the Royal Society of Tropical Medicine and Hygiene. **75**, 103-105
22 Dixon, M. W., Dearnley, M. K., Hanssen, E., Gilberger, T. and Tilley, L. (2012) Shape-shifting gametocytes: how and why does *P. falciparum* go banana-shaped? Trends in parasitology. **28**, 471-478
23 Sinden, R., Canning, E. U., Bray, R. and Smalley, M. (1978) Gametocyte and gamete development in *Plasmodium falciparum*. Proceedings of the Royal Society of London. Series B. Biological Sciences. **201**, 375-399
24 Kaslow, D., Okumu, F., Wells, T. and Rabinovich, R. (2017) malERA: An updated research agenda for diagnostics, drugs, vaccines, and vector control in malaria elimination and eradication. PLoS medicine. **14**, e1002455
25 Killeen, G. F., Tatarsky, A., Abdoulaye, D., Chaccour, C. J., Marshall, J. M., Okumu, F., Brunner, S., Newby, G., Williams, Y. A., Malone, D., Tusting, L. S. and Gosling, R. D. (2017) Developing an expanded vector control toolbox for malaria elimination. BMJ Global Health. **2**, e000211
26 Corbel, V., Chabi, J., Dabiré, R. K., Etang, J., Nwane, P., Pigeon, O., Akogbeto, M. and Hougard, J.-M. (2010) Field efficacy of a new mosaic long-lasting mosquito net (PermaNet® 3.0) against pyrethroid-resistant malaria vectors: a multi centre study in Western and Central Africa. Malaria Journal. **9**, 113
27 Nkumama, I. N., O'Meara, W. P. and Osier, F. H. (2017) Changes in malaria epidemiology in Africa and new challenges for elimination. Trends in parasitology. **33**, 128-140
28 World Health Organization. (2021) WHO guidelines for malaria
29 Ouji, M., Augereau, J.-M., Paloque, L. and Benoit Vical, F. (2018) *Plasmodium falciparum* resistance to artemisinin-based combination therapies: A sword of Damocles in the path toward malaria elimination. Parasite. **25**
30 Balikagala B, F. N., Ikeda M, Katuro OT, Tachibana SI, Yamauchi M, Opio W, Emoto S, Anywar DA, Kimura E, Palacpac NMQ, Odongo-Aginya EI, Ogwang M, Horii T, Mita T. . (2021) Evidence of Artemisinin-Resistant Malaria in Africa. New England Journal of Medicine. **385**, 1163-1171
31 Stokes, B. H., Dhingra, S. K., Rubiano, K., Mok, S., Straimer, J., Gnädig, N. F., Deni, I., Schindler, K. A., Bath, J. R. and Ward, K. E. (2021) *Plasmodium falciparum* K13 mutations in Africa and Asia impact artemisinin resistance and parasite fitness. Elife. **10**, e66277
32 Witmer, K., Dahalan, F. A., Delves, M. J., Yahiya, S., Watson, O. J., Straschil, U., Chiwcharoen, D., Sornboon, B., Pukrittayakamee, S. and Pearson, R. D. (2020) Transmission of artemisinin-resistant malaria parasites to mosquitoes under antimalarial drug pressure. Antimicrobial agents and chemotherapy. **65**, e00898-00820
33 Graves, P. M., Choi, L., Gelband, H. and Garner, P. (2018) Primaquine or other 8-aminoquinolines for reducing *Plasmodium falciparum* transmission. Cochrane Database of Systematic Reviews
34 Raman, J., Allen, E., Workman, L., Mabuza, A., Swanepoel, H., Malatje, G., Frean, J., Wiesner, L. and Barnes, K. I. (2019) Safety and tolerability of single low-dose primaquine in a low-intensity transmission area in South Africa: an open-label, randomized controlled trial. Malaria Journal. **18**, 1-13
35 Rampling, T., Ewer, K. J., Bowyer, G., Edwards, N. J., Wright, D., Sridhar, S., Payne, R., Powlson, J., Bliss, C. and Venkatraman, N. (2018) Safety and efficacy of novel malaria vaccine regimens of RTS, S/AS01B alone, or with concomitant ChAd63-MVA-vectored vaccines expressing ME-TRAP. npj Vaccines. **3**, 1-9

36 van den Berg, M., Ogutu, B., Sewankambo, N. K., Biller-Andorno, N. and Tanner, M. (2019) RTS, S malaria vaccine pilot studies: addressing the human realities in large-scale clinical trials. Trials. **20**, 1-4
37 Dobaño, C., Sanz, H., Sorgho, H., Dosoo, D., Mpina, M., Ubillos, I., Aguilar, R., Ford, T., Díez-Padrisa, N. and Williams, N. A. (2019) Concentration and avidity of antibodies to different circumsporozoite epitopes correlate with RTS, S/AS01E malaria vaccine efficacy. Nature communications. **10**, 1-13
38 Nadeem AY, S. A., Islam SU, Al-Suhaimi EA, Lee YS. (2022) Mosquirix™ RTS, S/AS01 vaccine development, immunogenicity, and efficacy. Vaccines (Basel). **30**, 713
39 Datoo, M. S., Magloire Natama, H., Somé, A., Traoré, O., Rouamba, T., Bellamy, D., Yameogo, P., Valia, D., Tegneri, M. and Ouedraogo, F. (2021) High efficacy of a low dose candidate malaria vaccine, R21 in 1 adjuvant matrix-M™, with seasonal administration to children in Burkina Faso.
40 Sulyok, Z., Fendel, R., Eder, B., Lorenz, F.-R., Kc, N., Karnahl, M., Lalremruata, A., Nguyen, T. T., Held, J. and Adjadi, F. A. C. (2021) Heterologous protection against malaria by a simple chemoattenuated PfSPZ vaccine regimen in a randomized trial. Nature communications. **12**, 1-10
41 Oneko, M., Steinhardt, L. C., Yego, R., Wiegand, R. E., Swanson, P. A., Kc, N., Akach, D., Sang, T., Gutman, J. R. and Nzuu, E. L. (2021) Safety, immunogenicity and efficacy of PfSPZ Vaccine against malaria in infants in western Kenya: a double-blind, randomized, placebo-controlled phase 2 trial. Nature Medicine. **27**, 1636-1645
42 Datoo, M. S., Natama, H. M., Somé, A., Bellamy, D., Traoré, O., Rouamba, T., Tahita, M. C., Ido, N. F. A., Yameogo, P. and Valia, D. (2022) Efficacy and immunogenicity of R21/Matrix-M vaccine against clinical malaria after 2 years' follow-up in children in Burkina Faso: a phase 1/2b randomised controlled trial. The Lancet Infectious Diseases
43 Martin, R. E., Henry, R. I., Abbey, J. L., Clements, J. D. and Kirk, K. (2005) The'permeome'of the malaria parasite: an overview of the membrane transport proteins of *Plasmodium falciparum*. Genome biology. **6**, R26
44 Staines, H. M., Derbyshire, E. T., Slavic, K., Tattersall, A., Vial, H. and Krishna, S. (2010) Exploiting the therapeutic potential of *Plasmodium falciparum* solute transporters. Trends in parasitology. **26**, 284-296
45 Martin, R. E. (2020) The transportome of the malaria parasite. Biological Reviews. **95**, 305-332
46 Kirk, K. (2004) Channels and transporters as drug targets in the *Plasmodium*-infected erythrocyte. Acta tropica. **89**, 285-298
47 Wishart, D. S., Knox, C., Guo, A. C., Shrivastava, S., Hassanali, M., Stothard, P., Chang, Z. and Woolsey, J. (2006) DrugBank: a comprehensive resource for *in silico* drug discovery and exploration. Nucleic acids research. **34**, D668-D672
48 Arinaminpathy, Y., Khurana, E., Engelman, D. M. and Gerstein, M. B. (2009) Computational analysis of membrane proteins: the largest class of drug targets. Drug discovery today. **14**, 1130-1135
49 Terstappen, G. C. and Reggiani, A. (2001) *In silico* research in drug discovery. Trends in pharmacological sciences. **22**, 23-26
50 Gardner, M. J., Hall, N., Fung, E., White, O., Berriman, M., Hyman, R. W., Carlton, J. M., Pain, A., Nelson, K. E. and Bowman, S. (2002) Genome sequence of the human malaria parasite *Plasmodium falciparum*. Nature. **419**, 498-511
51 Ren, Q., Chen, K. and Paulsen, I. T. (2007) TransportDB: a comprehensive database resource for cytoplasmic membrane transport systems and outer membrane channels. Nucleic acids research. **35**, D274-D279
52 Cowell, A. N., Istvan, E. S., Lukens, A. K., Gomez-Lorenzo, M. G., Vanaerschot, M., Sakata-Kato, T., Flannery, E. L., Magistrado, P., Owen, E. and Abraham, M. (2018) Mapping the malaria parasite druggable genome by using in vitro evolution and chemogenomics. Science. **359**, 191-199

53 Sanchez, C. P., Dave, A., Stein, W. D. and Lanzer, M. (2010) Transporters as mediators of drug resistance in *Plasmodium falciparum*. International journal for parasitology. **40**, 1109-1118
54 Martin, R. E. and Kirk, K. (2004) The malaria parasite's chloroquine resistance transporter is a member of the drug/metabolite transporter superfamily. Molecular biology and evolution. **21**, 1938-1949
55 Cowell, A. and Winzeler, E. (2018) Exploration of the *Plasmodium falciparum* resistome and druggable genome reveals new mechanisms of drug resistance and antimalarial targets. Microbiology insights. **11**, 1178636118808529
56 Hameed P, S., Solapure, S., Patil, V., Henrich, P. P., Magistrado, P. A., Bharath, S., Murugan, K., Viswanath, P., Puttur, J. and Srivastava, A. (2015) Triaminopyrimidine is a fast-killing and long-acting antimalarial clinical candidate. Nature Communications. **6**, 1-11
57 Rottmann, M., McNamara, C., Yeung, B. K., Lee, M. C., Zou, B., Russell, B., Seitz, P., Plouffe, D. M., Dharia, N. V. and Tan, J. (2010) Spiroindolones, a potent compound class for the treatment of malaria. science. **329**, 1175-1180
58 Dennis, A. S. M., Lehane, A. M., Ridgway, M. C., Holleran, J. P. and Kirk, K. (2018) Cell Swelling Induced by the Antimalarial KAE609 (Cipargamin) and Other PfATP4-Associated Antimalarials. Antimicrobial Agents and Chemotherapy. **62**, e00087-00018
59 Ndayisaba, G., Yeka, A., Asante, K. P., Grobusch, M. P., Karita, E., Mugerwa, H., Asiimwe, S., Oduro, A., Fofana, B. and Doumbia, S. (2021) Hepatic safety and tolerability of cipargamin (KAE609), in adult patients with *Plasmodium falciparum* malaria: a randomized, phase II, controlled, dose-escalation trial in sub-Saharan Africa. Malaria journal. **20**, 1-10
60 McCarthy, J. S., Abd-Rahman, A. N., Collins, K. A., Marquart, L., Griffin, P., Kümmel, A., Fuchs, A., Winnips, C., Mishra, V. and Csermak-Renner, K. (2021) Defining the antimalarial activity of cipargamin in healthy volunteers experimentally infected with blood-stage *Plasmodium falciparum*. Antimicrobial agents and chemotherapy. **65**, e01423-01420
61 del Pilar Crespo, M., Avery, T. D., Hanssen, E., Fox, E., Robinson, T. V., Valente, P., Taylor, D. K. and Tilley, L. (2008) Artemisinin and a series of novel endoperoxide antimalarials exert early effects on digestive vacuole morphology. Antimicrobial agents and chemotherapy. **52**, 98-109
62 Istvan, E. S., Das, S., Bhatnagar, S., Beck, J. R., Owen, E., Llinas, M., Ganesan, S. M., Niles, J. C., Winzeler, E. and Vaidya, A. B. (2019) *Plasmodium* Niemann-Pick type C1-related protein is a druggable target required for parasite membrane homeostasis. Elife. **8**, e40529
63 Erecińska, M. and Wilson, D. F. (1982) Regulation of cellular energy metabolism. Journal of Membrane Biology. **70**, 1-14
64 Zheng, J. (2012) Energy metabolism of cancer: Glycolysis versus oxidative phosphorylation. Oncology letters. **4**, 1151-1157
65 MacRae, J. I., Dixon, M. W., Dearnley, M. K., Chua, H. H., Chambers, J. M., Kenny, S., Bottova, I., Tilley, L. and McConville, M. J. (2013) Mitochondrial metabolism of sexual and asexual blood stages of the malaria parasite *Plasmodium falciparum*. BMC biology. **11**, 67
66 Salcedo-Sora, J. E., Caamano-Gutierrez, E., Ward, S. A. and Biagini, G. A. (2014) The proliferating cell hypothesis: a metabolic framework for *Plasmodium* growth and development. Trends in parasitology. **30**, 170-175
67 Cobbold, S. A., Vaughan, A. M., Lewis, I. A., Painter, H. J., Camargo, N., Perlman, D. H., Fishbaugher, M., Healer, J., Cowman, A. F. and Kappe, S. H. (2013) Kinetic flux profiling elucidates two independent acetyl-CoA biosynthetic pathways in *Plasmodium falciparum*. Journal of Biological Chemistry. **288**, 36338-36350
68 Storm, J., Sethia, S., Blackburn, G. J., Chokkathukalam, A., Watson, D. G., Breitling, R., Coombs, G. H. and Müller, S. (2014) Phosphoenolpyruvate carboxylase identified as a Key enzyme in erythrocytic *Plasmodium falciparum* carbon metabolism. PLoS pathogens. **10**, e1003876
69 Cobbold, S. A., V Tutor, M., Frasse, P., McHugh, E., Karnthaler, M., Creek, D. J., Odom John, A., Tilley, L., Ralph, S. A. and McConville, M. J. (2021) Non-canonical metabolic

pathways in the malaria parasite detected by isotope-tracing metabolomics. Molecular systems biology. **17**, e10023
70 Jacot, D., Waller, R. F., Soldati-Favre, D., MacPherson, D. A. and MacRae, J. I. (2016) Apicomplexan energy metabolism: carbon source promiscuity and the quiescence hyperbole. Trends in Parasitology. **32**, 56-70
71 Srivastava, A., Philip, N., Hughes, K. R., Georgiou, K., MacRae, J. I., Barrett, M. P., Creek, D. J., McConville, M. J. and Waters, A. P. (2016) Stage-specific changes in *Plasmodium* metabolism required for differentiation and adaptation to different host and vector environments. PLoS pathogens. **12**, e1006094
72 van Biljon, R. (2019) Integrative transcriptome and phenome analysis reveal unique regulatory cascades controlling the intraerythrocyti asexual and sexual development of human malaria parasites. In Biochemistry, Genetics and Microbiology ed.)^eds.). p. 133, University of Pretoria
73 Lasonder, E., Rijpma, S. R., van Schaijk, B. C., Hoeijmakers, W. A., Kensche, P. R., Gresnigt, M. S., Italiaander, A., Vos, M. W., Woestenenk, R. and Bousema, T. (2016) Integrated transcriptomic and proteomic analyses of *P. falciparum* gametocytes: molecular insight into sex-specific processes and translational repression. Nucleic acids research. **44**, 6087-6101
74 Ke, H., Lewis, I. A., Morrisey, J. M., McLean, K. J., Ganesan, S. M., Painter, H. J., Mather, M. W., Jacobs-Lorena, M., Llinás, M. and Vaidya, A. B. (2015) Genetic investigation of tricarboxylic acid metabolism during the *Plasmodium falciparum* life cycle. Cell reports. **11**, 164-174
75 Krungkrai, J., Prapunwattana, P. and Krungkrai, S. (2000) Ultrastructure and function of mitochondria in gametocytic stage of *Plasmodium falciparum*. Parasite. **7**, 19-26
76 Oppenheim, R. D., Creek, D. J., Macrae, J. I., Modrzynska, K. K., Pino, P., Limenitakis, J., Polonais, V., Seeber, F., Barrett, M. P. and Billker, O. (2014) BCKDH: the missing link in apicomplexan mitochondrial metabolism is required for full virulence of *Toxoplasma gondii* and *Plasmodium berghei*. PLoS pathogens. **10**, e1004263
77 Müller, M., Mentel, M., van Hellemond, J. J., Henze, K., Woehle, C., Gould, S. B., Yu, R.-Y., van der Giezen, M., Tielens, A. G. and Martin, W. F. (2012) Biochemistry and evolution of anaerobic energy metabolism in eukaryotes. Microbiology and Molecular Biology Reviews. **76**, 444-495
78 Woodrow, C. J., Penny, J. I. and Krishna, S. (1999) Intraerythrocytic *Plasmodium falciparum* expresses a high affinity facilitative hexose transporter. Journal of Biological Chemistry. **274**, 7272-7277
79 Elliot, J. L., Salbia, K. J. and Kirk, K. (2001) Transport of lactate and pyruvate in the intraerythrocytic malaria parasite, *Plasmodium falciparum*. Biochemical Journal. **355**, 733-739
80 Marchetti, R. V., Lehane, A. M., Shafik, S. H., Winterberg, M., Martin, R. E. and Kirk, K. (2015) A lactate and formate transporter in the intraerythrocytic malaria parasite, *Plasmodium falciparum*. Nature communications. **6**, 1-7
81 Huizing, M., Ruitenbeek, W., Thinnes, F. P., Depinto, V., Wendel, U., Trijbels, F. J., Smit, L. M., Ter Laak, H. J. and Van Den Heuvel, L. P. (1996) Deficiency of the voltage-dependent anion channel: a novel cause of mitochondriopathy. Pediatric research. **39**, 760-765
82 Klingenberg, M. (1970) Mitochondria metabolite transport. FEBS letters. **6**, 145-154
83 Papa, S., Francavilla, A., Paradies, G. and Meduri, B. (1971) The transport of pyruvate in rat liver mitochondria. FEBS letters. **12**, 285-288
84 Herzig, S., Raemy, E., Montessuit, S., Veuthey, J.-L., Zamboni, N., Westermann, B., Kunji, E. R. and Martinou, J.-C. (2012) Identification and functional expression of the mitochondrial pyruvate carrier. Science. **337**, 93-96
85 Bricker, D. K., Taylor, E. B., Schell, J. C., Orsak, T., Boutron, A., Chen, Y.-C., Cox, J. E., Cardon, C. M., Van Vranken, J. G. and Dephoure, N. (2012) A mitochondrial pyruvate carrier required for pyruvate uptake in yeast, *Drosophila,* and humans. Science. **337**, 96-100

86 Nagampalli, R. S. K., Quesñay, J. E. N., Adamoski, D., Islam, Z., Birch, J., Sebinelli, H. G., Girard, R. M. B. M., Ascenção, C. F. R., Fala, A. M. and Pauletti, B. A. (2018) Human mitochondrial pyruvate carrier 2 as an autonomous membrane transporter. Scientific reports. **8**, 1-13
87 Bowman, C. E., Zhao, L., Hartung, T. and Wolfgang, M. J. (2016) Requirement for the mitochondrial pyruvate carrier in mammalian development revealed by a hypomorphic allelic series. Molecular and cellular biology. **36**, 2089-2104
88 Vigueira, P. A., McCommis, K. S., Schweitzer, G. G., Remedi, M. S., Chambers, K. T., Fu, X., McDonald, W. G., Cole, S. L., Colca, J. R. and Kletzien, R. F. (2014) Mitochondrial pyruvate carrier 2 hypomorphism in mice leads to defects in glucose-stimulated insulin secretion. Cell reports. **7**, 2042-2053
89 Timón-Gómez, A., Proft, M. and Pascual-Ahuir, A. (2013) Differential regulation of mitochondrial pyruvate carrier genes modulates respiratory capacity and stress tolerance in yeast. PloS one. **8**, e79405
90 Štáfková, J., Mach, J., Biran, M., Verner, Z., Bringaud, F. and Tachezy, J. (2016) Mitochondrial pyruvate carrier in *Trypanosoma brucei*. Molecular Microbiology. **100**, 442-456
91 Negreiros, R. S., Lander, N., Chiurillo, M. A., Vercesi, A. E. and Docampo, R. (2021) Mitochondrial pyruvate carrier subunits are essential for pyruvate-driven respiration, infectivity, and intracellular replication of *Trypanosoma cruzi*. Mbio. **12**, e00540-00521
92 Schell, J. C. and Rutter, J. (2013) The long and winding road to the mitochondrial pyruvate carrier. Cancer & metabolism. **1**, 6
93 Tang, B. L. (2019) Targeting the mitochondrial pyruvate carrier for neuroprotection. Brain sciences. **9**, 238
94 Park, S., Safi, R., Liu, X., Baldi, R., Liu, W., Liu, J., Locasale, J. W., Chang, C.-y. and McDonnell, D. P. (2019) Inhibition of ERRα prevents mitochondrial pyruvate uptake exposing NADPH-generating pathways as targetable vulnerabilities in breast cancer. Cell reports. **27**, 3587-3601. e3584
95 Tavoulari, S., Thangaratnarajah, C., Mavridou, V., Harbour, M. E., Martinou, J. C. and Kunji, E. R. (2019) The yeast mitochondrial pyruvate carrier is a hetero-dimer in its functional state. The EMBO journal. **38**, e100785
96 Halestrap, A. P. (1976) The mechanism of the inhibition of the mitochondrial pyruvate transportater by α-cyanocinnamate derivatives. Biochemical Journal. **156**, 181
97 Divakaruni, A. S., Wiley, S. E., Rogers, G. W., Andreyev, A. Y., Petrosyan, S., Loviscach, M., Wall, E. A., Yadava, N., Heuck, A. P. and Ferrick, D. A. (2013) Thiazolidinediones are acute, specific inhibitors of the mitochondrial pyruvate carrier. Proceedings of the national academy of sciences. **110**, 5422-5427
98 Halestrap, A. P. and Denton, R. M. (1974) Specific inhibition of pyruvate transport in rat liver mitochondria and human erythrocytes by α-cyano-4-hydroxycinnamate. Biochemical Journal. **138**, 313
99 Halestrap, A. P. (1975) The mitochondrial pyruvate carrier: Kinetics and specificity for substrates and inhibitors. Biochemical Journal. **148**, 85-96
100 Zhang, M., Wang, C., Otto, T. D., Oberstaller, J., Liao, X., Adapa, S. R., Udenze, K., Bronner, I. F., Casandra, D. and Mayho, M. (2018) Uncovering the essential genes of the human malaria parasite *Plasmodium falciparum* by saturation mutagenesis. Science. **360**, eaap7847
101 Okombo, J., Kanai, M., Deni, I. and Fidock, D. A. (2021) Genomic and genetic approaches to studying antimalarial drug resistance and *Plasmodium* biology. Trends in Parasitology. **37**, 476-492
102 Birnbaum, J., Flemming, S., Reichard, N., Soares, A. B., Mesén-Ramírez, P., Jonscher, E., Bergmann, B. and Spielmann, T. (2017) A genetic system to study *Plasmodium falciparum* protein function. Nature methods. **14**, 450-460
103 White, J., Dhingra, S. K., Deng, X., El Mazouni, F., Lee, M. C., Afanador, G. A., Lawong, A., Tomchick, D. R., Ng, C. L. and Bath, J. (2018) Identification and mechanistic understanding

of dihydroorotate dehydrogenase point mutations in *Plasmodium falciparum* that confer *in vitro* resistance to the clinical candidate DSM265. ACS infectious diseases. **5**, 90-101
104 Collins, C. R., Das, S., Wong, E. H., Andenmatten, N., Stallmach, R., Hackett, F., Herman, J. P., Müller, S., Meissner, M. and Blackman, M. J. (2013) Robust inducible cre recombinase activity in the human malaria parasite *Plasmodium falciparum* enables efficient gene deletion within a single asexual erythrocytic growth cycle. Molecular microbiology. **88**, 687-701
105 Yap, A., Azevedo, M. F., Gilson, P. R., Weiss, G. E., O'Neill, M. T., Wilson, D. W., Crabb, B. S. and Cowman, A. F. (2014) Conditional expression of apical membrane antigen 1 in *Plasmodium falciparum* shows it is required for erythrocyte invasion by merozoites. Cellular microbiology. **16**, 642-656
106 Russo, I., Oksman, A., Vaupel, B. and Goldberg, D. E. (2009) A calpain unique to alveolates is essential in *Plasmodium falciparum* and its knockdown reveals an involvement in pre-S-phase development. Proceedings of the National Academy of Sciences. **106**, 1554-1559
107 Prommana, P., Uthaipibull, C., Wongsombat, C., Kamchonwongpaisan, S., Yuthavong, Y., Knuepfer, E., Holder, A. A. and Shaw, P. J. (2013) Inducible knockdown of *Plasmodium* gene expression using the *glmS* ribozyme. PloS one. **8**, e73783
108 Nkrumah, L. J., Muhle, R. A., Moura, P. A., Ghosh, P., Hatfull, G. F., Jacobs, W. R. and Fidock, D. A. (2006) Efficient site-specific integration in *Plasmodium falciparum* chromosomes mediated by mycobacteriophage Bxb1 integrase. Nature methods. **3**, 615-621
109 Naik, R. S., Krishnegowda, G. and Gowda, D. C. (2003) Glucosamine Inhibits inositol acylation of the glycosylphosphatidylinositol anchors in intraerythrocytic *Plasmodium falciparum*. Journal of Biological Chemistry. **278**, 2036-2042
110 Elsworth, B., Matthews, K., Nie, C. Q., Kalanon, M., Charnaud, S. C., Sanders, P. R., Chisholm, S. A., Counihan, N. A., Shaw, P. J. and Pino, P. (2014) PTEX is an essential nexus for protein export in malaria parasites. Nature. **511**, 587-591
111 Dvorin, J. D., Martyn, D. C., Patel, S. D., Grimley, J. S., Collins, C. R., Hopp, C. S., Bright, A. T., Westenberger, S., Winzeler, E. and Blackman, M. J. (2010) A plant-like kinase in *Plasmodium falciparum* regulates parasite egress from erythrocytes. Science. **328**, 910-912
112 Armstrong, C. M. and Goldberg, D. E. (2007) An FKBP destabilization domain modulates protein levels in *Plasmodium falciparum*. Nature methods. **4**, 1007-1009
113 Banaszynski, L. A., Chen, L.-c., Maynard-Smith, L. A., Ooi, A. L. and Wandless, T. J. (2006) A rapid, reversible, and tunable method to regulate protein function in living cells using synthetic small molecules. Cell. **126**, 995-1004
114 Wang, Y., Wang, Q., Huang, H., Huang, W., Chen, Y., McGarvey, P. B., Wu, C. H., Arighi, C. N. and Consortium, U. (2021) A crowdsourcing open platform for literature curation in UniProt. PLoS Biology. **19**, e3001464
115 Hall, B. G. (2013) Building phylogenetic trees from molecular data with MEGA. Molecular biology and evolution. **30**, 1229-1235
116 Jia, F., Lo, N. and Ho, S. Y. (2014) The impact of modelling rate heterogeneity among sites on phylogenetic estimates of intraspecific evolutionary rates and timescales. PLoS One. **9**, e95722
117 Hall, T., Biosciences, I. and Carlsbad, C. (2011) BioEdit: an important software for molecular biology. GERF Bull Biosci. **2**, 60-61
118 Hallgren, J., Tsirigos, K. D., Pedersen, M. D., Armenteros, J. J. A., Marcatili, P., Nielsen, H., Krogh, A. and Winther, O. (2022) DeepTMHMM predicts α and β transmembrane proteins using deep neural networks. bioRxiv
119 Blum, M., Chang, H.-Y., Chuguransky, S., Grego, T., Kandasaamy, S., Mitchell, A., Nuka, G., Paysan-Lafosse, T., Qureshi, M. and Raj, S. (2021) The InterPro protein families and domains database: 20 years on. Nucleic acids research. **49**, D344-D354
120 Tsirigos, K. D., Peters, C., Shu, N., Käll, L. and Elofsson, A. (2015) The TOPCONS web server for consensus prediction of membrane protein topology and signal peptides. Nucleic acids research. **43**, W401-W407

121 Claros, M. G. and Vincens, P. (1996) Computational method to predict mitochondrially imported proteins and their targeting sequences. European journal of biochemistry. **241**, 779-786
122 Allen, R. J. and Kirk, K. (2010) *Plasmodium falciparum* culture: the benefits of shaking. Molecular and biochemical parasitology. **169**, 63-65
123 Ginsburg, H., Krugliak, M., Eidelman, O. and Cabantchik, Z. I. (1983) New permeability pathways induced in membranes of *Plasmodium falciparum* infected erythrocytes. Molecular and biochemical parasitology. **8**, 177-190
124 Reader, J., Botha, M., Theron, A., Lauterbach, S. B., Rossouw, C., Engelbrecht, D., Wepener, M., Smit, A., Leroy, D. and Mancama, D. (2015) Nowhere to hide: interrogating different metabolic parameters of *Plasmodium falciparum* gametocytes in a transmission blocking drug discovery pipeline towards malaria elimination. Malaria journal. **14**, 213
125 Gupta, S. K., Schulman, S. and Vanderberg, J. P. (1985) Stage-Dependent Toxicity of N-Acetyl-Glucosamine to *Plasmodium falciparum*. The Journal of protozoology. **32**, 91-95
126 Dragan, A., Pavlovic, R., McGivney, J., Casas-Finet, J., Bishop, E., Strouse, R., Schenerman, M. and Geddes, C. (2012) SYBR Green I: fluorescence properties and interaction with DNA. Journal of fluorescence. **22**, 1189-1199
127 Makler, M. T. and Hinrichs, D. J. (1993) Measurement of the lactate dehydrogenase activity of *Plasmodium falciparum* as an assessment of parasitemia. The American journal of tropical medicine and hygiene. **48**, 205-210
128 D'Alessandro, S., Silvestrini, F., Dechering, K., Corbett, Y., Parapini, S., Timmerman, M., Galastri, L., Basilico, N., Sauerwein, R. and Alano, P. (2013) A *Plasmodium falciparum* screening assay for anti-gametocyte drugs based on parasite lactate dehydrogenase detection. Journal of Antimicrobial Chemotherapy. **68**, 2048-2058
129 Sugar, I. P. and Neumann, E. (1984) Stochastic model for electric field-induced membrane pores electroporation. Biophysical chemistry. **19**, 211-225
130 Goonewardene, R., Daily, J., Kaslow, D., Sullivan, T. J., Duffy, P., Carter, R., Mendis, K. and Wirth, D. (1993) Transfection of the malaria parasite and expression of firefly luciferase. Proceedings of the National Academy of Sciences. **90**, 5234-5236
131 Fidock, D. A. and Thomas, W. E. (1997) Transformation with human dihydrofolate reductase renders malaria parasites insensitive to WR99210 but does not affect the intrinsic activity of proguanil. Proceedings of the National Academy of Sciences of the United States of America. **94**, 10931-10936
132 Rodríguez-Trelles, F., Tarrío, R. and Ayala, F. J. (2005) Is ectopic expression caused by deregulatory mutations or due to gene-regulation leaks with evolutionary potential? BioEssays. **27**, 592-601
133 Adjalley, S. H., Johnston, G. L., Li, T., Eastman, R. T., Ekland, E. H., Eappen, A. G., Richman, A., Sim, B. K. L., Lee, M. C. and Hoffman, S. L. (2011) Quantitative assessment of *Plasmodium falciparum* sexual development reveals potent transmission-blocking activity by methylene blue. Proceedings of the National Academy of Sciences. **108**, E1214-E1223
134 Xu, L., Phelix, C. F. and Chen, L. Y. (2021) Structural insights into the human mitochondrial pyruvate carrier complexes. Journal of Chemical Information and Modeling. **61**, 5614-5625
135 Evers, F., Cabrera-Orefice, A., Elurbe, D. M., Kea-te Lindert, M., Boltryk, S. D., Voss, T. S., Huynen, M. A., Brandt, U. and Kooij, T. W. (2021) Composition and stage dynamics of mitochondrial complexes in *Plasmodium falciparum*. Nature communications. **12**, 1-17
136 Van Biljon, R., Niemand, J., van Wyk, R., Clark, K., Verlinden, B., Abrie, C., von Grüning, H., Smidt, W., Smit, A. and Reader, J. (2018) Inducing controlled cell cycle arrest and re-entry during asexual proliferation of *Plasmodium falciparum* malaria parasites. Scientific reports. **8**, 1-14
137 Naidu, R., Subramanian, G., Lim, Y. B., Lim, C. T. and Chandramohanadas, R. (2018) A reference document on Permissible Limits for solvents and buffers during in vitro antimalarial screening. Scientific reports. **8**, 1-8

138 Lamour, S. D., Straschil, U., Saric, J. and Delves, M. J. (2014) Changes in metabolic phenotypes of *Plasmodium falciparum in vitro* cultures during gametocyte development. Malaria journal. **13**, 468
139 Wiemer, E. A., Michels, P. A. and Opperdoes, F. R. (1995) The inhibition of pyruvate transport across the plasma membrane of the bloodstream form of *Trypanosoma brucei* and its metabolic implications. Biochemical Journal. **312**, 479-484
140 Painter, H. J., Carrasquilla, M. and Llinás, M. (2017) Capturing *in vivo* RNA transcriptional dynamics from the malaria parasite *Plasmodium falciparum*. Genome research. **27**, 1074-1086

# 7. Supplementary information

Supplementary Table 1 lists the forward and reverse primers used to amplify respective *mpc* gene regions which were subsequently ligated into SLI-TGD and SLI-*glmS* plasmids. Each primer contains a four nucleotide overhang region (underlined), either the *NotI* (5' GCGGCCGC 3') or *MluI* (5' ACGCGT 3') restriction enzyme cut site (bolded) and a *mpc* homology region. Additionally, the forward primer contains a stop codon (red) necessary for the SLI system to prevent episomal expression of the gene insert in the plasmid [102].

**Supplementary Table 1: Primer sequences used to amplify *mpc1* and *mpc2* regions for the SLI-TGD and SLI-*glmS* systems**

| Plasmid name | Gene insert | Forward primer (5'-3') | Reverse primer (5'-3') | Homology region (bp) |
|---|---|---|---|---|
| pSLI-*mpc1*-GFP | *mpc1* | AGAT**GCGGCCGC**TAATTAAGTATTATGCTTTGGGCTC | CGAT**ACGCGT**GGGTTCTTTCTTTAAATCGTTGCATCC | 219 |
| pSLI-*mpc2*-GFP | *mpc2* | CGCT**GCGGCCGC**TAATTTTATCCAAACATCATACC | AGAT**ACGCGT**TGCAATGTTGGCTAATGATATGGACC | 324 |
| pSLI-*mpc1-glmS* | *mpc1* | AGAT**GCGGCCGC**TAATTAAGTATTATGCTTTGGGCTC | CGCT**ACGCGT**TTTTGCTGTTATTTTTATTTTTTGATGTTTC | 399 |
| pSLI-*mpc1-glmS*-mut | *mpc1* | | | 399 |
| pSLI-*mpc2-glmS* | *mpc2* | AGAT**GCGGCCGC**TAATCATTAGCCAACATTGC | CGCT**ACGCGT**CCTTTCTTTTTCCTTCATATATAC | 561 |
| pSLI-*mpc2-glmS*-mut | *mpc2* | | | 561 |

Supplementary Figure 1 indicates the full 1.5 % agarose/TAE (w/v) gel of Figure 3.7B and 3.11B.

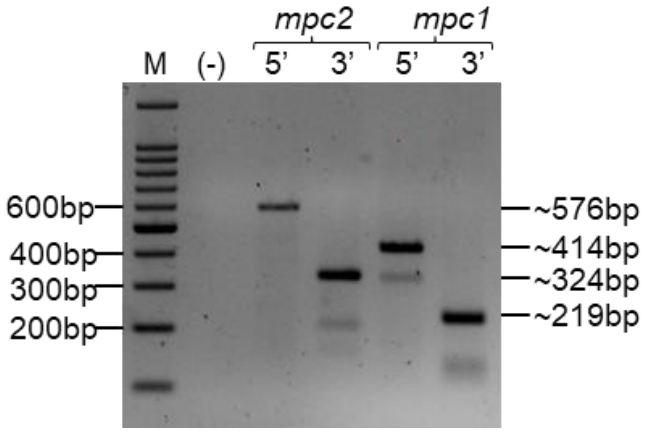


**Supplementary Figure 1: PCR amplification of the 5' and 3' fragments of *mpc1* and *mpc2*.** Complete 1.5 % agarose/TAE (w/v) gel stained with 0.5 mg/mL of EtBr after electrophoresis of Figure 3.7B and 3.11B representing the PCR products amplifying the 5' and 3' fragments of *mpc1* and *mpc2* genes for the incorporation into pSLI-GFP and pSLI-*glmS/glmS-mut* plasmids, respectively. M: 100 bp molecular marker (Promega, USA), (-): PCR sample loaded with water as a substitute for the DNA template, 5': 5' fragment and 3': 3; fragment.

Supplementary Figure 2 represents the complete 1.5 % agarose/TAE (w/v) gel of Figure 3.7C.

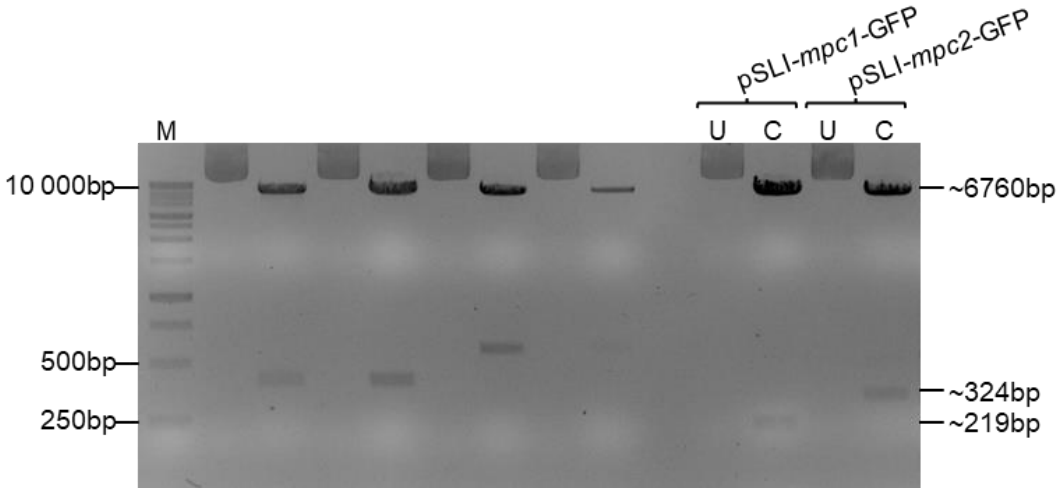


**Supplementary Figure 2: Restriction enzyme digestion of the recombinant pSLI-*mpc1*-GFP and pSLI-*mpc2*-GFP plasmids.** These constructs were digested with *NotI* and *MluI* and visualised on a 1.5 % agarose/TAE (w/v) gel stained with 0.5 mg/mL of EtBr after electrophoresis to validate the presence of respective *mpc* fragment inserts in each plasmid. M: 100 bp molecular marker (Promega, USA), U: undigested recombinant plasmid control and C: digested recombinant plasmid sample.

Supplementary Figure 3 represents the parasitaemia of NF54-epi(pSLI-*mpc1-glmS/glmS-mut*) and NF54-epi(pSLI-*mpc2-glmS/glmS-mut*) parasite lines during G418 selection (at 400, 300 and 200 µg/mL) and recovery. Parasites did not re-emerge for those under G418 selection at 400 µg/mL and 300 µg/mL after 50 days of selection and recovery (Supplementary Figure 3A and B). However, populations transfected with pSLI-*mpc2-glms* and pSLI-*mpc2-glms-mut* did re-emerge after 30-35 days of selection and recovery (15-20 days post-selection) (Supplementary Figure 3C). These populations were checked for genomic integration at the native *mpc2* locus (Supplementary Figure 4).

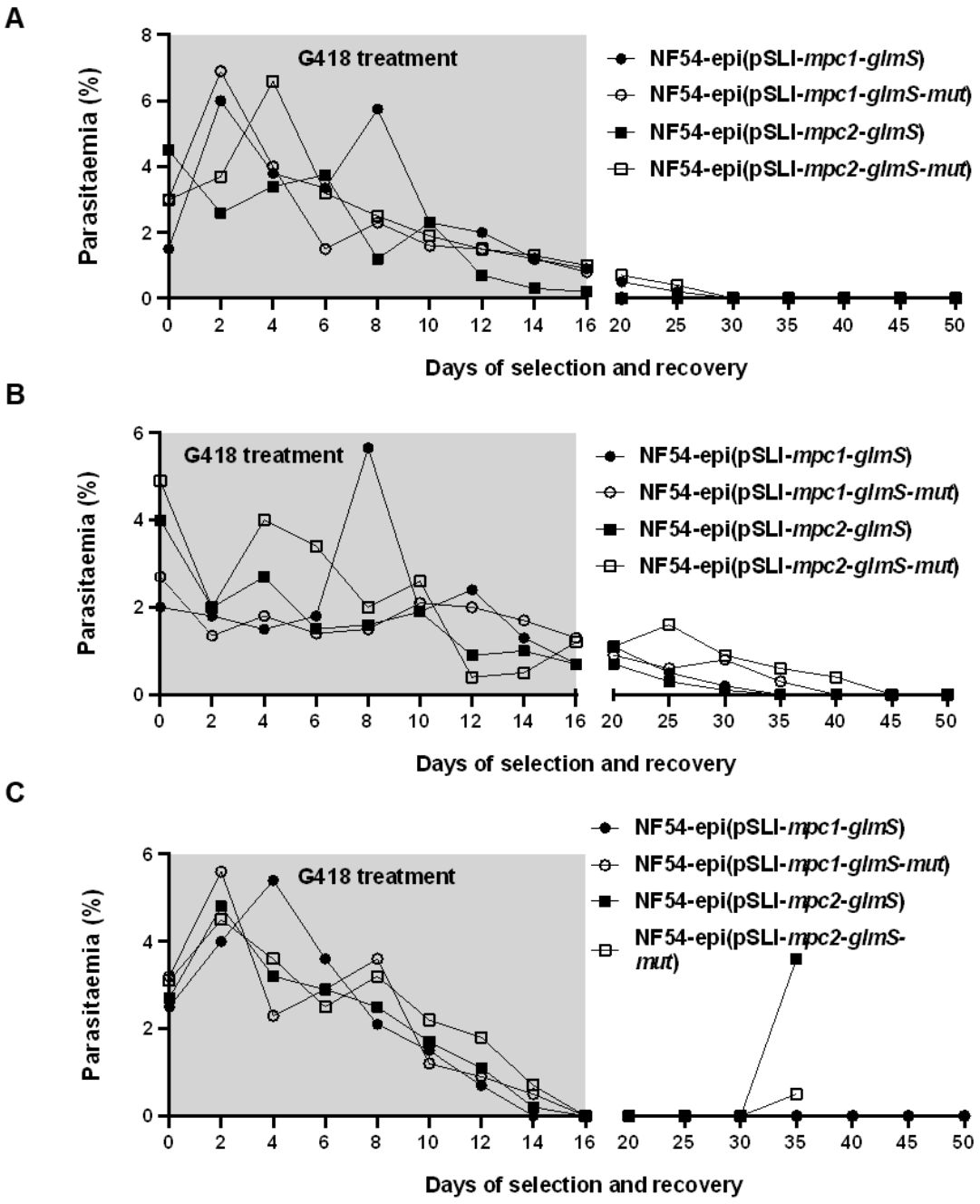


**Supplementary Figure 3: Parasitaemia of *P. falciparum* NF54-epi(pSLI-*mpc1-glmS/glmS-mut*) and NF54-epi(pSLI-*mpc2-glmS/glmS-mut*) parasite lines during G418 selection and recovery.** NF54-epi(pSLI-*mpc1-glmS/glmS-mut*) and NF54-epi(pSLI-*mpc2- glmS/glmS-mut*) parasite lines were treated with G418 at **(A)** 400 µg/mL, **(B)** 300 µg/mL, and **(C)** 200 µg/mL for a 16 day period (grey box) followed by a recovery period. The parasitaemia of each line was monitored every second day with light microscopy.

Supplementary Figure 4 indicates no integrants were obtained despite parasites re-emerging after 35 days of selection recovery with G418 selection at the low 200 µg/mL concentration for the populations transfected with pSLI-*mpc2-glms* and pSLI-*mpc2-glms-mut.* Upon checking for integration, the NF54 *mpc2* locus was detected in the wild type, NF54epi(pSLI-*mpc2-glmS)* and NF54epi(pSLI-*mpc2-glmS)* parasite populations (~1467 bp band) without 5' and 3' integration (incorrect band noted at 5' integration and no band detected at 3' integration). Additionally, the pSLI-*mpc2-glmS* and pSLI-*mpc2-glmS-mut* plasmids were not detected in the parasite populations. This would be due to plasmid removal from the parasite after multiple life cycles have progressed without plasmid integration.

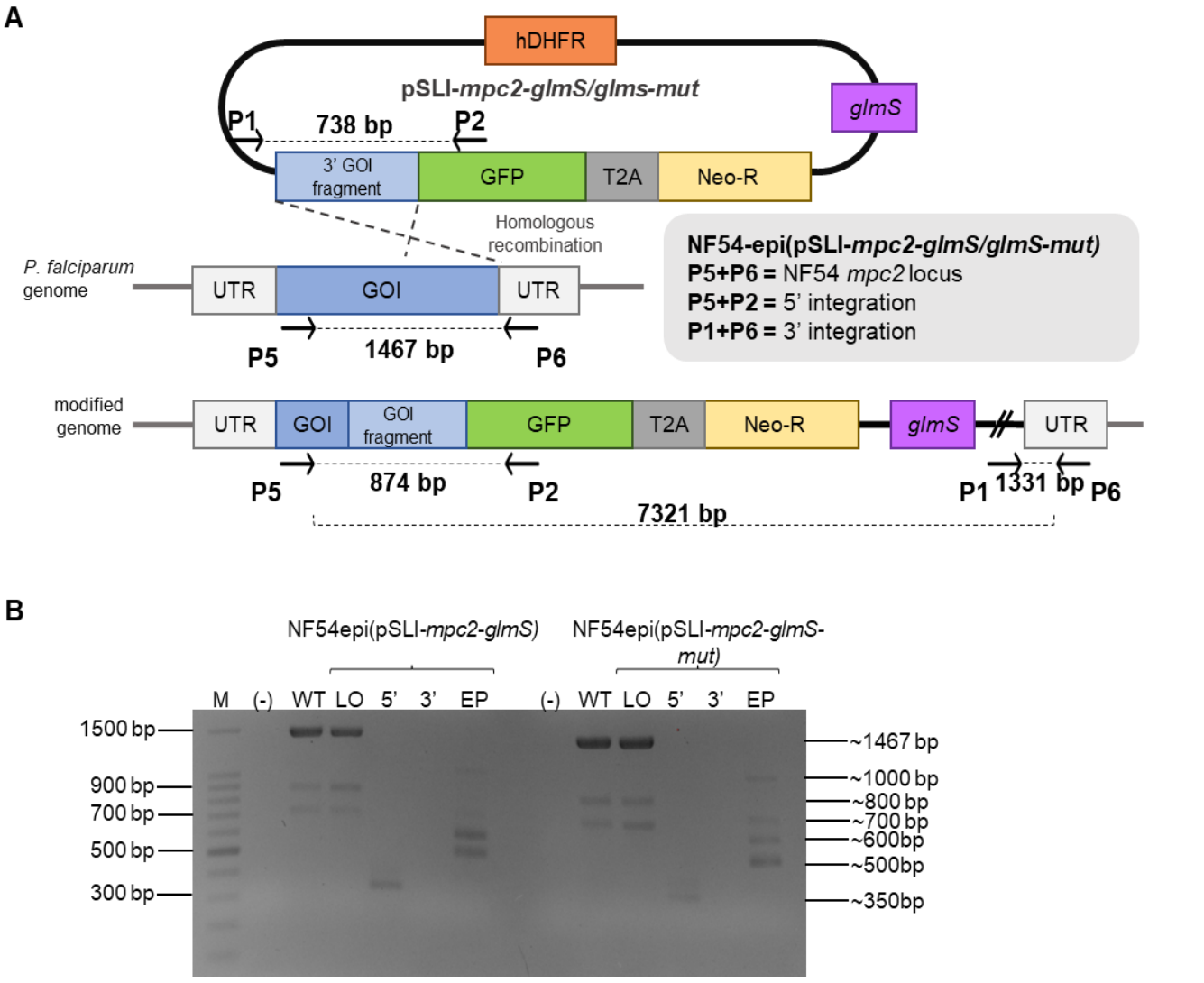


**Supplementary Figure 4: Genomic integration check on the NF54epi(pSLI-*mpc2-glmS)* and NF54epi(pSLI-*mpc2-glmS)* parasite populations. (A)** Schematic representation of the primer combinations used in screening the SLI-*glms* transgenic lines. **(B)** Parasite population suspected of integrating the pSLI-*mpc2-glmS* and pSLI-*mpc2-glmS-mut* plasmids were PCR screened for the presence of the 5' and 3' amplified region as well as the absence of the locus region. PCR products were visualised on a 1.5 % (w/v) agarose/TAE gel stained with 0.5 µg/mL EtBr after electrophoresis. M: 100 bp molecular marker (Promega, USA). (-): negative control without template DNA in PCR, WT: NF54 wildtype parasite template DNA, LO: NF54 *mpc2* locus region, 5': 5' integration region, 3': 3' integration region, EP: plasmid detection for episomal presence.

Supplementary Figure 5 represents the complete 1.5 % agarose/TAE (w/v) gel of Figure 3.17B.

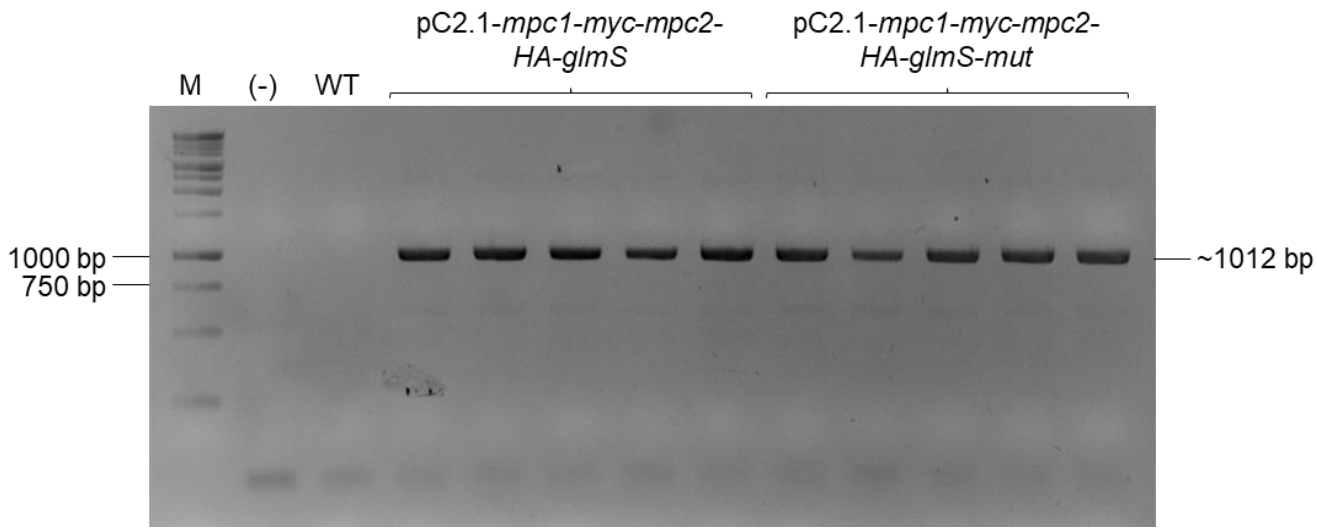


**Supplementary Figure 5: PCR screening for recombinant pCR2.1-*mpc1-myc-mpc2-HA* plasmids.** Bacterial colonies were screened for recombinant pCR2.1 plasmids with the *mpc1-myc-mpc2-HA* insert indicated by the 1012 bp band. PCR products were visualised on a 1.5 % (w/v) agarose/TAE gel stained with 0.5 µg/mL EtBr after electrophoresis. M: 1Kb molecular marker (Promega, USA), (-): no template control and (WT): LB-broth inoculated with water to indicate a negative screen.

Supplementary Figure 6 represents the complete 1.5 % agarose/TAE (w/v) gel of Figure 3.18A.

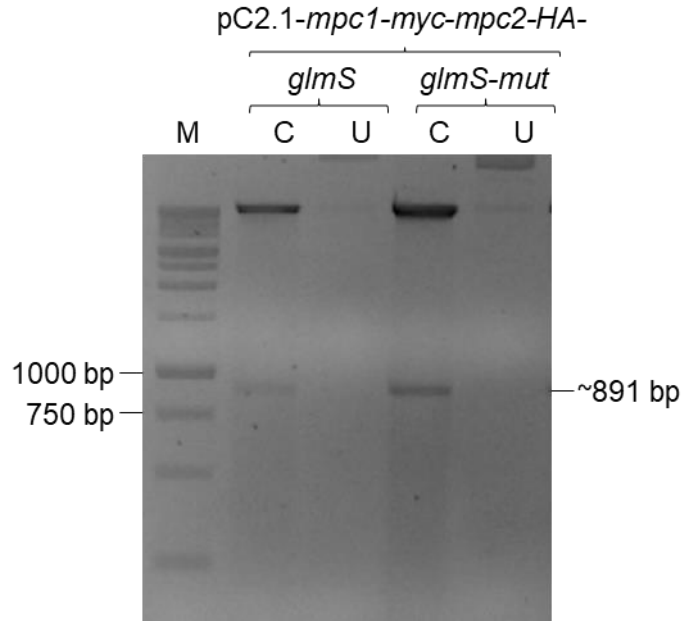


**Supplementary Figure 6: Validation of recombinant pCR2.1-*cam-mpc1-myc-mpc2-HA-glmS* and pCR2.1-*cam-mpc1-myc-mpc2-HA-glmS-mut* plasmids.** Restriction enzyme mapping of the recombinant pCR2.1-*cam-mpc1-myc-mpc2-HA-glmS* and pCR2.1-*cam-mpc1-myc-mpc2-HA-glmS-mut* plasmids with the *SalI* and *StuI* restriction enzymes. Digested constructs were visualized on a 1.5 % (w/v) agarose/TAE gel stained with EtBr 0.5 µg/mL. M: 1Kb molecular marker (Promega, USA), U: undigested plasmid sample and C: digested plasmid sample.

Supplementary Figure 7 represents the complete 1.5 % agarose/TAE (w/v) gel indicating the partial integration of NF54$^{attB}$ -*cam-mpc1-myc-mpc2-HA-glmS* parasite line as the original *cg6* gene was detected in both the wild type and integrated line indicated by the 681 bp band.

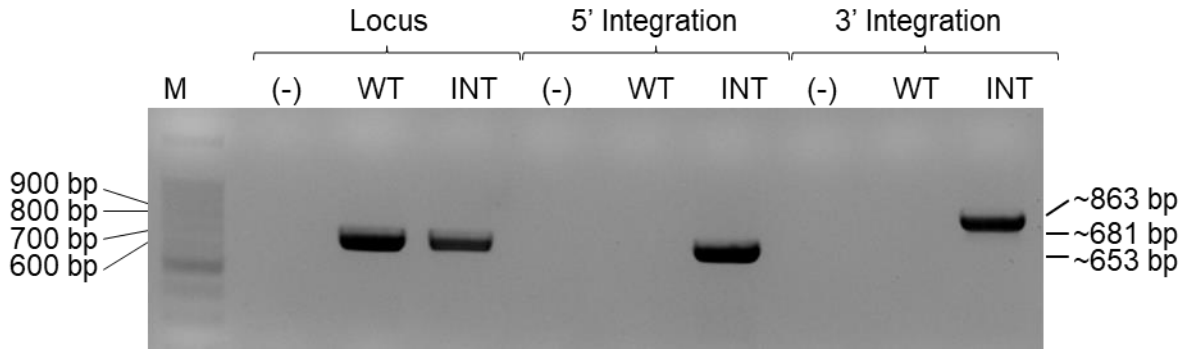


**Supplementary Figure 7: Partial genomic integration of the NF54-*cam-mpc1-myc-mpc2-HA-glmS* parasite line.** Parasite population suspected of integrating the pCR2.1-*cam-mpc1-myc-mpc2-HA* cassette were PCR screened for the presence of the 5' and 3' amplified region as well as the absence of the locus region. The NF54-*cam-mpc1-myc-mpc2-HA-glmS* parasite line was partially integrated with visible 5' (653 bp) and 3' (863 bp) fragments as well as the visible 681 bp band in the integrated line when checking the locus for the original *cg6* gene. PCR products were visualised on a 1.5 % (w/v) agarose/TAE gel stained with 0.5 µg/mL EtBr after electrophoresis. M: 100 bp molecular marker (Promega, USA). (-): negative control without template DNA in PCR, WT: NF54$^{attB}$ wildtype parasite template DNA, INT: NF54-*cam-mpc1-myc-mpc2-HA-glmS* parasite line template DNA.

Supplementary Figure 8 represents the parasitaemia of the partially integrated NF54$^{attB}$-*cam-mpc1-myc-mpc2-HA-glmS* parasite line after the second period of WR99210 drug pressure. This parasitaemia did not reduce to 0 % as with the first selection cycle (Figure 3.19) due to the presence of partially integrated parasites within the population. The parasitaemia increased between day 5-9 after the 6 day selection cycle with WR99210. Following this, the parasite population was checked and confirmed through with PCR for genomic integration of the *mpc1-myc-mpc2-HA-glmS* fragment into the *cg6* gene.

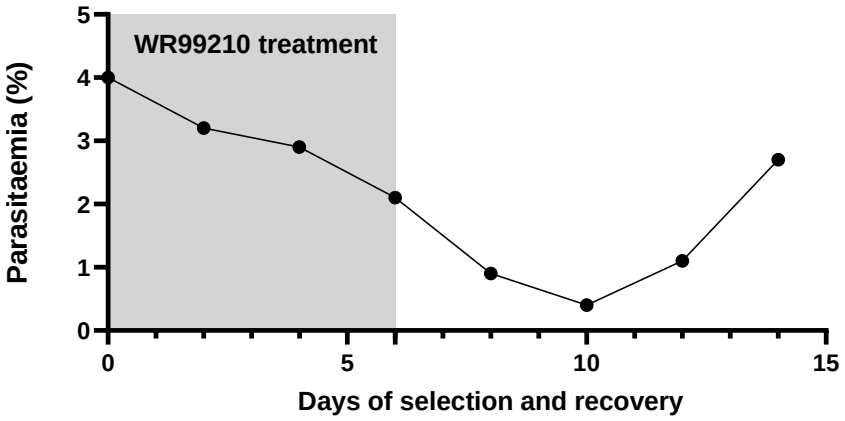


**Supplementary Figure 8: Parasitaemia of *P. falciparum* the NF54$^{attB}$-*cam-mpc1-myc-mpc2-HA-glmS* parasite line during WR99210 selection and recovery.** NF54$^{attB}$-*cam-mpc1-myc-mpc2-HA-glmS* partially integrated parasite line was treated with WR99210 for 6 days (grey box) to obtain a fully integrated transgenic line followed by a recovery period. The parasitaemia of each line was monitored every second day with light microscopy.